Avertissements au lecteur

Ce document est le produit d'un projet de master réalisé à l'EPFL dans le laboratoire d'Ecohydrologie sur une période de quatre mois. Son contenu n'engage que son auteur et n'est reproductible qu'avec le consentement écrits de ce dernier.

Warning to the reader

This document is the product of a master's project done at EPFL in the laboratory of Ecohydrology during a four month period. Its content commits solely it author and can be reproduced only with the written consent of the latter.

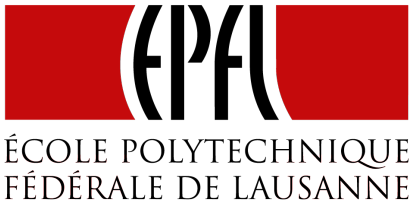

École polytechnique fédérale de Lausanne

Master Thesis

Hydrology and Pesticide Transport Modelling in the Petite Chamberonne catchment

---

Author:
Pascal Stalder

Supervisors:
Pierre Queloz
Bettina Schaefli
Enrico Bertuzzo
Prof. Andrea Rinaldo

Laboratory of Ecohydrology (ECHO)

June 19, 2013

Abstract

This project studied hydrological models used in the catchment of the Petite Chamberonne north-west of Lausanne. In a first step, input data have been analysed and prepared for the spatially explicit, conceptual hydrological model SEHR-ECHO. It has been proved that rainfall data can be taken and homogeneously distributed over the catchment from a nearby rain gauge (Crissier). The 9 months of discharge data proved to be of good quality; 9 months of data however is rather short for automatic calibration. Unique annual events influence the calibration of the hydrological model strongly and had to be removed and tested manually. First results showed a mediocre performance of the standard version of SEHR-ECHO. In order to improve the results of the simulation, several adaptations of the model have been tested. The best variant showed to be SEHR-ECHO, using reservoirs in series (instead of parallel) and Horton's mechanism for surface runoff production (instead of Dunne's mechanism). A NSE of 0.77 has been achieved. Based on this hydrological model, two types of pesticide transport models have been developed and tested. Though not yet calibrated (due to the lack of data), it has been observed that the two models give results that are sensitive to the chemical properties of the simulated pesticide and that the results show similarities to what has been observed in previous studies (e.g. [Leu et al., 2004a]). A further effort in calibration using more date will have to be undertaken in order to improve and validate the hydrological simulations. At last, the pesticide transport model will have to be calibrated and its results interpreted once data is available.

Résumé

Ce projet visait à étudier les modèles hydrologiques du bassin versant de la Petite Chambronne situé au nord-ouest de Lausanne ainsi que le transport des pesticides à l'échelle du bassin versant. Dans un premier temps, les données d'entrée sont été analysées et préparées pour le modèle hyrologique conceptuel et spatialement explicite SEHR-ECHO. Il a été prouvé que les données pluviométriques peuvent être relevées dans une jauge de pluie (Crissier) et être distribuées homogénéiquement sur le bassin versant. Les données de débits mesurés pendant 9 mois étaient de bonnes qualités cependant 9 mois de mesures ne suffisent guère pour une calibration automatique du modèle hydrologique. Des événements annuels exceptionnels influencent fortement la calibration du modèle hydrologique et doivent donc être retirés et testés manuellement. Les premiers résultats ont montré une performance limitée de la version standard de SEHR-ECHO. Dans le but d'améliorer les résultats des simulations, plusieurs adaptations du modèle ont été testées. La meilleure variante de SEHR-ECHO s'est avérée être celle utilisant les réservoirs en séries (au lieu des réservoirs en parallèle) et le mécanisme d'Horton (au lieu du mécanisme de Dunne) pour la production d'eaux de ruissellements. Un NSE de 0.77 a été atteint. Sur la base de ce modèle hydrologique, deux types de modèle de transports de pesticides ont été développés et testés. Bien qu'ils ne soient pas encore calibrés (en raison du manque de données), il a été observé que les deux modèles donnent des résultats qui sont sensibles aux propriétés chimiques des pesticides étudiés et que les résultats étaient cohérents avec les observations de précédentes études (par exemple [Leu et al., 2004a]). Un effort supplémentaire sur la calibration en utilisant plus de données devra être entrepris afin d'améliorer et de valider les simulations hydrologiques. Enfin, le modèle de transport des pesticides devra être calibré et ses résultats interprétés une fois les données disponibles.

Acknowledgements

I would like to thank Prof. Andrea Rinaldo for giving me the opportunity to work in the laboratory of ecohydrology (ECHO). Special thanks go to Bettina Schaefli, without whom the hydrological modelling part of this project would not be what it has become. I also thank Pierre Queloz for his constant input of ideas and remarks on pesticide modelling. Further thanks go to Enrico Bertuzzo, for his inputs on pesticide transport models. I was glad working in this lab, and I thank all the collaborators of the ECHO-lab for their comments, help and discussions. Furthermore, I thank my family for their constant support and for making my studies at EPFL possible. Their feedback, not only on this last project, has always been important and useful to me. I also would like to thank my girlfriend Célia for her unconditional love and support during all these years.

Contents

List of Figures

List of Tables

Chapter 1

Introduction

Even long before the industrialization, farmers used natural pesticides in order to prevent damages to theirs crop. These substances target any undesirable species that grow on the fields along with the main culture and decrease productivity. Natural pesticides (such as toxic metals) have however not been used as frequently and abundantly as nowadays pesticides. During the 1940s, industrial production of pesticides began to increase [Daly et al., 1998]. Worldwide, the majority of pesticides are used in developed countries, but developing countries are catching up. In Switzerland, the sale of pesticides increased by 15 % from 2006 to 2011 [BFS, 2012], and are expected to still rise in the near future. A total of 2225.1 tons of active substances have been sold in 2011 [BFS, 2012].

As these chemical reactants are applied to what finally becomes our food, one has to know the inherent danger of these substances for our health. Assessments of the ecotoxicology of almost all substances used as pesticides are available. One well known example is DDT (dichlorodiphenyltrichloroethane), which has been widely used as an insecticide. One of its major aims was to fight the *Anopheles* mosquitoes, vector of malaria. It was thought that diminishing the population of these mosquitoes will eventually decrease the number of deaths due to malara. It did - but had a major side effect. DDT proved to be bioaccumulating and proved to be hormone active and may cause cancer. The persistence and bioaccumulation of DDT has thus been studied all over the world (e.g. Egypt [El Nemr et al., 2013], China [Yu et al., 2013], or USA [EPA, 2011]). In the case of DDT, these studies led to an interdiction of the product. Under the Stockholm Convention, limited uses as vector control for preventing malaria are still allowed. This shows the importance of knowing how these pesticides behave in nature. It has to be pointed out that each pesticide has different chemical properties and can therefore show different behaviours. It is especially important to know how these substances move in nature. In most of the cases, these substances are transported by water, along a river network, ending in a lake or ocean, where they are eventually degraded or ingested by animals, or simply accumulated at the bottom of the water body. The transport of pesticides in nature has been less studied than their ecotoxicology. This is mainly due to the fact that the transport of pesticides has to be linked to a hydrological model, and that the hydrological models itself are not always easy to deal with (as the present project will show).

In a study by [Leu et al., 2004a], the processes leading to a transport of three pesticides (atrazine, dimethenamid, and metolachlor) from their point of application to surface waters have been analysed. The authors report the importance of the two first precipitation events following an application, which lead to a high surface runoff, washing off a major fraction of the pesticides. However, they did not model these processes. In a companion paper [Leu et al., 2004b], they report the variability of herbicide concentration for similar meteorological conditions due to variable properties of the fields. Even so, no follow-up paper did try to turn these results into a model. These two, and a third by the same author [Leu et al., 2005] can however be used as a comparison for future model results. Other studies exist that predict the transport of pesticides. An example would be SWAT (Soil and Water Assessment Tool, [Larose et al., 2007], [Neitsch et al., 2009]) by the College of Agriculture and Life Sciences (Texas, USA), which couples hydrological simulations and pesticide transport modelling using a physically based modelling approach. In Switzerland, similar models exist, but are not as much used in policy making than in the US (e.g. [Bertuzzo et al., 2013]).

It is therefore clear that the next step has to be taken. That is, develop an new input-output model that predicts the transport of herbicides on the catchment scale for small catchments, using meteorological data as input. Enveloped in the project "Catch-Herb" of Ecohydrology laboratory (ECHO-lab) at EPFL, this Master's thesis is taking the first few steps for such a model. The catchment of the Petite Chamberonne north-west of Lausanne, VD-CH which this Master's thesis focusses on, has been selected as a pilot catchment. The project Catch-Herb itself is funded by the Swiss National Science Foundation and takes place from 2011 to 2014.

In order to achieve these goals, at first, the spatially explicit hydrological response model of ECHO-lab (SEHR-ECHO) will be adapted and calibrated for the catchment of the Petite Chamberonne. The catchment and the usage of pesticides in the study area are described in chapter 2. In chapter 3, the methods used to obtain the resulting pesticide model are presented. At first, SEHR-ECHO will be adapted and calibrated for the catchment Petite Chamberonne using meteorological input data. Based on these results, an extension for SEHR-ECHO allowing the simulation of pesticide transport is written. Two different types of models will be tested: first, a simple model using a well mixed assumption and second, a model that uses the concept of water age. It has to be noted that during this project, no measurements of pesticide concentrations have been available. Therefore, calibrating the pesticide transport model is not yet possible. A general evaluation of the two tested models is however done, based on three case studies.

Chapter 2

Background information

In this chapter, information on the catchment is provided. The information on the Chamberonne catchment are mainly based on the semester project of 2012 [Stalder, 2012]. During this previous project, the Chamberonne catchment and more specifically the application of pesticides in the subcatchment of the Petite Chamberonne have been studied.

2.1 The Chamberonne catchment

2.1.1 Description of the catchment

SEHR-ECHO has been applied to the catchment of the Chamberonne river for previous studies (e.g. [Imfeld, 2011], [Nicótina et al., 2008]), situated west of Lausanne. The catchment can be divided in two major sections based on the land use. The northern part of the catchment consists mainly of agricultural area, with some rural villages. The southern part, adjacent to the lake of Geneva, is highly urbanised.

The slope of the rivers change accordingly. In the northern rural area, the rivers flow along a gentle slope. Between Cheseaux and the campus of the EPFL, the slope of the rivers gets steeper (up to 0.04). The slope for the Sorge and Chamberonne is illustrated in Fig. A.1, Appendix A.

Both rivers, the Mèbre in the east and the Sorge in the west, flow in the south direction towards the lake. They cross the city of Lausanne, where the rivers are highly influenced by human activities. This includes the construction of retention basins for flood control, storm sewers as well as impervious surfaces [Schleiss, 2012]. The overall impermeability of the catchment is approximately 37 % [Queloz, 2012]. The land use of the area contributing to the Chamberonne river network can be seen in Fig. A.2. The Chamberonne has a Q_{347} of 0.226 m^3/s [Stalder, 2012].

2.1.2 The subcatchment of the Petite Chamberonne

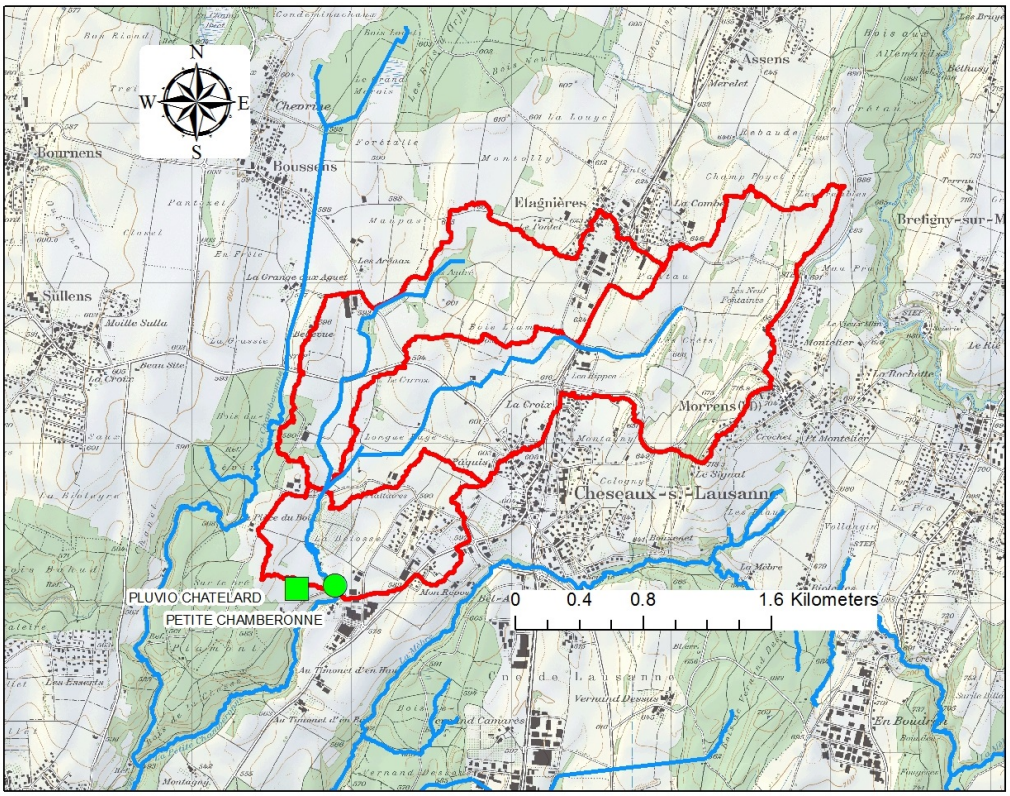

Figure 2.1: Calculated catchment of the Petite Chamberonne [SwissTopo, 2012]

For this master thesis, the subcatchment of the Petite Chamberonne has been studied. Lying in the northern part of the catchment of the Chamberonne, the subcatchment of the Petite Chamberonne has been selected as a pilot catchment, where measurements of pesticides are taken and a first attempt of pesticide transport modelling is undertaken. The subcatchment of the Petite Chamberonne is composed of mainly agricultural surfaces, with a minor area covered with forest and infrastructure. The subcatchment has been studied during the semester project 2012 [Stalder, 2012]. A survey has been conducted on the application of pesticides in the area. Furthermore, information on the drainage systems in the study area has been gathered. The results of this survey can be found in the appendix A, Fig. A.4. During the master thesis, the subcatchment of the Petite Chamberonne has been calculated using TauDEM on Mapwindow GIS [Tarboton, 2013] . The calculated area is approximately 4.6 km^2, representing roughly 10% of the total area of the catchment of the Chamberonne (Fig. 2.1). It has to be noted that the surface area of the Chamberonne catchment is expected to be estimated with an unknown error, due to the fact that the there is little knowledge about the drainage system of the area. For further information on this issue, refer to section 3.1.1.

2.1.3 Measurement stations

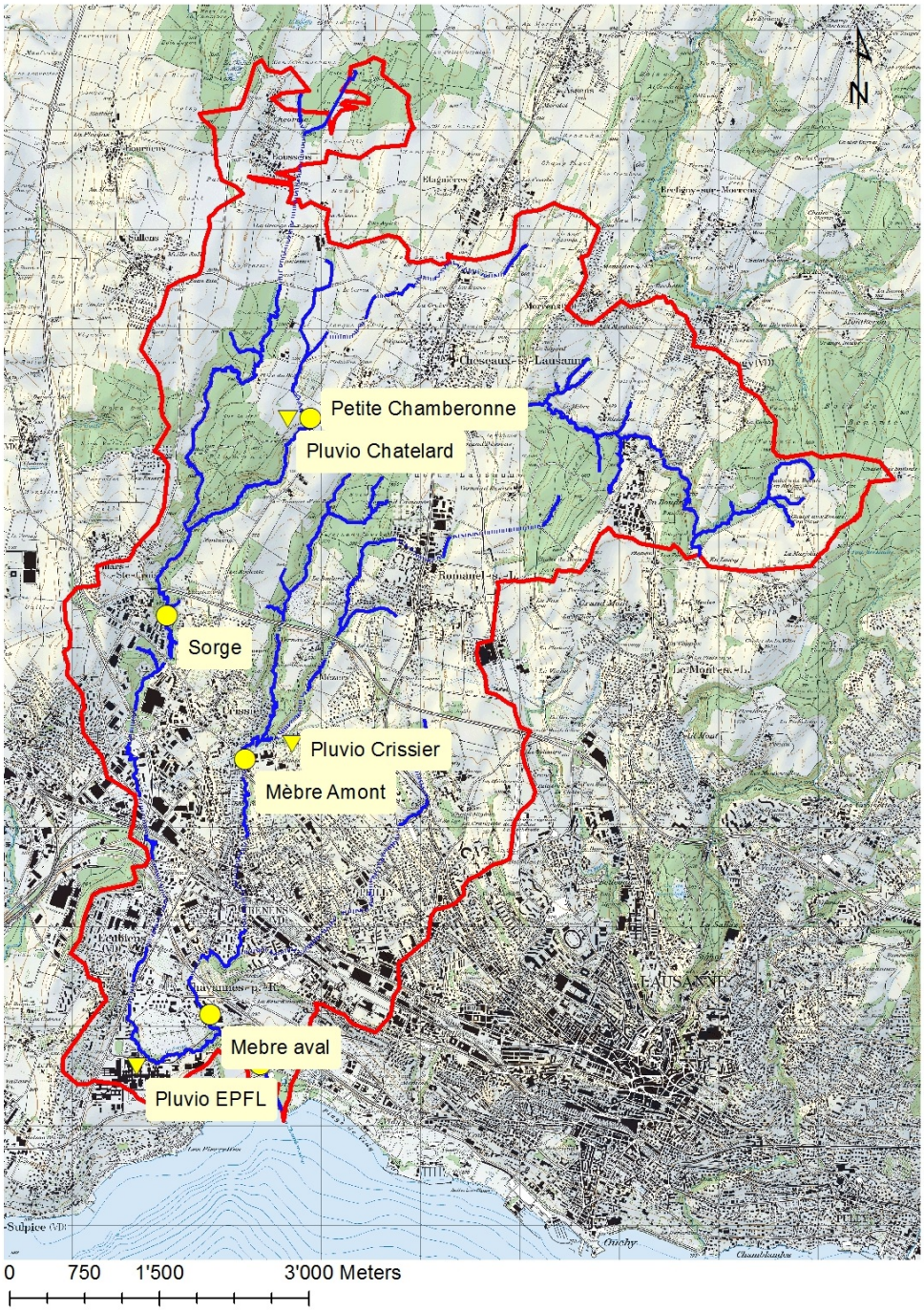

Figure 2.2: Overview of the Chamberonne catchment

The ECHO laboratory disposes of and runs several measurement stations across the catchment of the Chamberonne. The location of each station is indicated in

Fig. 2.2. The station of particular interest for this study is located at the "Petite Chamberonne", as this station measures discharge, temperature and electrical conductivity and takes water samples at the location downstream of the sub-catchment of the Petite Chamberonne. These water samples can be used for the calibration of a future pesticide transport model.

The stations measure following parameters:

1. Petite Chamberonne: water level [m], water temperature [°C], conductivity of the water [$\mu S/cm$] @ 25°C. A measurement is taken every 5 minutes. First recording on 30.04.2012 (ongoing).

2. Sorge: water level [m], water temperature [°C], conductivity of the water [$\mu S/cm$] @ 25°C. A measurement is taken every 5 minutes. First recording on 08.12.2009 (ongoing).

3. Mèbre Amont: This station was located at the gallery from 15.12.2009, and on the 27.04.2012 a second station has been installed at the crossover located 100m further downstream. The main purpose was to increase the reliability of th measurements, as the flow at the crossover is more uniform and thus poses less problems than at the gallery. The station at the gallery measures only water levels [m], whereas at the crossover, water temperature [°C] and conductivity of the water [$\mu S/cm$] are measured additionally.

4. Mèbre Aval:only water levels [m] are measured every 5 minutes, first recording 11.12.2009.

5. Chamberonne/UNIL: water level [m], water temperature [°C], conductivity of the water [$\mu S/cm$] @ 25°C. A mesaurement is taken every 5 minutes.

6. Pluviometer Chatelard: Precipitation data is being collected at the rain gauge at the rain gauge Chatelard (see Fig. 2.2). The unit used is a "PluvioMadd" by Madd Technologies SARL. The tipping bucket rain gauge measures the time between each 0.2 l/ m^2. This corresponds to 0.2 mm of precipitation at the measured time.

7. Meteostation EPFL: At this stations, precipitation is measured using a heated gauge. Furthermore, wind speed and direction are measured, as well as the incoming solar radiation. Lastly, the temperature is measured at 3 different, heights (5, 10 and 20cm above ground level), and the humidity of the air is recorded.

2.2 Semester Project 2012

During autumn 2012, a project trying to identify the pesticides used in the sub-catchment of the Petite Chamberonne, as well in quantity and their specific application dates has been conducted [Stalder, 2012]. The results aid delimiting the time where samples should be taken, and give a general idea of the kind of pesticides present in the river water. The information gathered during this

project are based on the report of the AGRIDEA [Favre et al., 2010], as well as a telephone survey amongst the farmers exploiting the agricultural fields of interest.

As for the dates of application, it has been found that mainly two periods of application exist: late summer/early autumn and spring. The exact dates depend however on the plant cultures. The major plant cultures in the study area are corn, wheat, colza and barley. Each culture will be treated at a different development state, or reach a specific development state at a different point in time. Overall, it can be expected that the major fraction of pesticides will be measured in April and September of each year [Favre et al., 2010] [Stalder, 2012].

The substances used also depend on the specific plant species. Several dozen different pesticides are recurrently used, the five major groups (by applied mass) being isoproturon, mancozeb, chlorothalonil, glyphosate and metamitron. The amount of applied pesticide depends on the type of culture and severity of the pest. The mean application for isoproturon is 0.217 kg/ha, mancozeb 0.212 kg/ha, chlorothalonil 0.116 kg/ha, glyphosate 0.116 kg/ha and metamitron 0.080 kg/ha [Favre et al., 2010].

These results show the importance of having samples of river water during April of each year to be studied. These data could then be used to calibrate and validate the newly developed extension for the hydrological model.

Chapter 3

Method

In this chapter, the theory and models used for the present project are presented. At first, the hydrological response model used will be described, and the studied variants are presented. In section 3.2 thereafter, two different types of pesticide transport models are presented. The last section is explaining the calibration process.

3.1 Hydrological Modelling

Hydrological models can be used in many ways. They can predict not only discharge and water flows in the near to not-so-near future, they can also predict the impact of climate change and land use change (e.g. [Praskievicz and Chang, 2009]). On the other hand, not every model works in the same way. Three types of models exist [Pechlivanidis et al., 2011]).

- Empirical models: They simulate discharge (or other hydrologically relevant data) based on observations. These observations are then transformed into discharge using empirical equations. One early example of this approach is the unit hydrograph approach.
- Conceptual models: Based on a pre-defined model structure, these input-output models are based on a number of parameters. These parameters can be chosen according to the requirements and do not always represent physical properties of the processes. Therefore, these parameters have often to be estimated by calibrating the simulation using observation data.
- Physical models: These models simulate the processes, such as evapotranspiration, percolation, infiltration, using the specific governing equation of motion. These equations have often to be solved numerically using finite element spatial or temporal discretisation.

The models can be classified as lumped or distributed models, where the first signifies a homogeneous behaviour across a large section and the second a more heterogeneous behaviour. The computational requirements are clearly higher for distributed models. Furthermore, models can be deterministic (one single

answer) or stochastic, where random variables are used to represent uncertainty in process modelling and input data.

3.1.1 Input preparation

Before any simulation can be done, all input data have to be prepared and reformatted, in order to meet the input format required for the specific model used. The inputs here will be prepared for SEHR-ECHO. Each input is briefly described, it is explained how it has been prepared, and the kind of problems encountered during the preparation are illustrated. A general interpretation and comments on the input data are given where it has proven to be of significance.

Overview on input data

Required input data are:

1. Observed discharge at a specific point/section. The discharge is measured and can therefore be compared to the simulated discharge. This allows the calibration of the model.

2. Precipitation data. This data is required in order to be transformed into discharge and represents the main input for hydrological models. The major input in the Chamberonne catchment is rain, as no glacier or permanent snow covers are present in the catchment.

3. Temperature data. The model decides which fraction of the precipitation falls as snow and how much snow melts, where the temperature plays a leading role.

4. Potential evapotranspiration (PET). An important fraction of the precipitation is directly intercepted by vegetation and evaporated and transpired. This water therefore never reaches the channel and does not contribute to the total discharge of the river. The PET measures the maximum volume of water that can be evapotranspirated.

5. Network geometry. This geometry describes the setup of the river network.

   As an example, the network geometry of the sub-catchment of the "Petite Chamberonne" is given below.

   In figure 3.1, the layout of the network is displayed, with the information on the number of stretches and each section's length. This layout, especially the length of each stretch plays a major role in the routing of the discharge.

6. Hydraulic conductivities. In order to be able to simulate the subsurface and deep reservoir fluxes, the model requires information on the composition of the subsurface, especially the hydraulic conductivities of each section of the catchment. This is then used to calculate the leaching from the active soil layer to the reservoirs, according to equation 3.7.

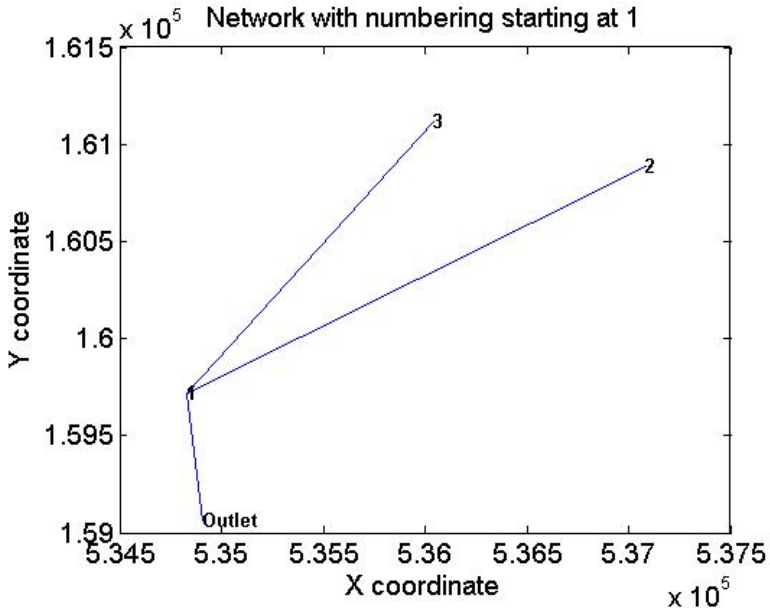

Figure 3.1: Network geometry of the sub-catchment of the "Petite Chamberonne"

7. Altitudes. The temperature data is measured at EPFL, at an altitude of 395 m.a.s.l. The temperature therefore has to be extrapolated for higher altitudes, in order to get representative snow-rain distributions.

8. Impervious area. An important fraction of the precipitation contributes directly to the surface run-off. This is especially true for impermeable areas, where the water cannot penetrate the soil and flows freely on the surface. It is therefore important to know the percentage of impermeable areas (such as roads, parking lots, houses) in each subcatchment.

Discharge

- Measured data: water level [m] at 6 stations
- Required input format for model: observed discharge [m^3/s] for specific station

Establishing rating curves During the year 2012 and 2013, several measurements of discharge-water level couples have been taken. These couples can be used to establish rating curves, which relate water levels [m] to a discharge [m^3/s]. Rating curves have been established for each station separately, in order to convert the measured water level to a corresponding discharge. Two methods of interpolation have been used:

1. The Power law which is the most widely used form for fitting rating curves [ASCE, 1996]. It has the following general form:

$$Q = a_1 * x^{a_2} \tag{3.1}$$

2. The Parabolic law having a general form of

$$Q = b_1 * x^2 * b_2 * x + b_3 \tag{3.2}$$

As an example, the fitted rating curves for the station "Petite Chamberonne" is given below (Figures for each station can be found in appendix B).

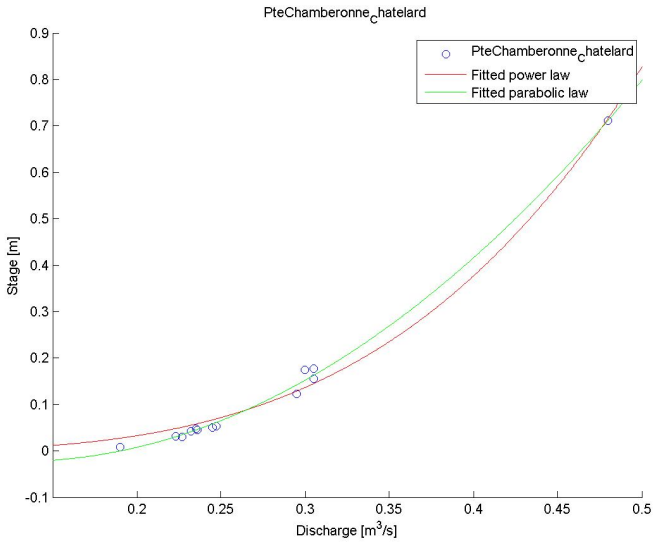

Figure 3.2: Rating curve, Petite Chamberonne

A good fit can be observed for the majority of the points using both laws. However, the limited number of measurements at high water levels and correspondingly high discharge increase the uncertainty at higher discharges. The highest measured water level at the station "Petite Chamberonne" for the year 2012 was 0.6 meters, and one could estimate a corresponding discharge using Manning's law:

$$\begin{aligned} Q &= A * v \\ &= A * k * S^{1/2} * R_h^{2/3} \end{aligned} \tag{3.3}$$

S being the slope of the channel bed, k the Manning-Strickler coefficient and R_h the hydraulic radius. The section can be assumed being rectangular for up to a height of 1.5 meters. The Manning-Strickler coefficient on the one hand as well as the slope on the other hand are unknown. $k * s^{0.5}$ can be estimated using the measurements; the results of this operation show a large variability of one

couple to another. It is therefore questionable whether Manning-Strickler can be applied at this location.

Therefore, the interpolation of the water level measurements at each station has been done using both laws for comparison and without any additional points calculated with Manning's equation. Although the two laws show similar behaviour, the parabolic law has a major flaw: it produces negative discharges for small water levels. This being physically impossible, the power law has been chosen for the interpolation of the water levels.

The observed discharge at the Petite Chamberonne is shown in Fig. 3.3 below. A clearly distinguishable period of a lower discharge can be observed during summer, whereas the winter 2012/2013 is showing a rather high discharge. This observation is consistent with the observed rainfall patterns. The peaks however seem to be large compared to the baseflow. This may be due to the interpolation and the stage-discharge curves, i.e. uncertainty in the creation of the power law (or correspondingly the parabolic law). This uncertainty is measured using several measures of fitted data, which are summarized in the appendix B. For the station at the Petite Chamberonne, the root mean square error (RSME) is 0.011699, which is close to 0 and therefore an indication of a good fit for the rating curve. Taking the other indicators into account, the good fit is confirmed.

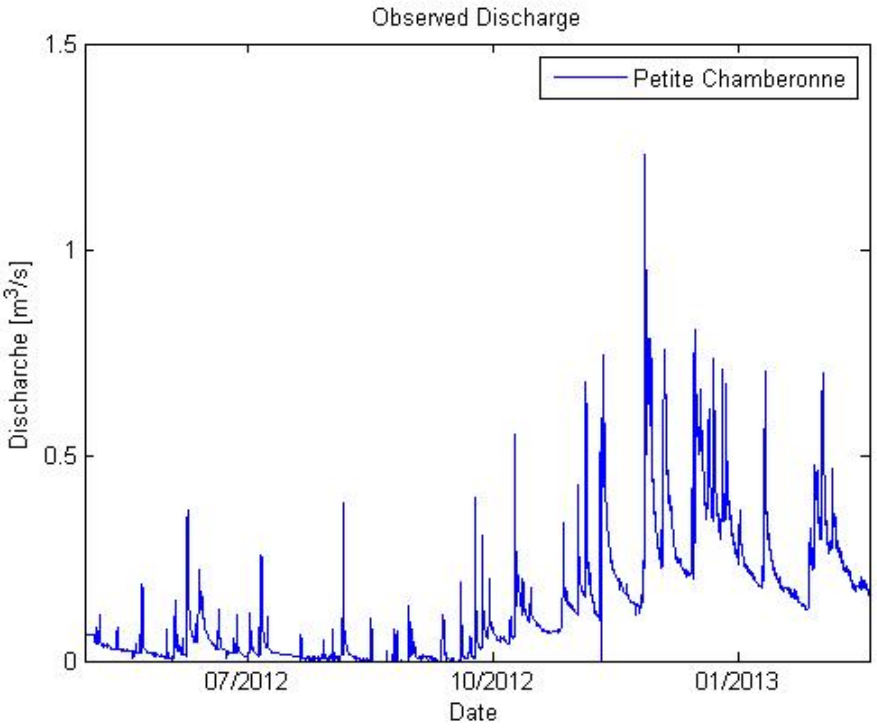

Figure 3.3: Observed discharge at the station Petite Chamberonne, interpolated from water levels using the power law

A recent study on the river Po in Italy [Domeneghetti et al., 2012] showed that the uncertainty in the rating curve are however not negligible. This is especially true for discharges that have to be extrapolated, i.e. it is important having measurements of stage-discharge at high stages (and correspondingly high discharges). Exploring the two types of rating curves, the power law and parabolic law, this finding is reflected in the fact that the two curves show significant differences for large stages. Another study states that discharge measurements at low stages tend to be more uncertain, and more importantly, that the uncertainty is not uniform across time [Tomkins, 2012]. It is therefore important to have several measurements of stage-discharge couples at different points in time, and also having captured the highest possible discharge. This decreases the rating curve uncertainty. However, it has to be noted that the previously mentioned studies have been made on large streams, whereas the present project is studying a small stream.

The discharge of the Petite Chamberonne has been compared to the discharge at the station Sorge (see Figure 2.2 for location) in order to confirm the discharge and increase the confidence in the data. The Sorge, located north of the urbanized region of Lausanne, should show a similar behaviour to rain forcing as the Petite Chamberonne. The area of the subcatchment of the Sorge is however bigger (based on visual estimates, not calculated) and should therefore lead to a bigger response. The peaks of discharge are expected to be bigger for the Sorge. Furthermore, it can be expected that the falling time of a peak is longer, as the farthest distance from the measuring station is bigger for the Sorge than for the Petite Chamberonne. These assumptions are confirmed visually (see Fig. 3.4) [1]. It can therefore be concluded that the measurements of the discharge have a high reliability and can be used without expecting large errors during the calibration process.

[1] The interpolation for the discharge at the station Sorge has been done using a parabolic law. This should prevent unreasonable high discharge peaks, which are due to the behaviour of the fitted power law (see B.2) for the rating curve of the station Sorge. As the comparison is done visually, the choice of the law is not of major importance and has been done for the sole purpose of the best visualization

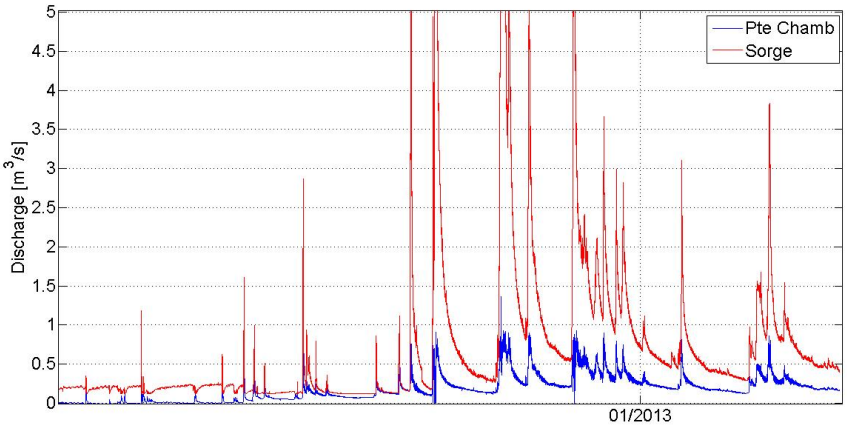

Figure 3.4: Zoom on the observed discharge at the stations Petite Chamberonne and Sorge

Precipitation data

- Measured data: 4 different stations with different formats for rainfall
- Required input format: continuous precipitation in mm/h

A rain gauge has been installed at the location Chatelard. The precipitation measured at this location was supposed to be used for the simulation of discharge at the Petite Chamberonne. However, upon analysis of the precipitation data, major issues with the station at Chatelard have been detected. It appears that the rain gauge at Chatelard has not been working properly during summer 2012, and has not been measuring any rain. While 2 to 3 weeks without rain seem possible, 3 months without rain clearly signal a problem. The annual precipitation at Chatelard would have summed up to roughly 900 mm, which is small compared to other nearby stations. The fact that there was a problem during the summer months becomes evident when plotting the cumulative precipitation of this station together with other nearby stations (Fig. 3.5). Hence, the measured time-series could not be used per se, and a solution for this problem had to be found. Especially as this precipitation data is the main input for the hydrological model, a close match to the actual rainfall had to be found. A script which allows the conversion to same formats as well as a comparison of the three stations in the proximity of Chatelard (Pully, EPFL and Crissier) has been written (see appendix C for complete code and additional figures). Hourly, daily and monthly values also have been used for comparison. Visually, the four stations can be compared using Fig. 3.5. A close match of the stations at Chatelard and Crissier even at an hourly level can be observed (Fig. C.3).

The three stations at the EPFL, in Crissier and Pully show a similar behaviour, with a small difference in the total cumulated rainfall for the observed period. Pully and EPFL have slightly more rainfall than Crissier, which can have two reasons. Firstly, EPFL and Pully are heated rain gauges, where snow is

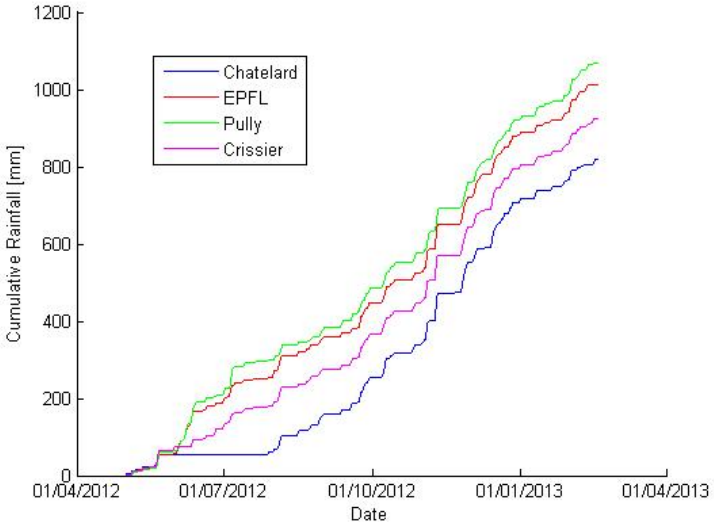

Figure 3.5: Cumulative precipitation for each station

melted and measured more correctly than in Crissier, where the rain gauge is not heated. Secondly, the stations at EPFL and Pully are closer to the lake than the station in Crissier, which may lead to a minor difference in total precipitation.

As an intermediate solution, it is proposed to use the measured precipitation data for Chatelard starting after the prolonged period of no rainfall (i.e. starting August 2012), adding the rainfall of Crissier before that date. Crissier's rainfall has been chosen due to its close match, both geographically and in terms of rainfall data. A reconstructed rainfall period of a little more than 9 months has thus been created (from 01-May-2012 to 01-Feb-2013).

The reconstructed rainfall sums up to 1016 mm for the nine months period. Assuming a uniform distribution over the year, we can estimate the yearly rainfall to be approximately 1350 mm (12/9 of 1016 mm). This value corresponds well to measured data, which show 1458 mm of annual rainfall in Switzerland (1961–1990) [Spreafico and Weingartner, 2005]. The rainfall is homogeneous over the catchment.

The 95 percentile of rainfall is 0.8875 mm/h, when no-rain events are taken into account, and 2.2 mm/h when only rain events are taken into account. This shows that there are very few extreme events during the study period. The rainfall distribution could be modelled using an exponential law. See figures in appendix C.

Apart from the problems occurring during the summer 2012, general problems may come up during winter months. An important point of measuring precipitation is how to measure precipitation in form of snow. Measuring snow implies several difficulties. The measurement of precipitation in form of snow is far from easy, and can yield systematic measurement errors. The origin of these errors are mainly twofold: firstly, the wind field around the measuring gauge is highly turbulent, and therefore a great amount of snow is deviated around the

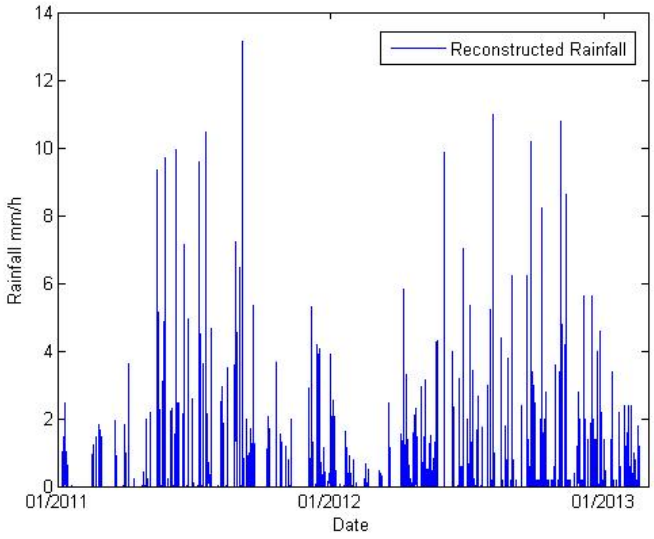

Figure 3.6: Reconstructed rainfall, combination of Crisser and Chatelard

gauge. Secondly, snow has to be melted in order to be measured by the tipping bucket. This heating can yield to losses. Depending highly on the type of gauge used to measure precipitation, losses up to 47 % can be expected (Forland (1982), in [Zweifel and Sevruk, 2002]. For tipping buckets, as used in Chatelard and Crissier, a systematic error of about 10 % can be expected (Forland (1982), in [Zweifel and Sevruk, 2002]). When accounting for this measurement error, real precipitation could be higher than measured; which ultimately would lead to higher discharges (or simulated discharges being too small). These difficulties do interfere directly with the simulation process, as the calibration can be biased by the erroneous precipitation measurements.

Lastly, the precipitation and discharge are plotted on the same figure down below. This allows to identify any issues with the input data. For this series, a good match between precipitation and discharge can be observed. One peak in discharge however (marked in green) does not have any preceding rainfall event. The data otherwise does not show any peak in discharge without a preceding rainfall. It can therefore be concluded that this is a singular event, although the reasons for this event remain unknown. As the available data covers only 9 months, this single event has a big influence on the calibration processes. In order to improve the calibrations, this discharge peak has been removed and replaced with the mean discharge during summer.

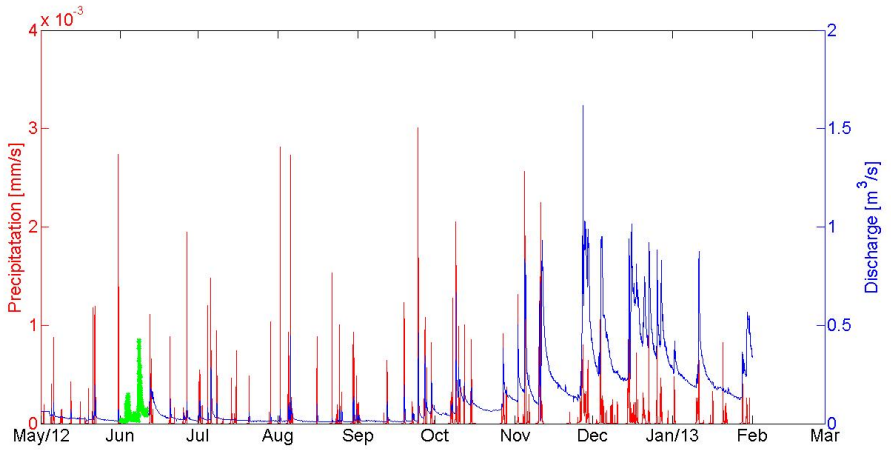

Figure 3.7: Overlay of precipitation and discharge measurements. All peaks of precipitation result in a peak of discharge, one peak in discharge (in green) however does not follow any precipitation event.

Temperature data

- Measured data at meteo station at EPFL
- Input data: continuous temperature data in Celsius

Temperature data have been measured by a weather station at EPFL. All meteorological data have been provided, and temperature data has been extracted for the desired time span.

Potential Evapotranspiration

- Available data: Model developed by Federico Croci & Meteostation EPFL
- Required data: Potential evapotranspiration in mm/h, hourly timestep for the study period

The potential evapotranspiration (PET) is calculated using a Penman-Monteith model [Penman, 1948] [Monteith, 1965]. A code which has been developed at EPFL by Federico Croci has been used for this purpose.

Using this model, the PET can be estimated for the desired period. Note that the calculated PET is not calibrated and uses the meteo data from the station EPFL. It is therefore questionable whether the calculated PET can be used for further hydrological modelling. The total potential evapotranspiration calculated with the simplified equation for the 9 months period is 419 mm. This is close to the PET to be expected. Lausanne, as well as all of the northern shore of lake Geneva, has amongst the highest PET in Switzerland with up to a maximum of 700 mm PET per year (correspondingly 9/12 = 600 mm). The mean actual ET in Switzerland is 484 mm, which corresponds to approximately

80 % of the potential evapotranspiration [Spreafico and Weingartner, 2005]. For further information on the calculation of the PET, refer to Federico Croci's work.

Digital elevation model

- Available data: DEM of the area around Lausanne
- Required input: Treated network geometry file

The digital elevation model (DEM) provides information on the topographical shape of the study region, i.e. each point of the raster image has a corresponding altitude. Using the DEM, two things can be calculated. Firstly, one can calculate the area of the catchment and the subcatchments within it, and secondly, calculate the network geometry of the channel network. The area of the catchment is required to know the area of influence, for example to convert the precipitation from mm into a volume (m^3). The different subcatchments are calculated in order to have a spatially explicit (semi-distributed) model, and to be able to route discharges amongst the different sections of the catchment. The network geometry is required to know how to route the water along the river network.

The calculation of the area of the catchment and subcatchments is done using TauDEM on MapWindow GIS [Tarboton, 2013]. The DEM used for the calculations is the swissALTI3D, provided by SwissTopo, at a grid size of 2m.

In the catchment of the Petite Chamberonne, several sections of the river lie underground. The DEM does therefore not represent the draining function of the terrain, i.e. it falsely drains water towards another catchment. When the contributing area for the station "Petite Chamberonne" is calculated, the area of the catchment is hence not calculated correctly. In a first attempt to solve this problem, a manual adjustment of the DEM was introduced: an artificial, 999 meters high "barrier" was added into the DEM. This wall avoids any spills from adjacent subcatchments, but is a rather crude operation. Another solution had to be found in order to counter the issue of subsurface channels.

Accordingly, a "burn in" function has been used. This function, which is implemented in MapWindow GIS, uses a pre-defined channel shapefile and burns its outline into the DEM. The altitude of the DEM is changed in such a way, that the terrain drains according to the burnt in channel. The shapefile used for this purpose is the official vector shapefile (VEC25_gwn_l_Clip), used previously in the semester project [Stalder, 2012]. During a visit on the terrain, Pierre Queloz observed that the channel passes further north than the official vector shapefile. This stretch has then been added manually to the shapefile and used for the calculation of the total area of the catchment. The result of this operation can be seen in Fig. 2.1, chapter 2.1.2.

There are however still several uncertainties influencing the size of the catchment. The exact number, size and direction of the drainages is unknown. It can be expected that a huge number of drainages are present in the agricultural zones. Furthermore, it is not known where the canalisation passes. This will ultimately influence the size of the catchment, and accordingly the total volume of

precipitation it receives. In order to minimize this issue, an additional parameter (SS) has been introduced (see section 3.3.3 for further details).

Hydraulic conductivities

In SEHR-ECHO, each subcatchment (called "section" later on) of the catchment possess its own hydraulic conductivity, K_{sat}. The difference between the sections is expressed as a ratio to the calibration parameter K_c, according to following equation:

$$Ksat = \frac{R_{ks} * K_c}{3600} \tag{3.4}$$

where R_{ks} is the said ratio. This ratio is obtained using the function *subcatchstatTaudemV02.m*, provided with the model. This function determines the dominant land use for each section. The sections are the same as the ones calculated previously (see section 3.1.1), whereas the land use is taken from geostatistical data from SwissTopo (Swiss Federal Office for Statistics: Geostat - Version 1997, Bern, Switzerland, 2001). The link of a land use to a hydraulic conductivity is made passing by the runoff coefficients. Runoff coefficients have a connection to the infiltration trends and hence with hydraulic conductivities. Furthermore, runoff coefficients can be linked to land use more easily than hydraulic conductivities. The link of runoff coefficients and land use is based on data by the service of conservation of natural resources of the U.S. Department of Agriculture (in [Da Ronco, 2013]).

At first, an overall runoff coefficient per section is calculated (composed of all the land uses in the section, on a grid of equal size of the DEM). This overall value is normalized by dividing it by the runoff coefficient of the dominant class in the section [Da Ronco, 2013]. The overall value is then stored as R_{ks}, and used as in equation 3.4.

In order to increase the speed of the calibrations, R_{ks} can also be fixed to 1 for each subcatchment. This signifies that each subcatchment possess the same hydraulic conductivity, even after calibration. For the catchment of the Petite Chamberonne, this assumption seems valid, as the main land use is agricultural fields and forests. It can therefore be expected that the sections each express similar hydraulic conductivities. Furthermore, hydraulic conductivities are strongly influenced by drainage systems made by men. It is therefore questionable whether the approach proposed by the *subcatchstatTaudemV02.m* function is applicable for this specific catchment.

3.1.2 SEHR-model of ECHO-lab

This section describes the spatially explicit hydrological response (SEHR) model used for this project. The summarized description is based on two previous Master's theses. For a more detailed explanation of the model and its functioning, refer to either Cédric Imfeld's [Imfeld, 2011] or Pierfrancesco Da Ronco's [Da Ronco, 2013] respective master thesis or the paper presenting the model [Nicótina et al., 2008]. It has to be noted that the description here matches the

original state of the model. During this project, several adaptations have been made to the model, which are described in chapter 3.1.3.

Functions and Modules

SEHR-ECHO simulates discharge based on previously mentioned inputs for an hourly or daily timestep through a conceptual, semi-lumped approach. For this project, an hourly timestep has been chosen. The catchment is represented by several sections (as shown in Fig. 2.1), each having a different homogeneous hydrological behaviour. Each section receives meteorological forcing based on nearby weather stations data series. A snow/rain separation with a corresponding snow accumulation, based an a critical temperature, is simulated. The equivalent rainfall is then transformed into runoff and subsurface discharge in a reservoir based approach. The resulting fluxes are then routed along the channel network resulting in the total discharge at a given measurement station. In the following, the different steps of SEHR-ECHO are described in more detail. The workflow is also illustrated in Fig. 3.9.

1. Rain is intercepted, for example by vegetation. This intercepted precipitation is directly evaporated and does not reach the ground. This is calculated by the interception module of the model (icept.m)

2. The rainfall after interception undergoes a second separation into snow and rain. Based on a critical temperature (here, 1°C is used), rainfall is transformed into snowfall as soon as temperature falls below the critical temperature. Snow is then stored in the snow reservoir and melts according to temperature. This process retains a certain volume of the precipitation and releases it as soon as the temperature rises above the melt point. The output of the snow module is the equivalent precipitation.

3. The equivalent precipitation is then introduced to the soil moisture module. In a first step , the precipitation is split into a direct surface runoff, using Dunne's model according to following equation:

$$R_s = J\frac{A_{imp}}{A_{sc}} + J - (\frac{\rho * Zr}{dt} * (s_1 - s) + K_{sat} * s^c) \tag{3.5}$$

   where A_{imp}/A_{sc} is the fraction of impermeable surfaces in the subcatchment, ρ the porosity and Zr the thickness (in mm) of the active soil layer, s the soil humidity and s_1 the soil moisture stress point and J the equivalent precipitation. According to this equation, rainfall first saturates the soil. Once the soil is fully saturated, it produces surface runoff.

4. The soil-module transforms the water in the active soil layer (coming from infiltration) into leaching and transpiration. It is assumed that evaporation is negligible once the water reached the active soil layer. Transpiration is calculated using a potential evapotranspiration, which has be calculated using a Penmna-Monteith model (see chapter 3.1.1). The actual transpiration

is then calculated using

$$ET = PET * \frac{s - s_w}{s_1 - s_w} \tag{3.6}$$

s_1 is the soil moisture stress point and s_w the soil moisture wilting point. This follows the idea of a water stressed transpiration as long as the soil humidity is lower than the soil stress point, according to Fig. 3.8. Leaching is calculated using the relationship developed by Clapp and Hornberger [Clapp and Hornberger, 1978]

$$L = K_{sat} * s^c \tag{3.7}$$

where c is the Clapp-Hornberger exponent. In the case of SEHR-ECHO, c is also a calibration parameter.

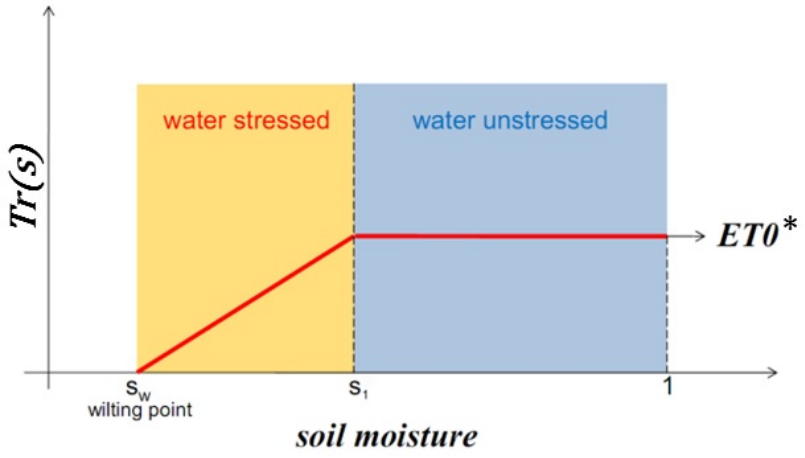

Figure 3.8: Conceptualisation of Transpiration

5. The leached water is distributed amongst two sub-surface reservoirs: a "deep" and a "subsurface" reservoir. This distribution is done using the "ϕ index". The ϕ index gives a constant recharge to the deep reservoir and can be calibrated. Although the nomenclature of the two reservoirs does not necessarily represent their geological disposition, the two reservoirs can be distinguished based upon their response time. The deep reservoir is considered having a longer (several times more) response time than the subsurface reservoir. These response times are represented in the calibration parameters t_s and t_d. Both reservoirs have a linear response, in the form of

$$Q = k * S \tag{3.8}$$

where S is the available storage in the given reservoir. It has to be pointed out that these subsurface processes are of major importance for the transport of pesticides and the implementation of these subsurface processes will therefore dictate the implementation of the transport of pesticides.

6. Lastly, the different discharges produced by the various modules are routed together in order to have the total discharge at a specific section. Using the discharge from every single section, the peaks are at first distributed within the section using a instantaneous unitary hydrograph approach. This approach is based on the probability distribution function issued from the advection-diffusion equation. Finally, the (distributed) discharges from the different sections are summed up for the final total discharge at the studied intersection [Da Ronco, 2013] [Imfeld, 2011].

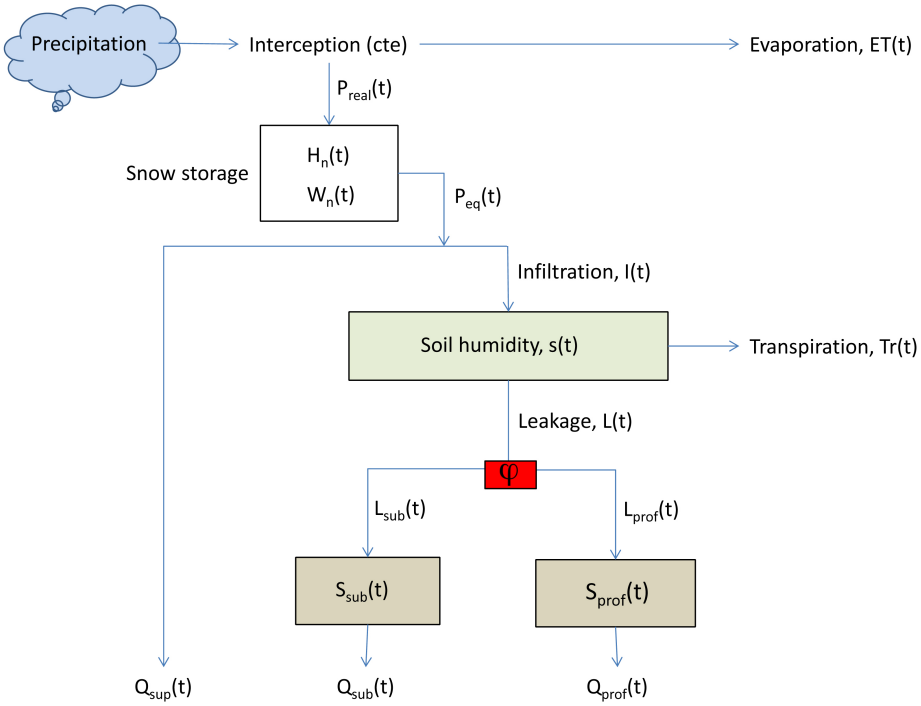

Figure 3.9: Conceptualisation of the SEHR model

Calibration parameters

This model allows and requires the calibration of following parameters [Schaefli, 2013, setupfunction]. These calibration parameters and their respective search interval have been extensively described by Imfeld [Imfeld, 2011]; here, it is pointed out which parameter is having more importance for this thesis, i.e. for the transport of pesticides.

1. K_c: Calibration parameter for the saturated hydraulic conductivity [mm/h]. Together with the input of the spatially distributed ratio Ks (R_{Ks}, 6), this parameter is used to describe the hydraulic conductivity found in each section.

2. c: Exponent of the Clapp-Hornberger equation for the non-linear loss from the root zone [-]. The search interval is based on suggested values by Clapp and Hornberger [Clapp and Hornberger, 1978] in [Imfeld, 2011].

3. Zr: Depth of the active soil layer [mm]. This parameter is representing the reservoir of humidity in the top-soil and is of importance for this thesis, as the top-soil layer is the most important factor for the transport and metabolism of pesticides.

4. t_s: Parameter for the mean subsurface residence time [h].

5. $s*$: Soil moisture treshold for plant-stress condition [-].

6. s_w: Soil moisture at permanent wilting point [-]. This parameter, as well as the previous, can be observed in the field. The search intervals are therefore based on field observations.

7. ϕ: Constant maximum recharge of baseflow reservoir ("deep flow") mm/h.

8. $t_{d,scal}$: Scaling parameter to increase the residence time of the deep baseflow reservoir with respect to ts, where the minimum of this parameter is 1. The overall residence time of water (and inherently of pesticides) - t_s and $t_{d,scal}$ - in the system influences the total amount of degraded matter and is therefore of major importance.

9. a_n: Degree-day melt factor [mm/°C/day]. Previous studies have shown that this parameter is very little sensitive, and it does not have to be calibrated with much precision. For this project, it has been fixed at 3 mm/°C/day.

10. θ_{cr}: Snowpack retention capacity [-]

11. cst_m: Constant winter melt at soil/snow interface, mm/day

12. $a_{ice,scal}$: Scaling parameter for ice degree-day factor (a_{ice}=a_n*$a_{ice,scal}$)

13. t_{ice}: Mean residence time in hours of glacier melt linear reservoir [h]

The ranges of each parameter are summarized in tables 3.1 [Imfeld, 2011]. The example parameter set is used for the general appreciation of the various variants tested during this project (see chapter 4.1 for results). This example parameter set is based on the parameters used for the Chamberonne catchment (after [Imfeld, 2011]), with minor adaptations based on visual exploration of the simulations.

	K_c	c	Zr	t_s	$s*$	Rs_w	ϕ	$t_{d,scal}$	SS	α
min	0.03	3.3	50	1	0.2	0.01	0	1	1	1
ex	100	9.72	1128	2	0.8	0.1	0.001	4	1	5
max	360	30	2000	250	0.8	0.99	20	2000	2	25

Table 3.1: Parameter ranges and example parameter set

3.1.3 Changes, adaptations and variants of the SEHR-model

During the project, several changes and additions to the SEHR model have been made. These include several bug-fixes, which can be found in the appendix as well as the implementation of initialized storages. Furthermore, some technical issues where resolved. Most importantly, the model has been adapted in order to improve its performance. These variants are then studied in further detail.

Initialization strategy

Previous versions initialized the reservoirs as empty, containing no water. As the available data for the Petite Chamberonne stretch only over 9 months, this poses a significant problem. Calibrations have shown that the reservoirs are filled during the first two to three months, depending on the specific parameter set. Only after the reservoirs have been filled, a response was produced. In order to minimize this problem, Bettina Schaefli implemented an initialization of the reservoirs that depends on the observed discharge. Running the model and discarding the first months in terms of simulated data is no option due to the fact that only 9 months of data are available. Therefore, the initialization strategy chosen is as follows: The soil moisture, s, is initialized as half its retention capacity

$$s_0 = s_w + \frac{s_1 - s_w}{2} \tag{3.9}$$

where s_0 is the initial soil moisture, s_w, the soil moisture wilting point and s_1 the soil moisture stress point. The subsurface reservoir, Ssub, is initialized as

$$S_{sub,0} = \frac{Q_{sub,0}}{k_{sub}} \tag{3.10}$$

where $S_{sub,0}$ is the initial subsurface reservoir storage, $Q_{sub,0}$ 10 % of the mean annual discharge and finally k_{sub} the sub-superficial discharge rate depending on the calibration parameter t_s. The deep storage is initialized in the same way as the subsurface storage.

However, it has to be noted that the simulations showed a much less important storage for both of the reservoirs than proposed by the above initialisation. Therefore, the initial storages for the catchment of the Petite Chamberonne have been fixed manually:

- initial soil moisture: 0.4
- initial subsurface storage: 0.5 mm
- initial deep storage: 0.5 mm

Changes in hydrological processes modelling

In order to improve the performance of the model, several different variations of the model are tested and calibrated. These variations include options that can be selected or deactivated and/or processes that are modelled using different equations. The variations namely include:

1. Snow module: inactive/active. During the calibration process, the snow module can be deactivated. This signifies that the equivalent precipitation is equal to the precipitation after interception. In other words, precipitation is not transformed into snow, and the snow reservoir is always empty.

2. Reservoir subsurface: linear/nonlinear. The empty function of the reservoirs in the original model is linear, as described in chapter 3.1.2. Changing the empty function to a non-linear equation allows a faster decline when the reservoir has a certain volume stored. The according (non-linear) equation is therefore:

$$Q_{sub} = K_{sat} * S_{sub}^{\alpha} \tag{3.11}$$

where α is equal to 2 in our case. If required, it could easily be made a calibration parameter.

3. Reservoirs: in series/parallel. In the original SEHR-module, the two subsurface reservoirs are in parallel. This signifies that the leaching water from the active soil layer is distributed amongst the two reservoirs. This can be changed, so that the reservoirs work in series. When they are in series, the subsurface reservoir aliments the deep reservoir (Fig. 3.10). In other words, the leaching water from the active soil layer is leached in one single reservoir.

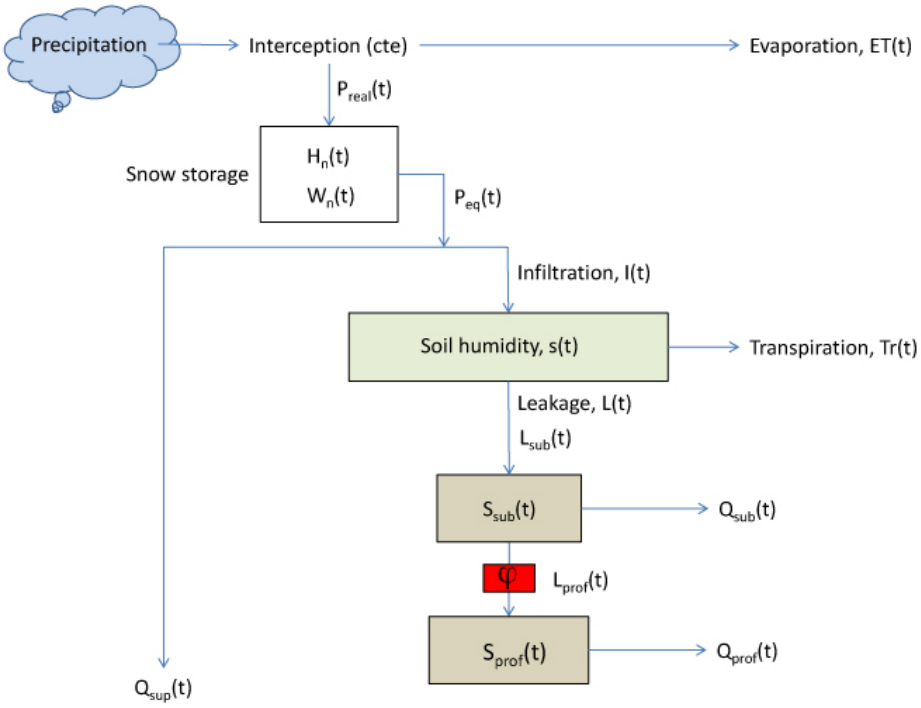

Figure 3.10: Conceptualisation of the workflow with reservoirs in series

4. Runoff: Horton/Dunne. Early in the calibration process, it has been re-

marked that the infiltration modelled with Dunne's equation (see section 3.1.2, equation 3.5) does not allow the fast responses that are observed in the data. In order to minimize this problem, it is tested whether Horton's equation improves the results. Horton's mode of surface runoff can be computed using

$$R_s = (1 - (\frac{s}{s_1})^{\alpha}) * P_{eq} \tag{3.12}$$

The major difference to Dunne's mode of surface runoff is that runoff is produced even before the soil is fully saturated. The infiltration calculated using Horton's equation depends however on the calibration parameter α. The influence of this parameter is shown in Fig. 3.11 below. It can be said that, the bigger α is, the closer we get to Dunne's mode of infiltration. For large α, the soil has to be close to be fully saturated before any runoff is produced.

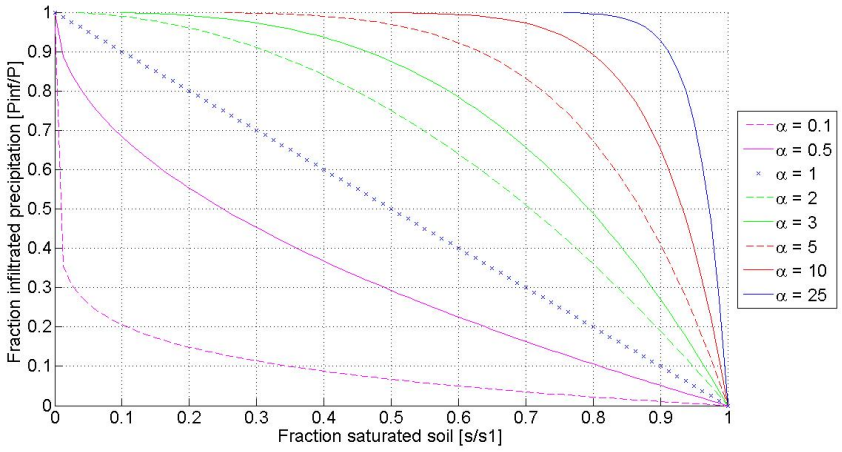

Figure 3.11: Influence of α on the fraction infiltration as a function of the fraction of soil saturation

At last, when combining all possibilities, a total of 2^4=16 different combinations are given. Each possible on/off choices will at first be compared with each other, in order to detect their influence on the simulation. This allows to group the combinations into families with similar behaviour, which then are commented and analysed in further detail (see section 4.1.5)

Change in overall workflow of SEHR-ECHO

The development of a pesticide transport module showed that it could be interesting to change the concept of SEHR-ECHO. Instead of having a single active soil layer, which is connected to two reservoirs, one could realise a model with two active soil layers each connected to its own reservoir (see Fig. 3.12 for conceptualisation). Each of the soil layers has furthermore its own soil humidity

with a distinguishable behaviour in time. The reservoirs correspond, as in the original SEHR-ECHO, to the response times of the layers.

The two soil layers each possesses a hydraulic conductivity which is specific to their response time. Using an additional parameter, RKc, the previous calibration parameter Kc is adjusted to the slow response using following equation:

$$RKc = \frac{K_{c,fast}}{K_{c,slow}} \tag{3.13}$$

This additional parameter has hence to be calibrated in the intervall [0,1].

The ϕ-method applies not on the level of the reservoirs, but before the soil layer. Previously, the ϕ-method distributed the leaching water amongst the two reservoirs. In the new version of the model, the ϕ-method distributes the equivalent rain, P_{eq}, amongst the two soil layers. The parameter ϕ can still be calibrated as before.

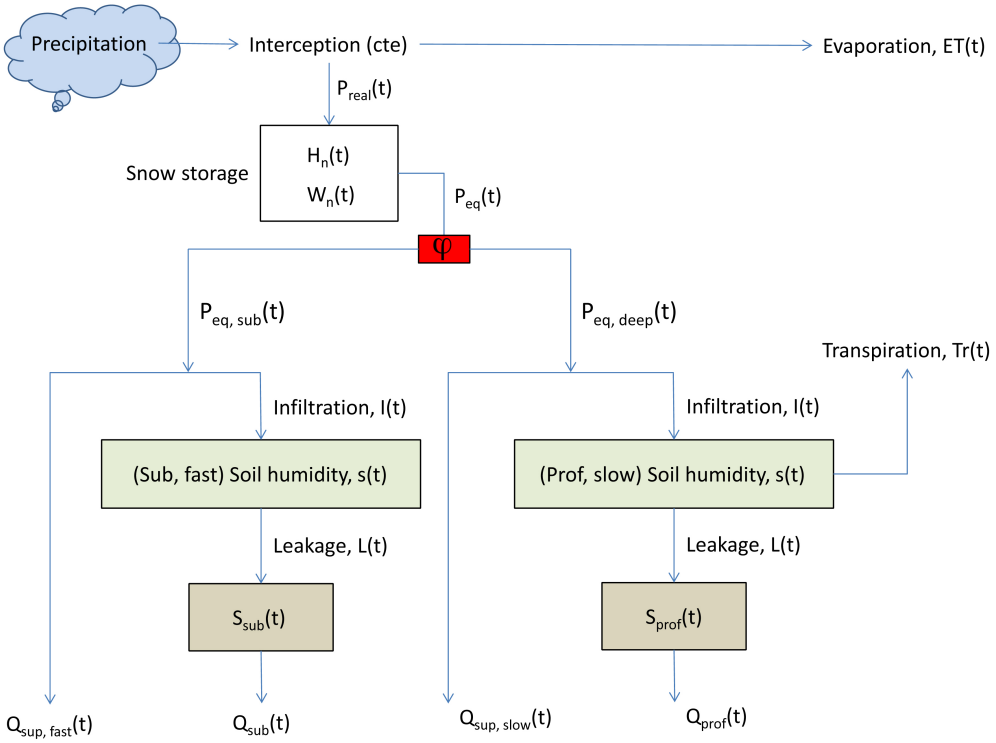

Figure 3.12: Conceptualisation of the new workflow of SEHR-ECHO

Technical issues

Several minor issues with SEHR-ECHO have been detected and resolved. These issues are global and apply to every new (and old) version of SEHR-ECHO.

- Changed the implementation of the parameters of soil moisture (s_w and $s*$). In previous versions, the soil moisture wilting point could be above the soil moisture stress point, when automatic optimizers are used for the

calibration of the two parameters. This is however physically impossible. The new version expresses the soil moisture wilting point as a ration of the stress point, where the ratio is between 0.01 and 0.99.

$$s_w = R_{sw} * s_1 \tag{3.14}$$

- In the original version of the model, the empty function and the update of the reservoirs have been done directly in the soil moisture module. It was therefore tedious to change these equations, especially when one wanted to change from a linear to a non-linear empty function for the two reservoirs. In order to facilitate the handling of these equations, two separate functions have been written (*emptyV02.m* and *stockupdateV02.m*, see appendix F). Furthermore, the calculation of the fluxes resulting from the soil layer as well as the storages is also done in newly written functions (*estSEHRfluxesV02.m*, appendix F.2 and *estSTOREflux.m*, appendix F.1). These functions can be used with any of the previously presented versions of the model.

- Lastly, the setup function of the model has been extended, in order to include the different options. Two model options can now be selected: having a linear or nonlinear response, having the reservoirs in series or in parallel and having Horton or Dunne infiltration. For explanations on the different options, see chapter 3.1.3.

3.2 Pesticide transport model

Pesticides transport models are, as mentioned in the introduction, clearly fewer in number than hydrological models. Some examples can still be given. One model used for modelling the fate of pesticides is SWAT (Soil and Water Assessment Tool), which couples the simulation of hydrological response and transport of pesticides using a spatially distributed, physically based approach [Neitsch et al., 2009]. Studies have been conducted in order to validate the predictions made by SWAT (e.g. [Larose et al., 2007]). The authors of said article state that the model predicts discharge adequately (NSE=0.5-0.7), and gives a satisfying prediction of monthly and daily trends in Atrazine concentrations.

For the present project, two types of models will be developed for the transport of pesticides. The first one is using the assumption of well-mixed reservoirs (section 3.2.2), whereas the second uses the principles of water age (section 3.2.3). These two model have not yet been calibrated, as no data are available to date. In order to explore the capabilities of the two different models and test the sensitivity to different parameters, they are compared against each other using three case studies (Section 4.2). Both models are using the SEHR-model for the hydrological modelling. All fluxes and storages of water are calculated by the SEHR-model.

3.2.1 Important points on pesticide transport modelling

In order to be able to model the transport of pesticides, one has to know their properties. Many properties can be considered important. A (non-exhaustive) list is given below:

- Solubility. The solubility determines the fraction of the total mass that is dissolved in water. Concerning pesticide transport modelling, the dissolved fraction corresponds to the mobile fraction, whereas the sorbed fraction will stick to particles and remain immobile.
- Soil partition coefficient, K_D. The partition coefficient is of similar use to the solubility. K_D represents the potential of adsorption of a given pesticide. Furthermore, K_D can be linked to the retardation of the pesticide in the soil, as proposed by [Wilson et al., 1990].
- Henry's law constant, K_H. This constant represents the volatility of the pesticide. The more volatile a given pesticide is, the bigger the losses to the atmosphere. The transport towards groundwaters is therefore diminished. It has to be expected that pesticides are mostly non-volatile.
- Half life, DT_{50}. The degradation of a chemical substance can be expressed in multiple ways, one of them being the half life. The half life is the time after which a substance has decreased by 50% in total mass. The half life is to be preferred over rate constants, as the half life can be linked to a specific environment, for example the active soil layer or deep groundwater. Furthermore, several studies exists that describe the half life of pesticides in various environments (see 4.2 for examples).
- Bioconcentration. This property, although of less importance for pesticide transport modelling, can be interesting to study. It represents the capability of the pesticide to accumulate and concentrate in biomass (such as fish, birds and ultimately humans). On the catchment scale, especially in the Petite Chamberonne, this property can however be neglected, as, for example, there are no fishes in the river.

For the models developed during this project, the partition coefficient K_D and the half life DT_{50} are used.

3.2.2 Simple model: Using completely-mixed assumption

The simple model uses the assumption that each reservoir, the soil layer as well as the surface crust are well mixed. In other words, the mass that enters a given reservoir is mixed with the total volume of water in the reservoir.

Pesticides are applied to a surface crust, where they are partitioned into a mobile and an immobile fraction. The mobile fraction can then be infiltrated into the soil layer, and flow towards the river with surface runoff. In the reservoirs, the mass is released according to the prevailing concentration and as a fraction

of the available stock of water. At last, the different contributions are summed up in order to result in a total concentration.

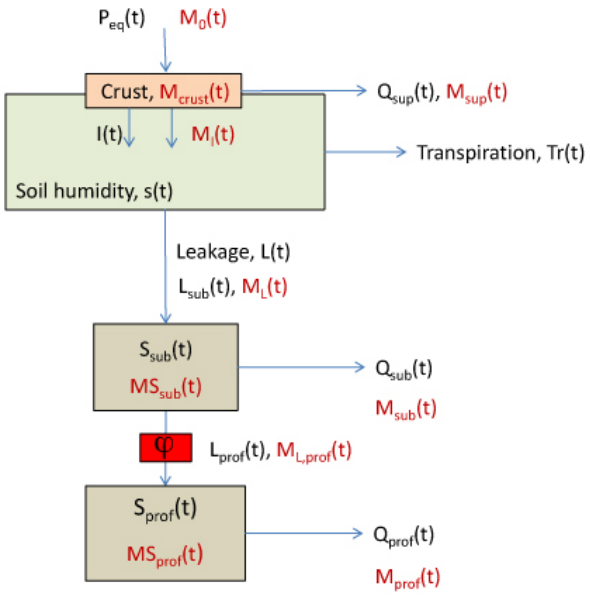

Figure 3.13: Workflow of the simple pesticide transport model in case of reservoirs in series (the workflow the model in case of parallel reservoir can be found in Appendix H, Fig. H.6)

Mathematical concept

A simple model for pesticide transport has been developed based on the previous work by Bertuzzo et al. [Bertuzzo et al., 2013]. In this article, the authors describe a simple model for the transport of pesticides at the catchment scale.

The simple model uses a surface crust onto which pesticides are applied. In this surface crust, the pesticide is partitioned into a mobile and immobile fraction. While the immobile fraction of the applied pesticides sticks to the soil particles, the remaining fraction dissolves into water. The partitioning is done using the partition coefficient K_D for the given pesticide, according to following equation:

$$M_{crust,dis}[kg] = \frac{M_{crust,tot}}{\phi * \frac{K_D}{\theta} + 1} \tag{3.15}$$

where ϕ is the mass of soil per total volume and θ the saturation of the crust. Assuming a fully saturated surface crust, θ equals 1.

Accordingly, the concentration of pesticide in the surface crust is as follows:

$$C_{crust,dis}[\frac{kg}{m^3}] = \frac{M_{crust,dis}}{d_{crust} * A * \theta} \tag{3.16}$$

where A is the total surface area for each subcatchment. The concentration is hence distributed and may differ for each subcatchment, according to the application of pesticides in each subcatchment. Here, the importance of the thickness of the surface crust, d_{crust}, is evident. This thickness influences directly the concentration of the pesticide, as it is used for the calculation of the total volume of water (V_{water}=d_{crust}*A). $C_{crust,dis}$ is used when water leaves the surface crust. Water may leave the surface crust in two ways: toward the soil layer with infiltration, or with surface runoff towards the river.

Infiltrated mass of pesticides is given as:

$$M_{inf}[kg] = C_{crust,dis} * Q_{inf} * A * \delta t \tag{3.17}$$

and the mass of pesticide in surface runoff as

$$QM_{sup}[kg] = C_{crust,dis} * Q_{sup,NR} \tag{3.18}$$

Pesticides undergo chemical degradation in the surface crust, which follows a first order chemical degradation with a degradation rate of k_{dis}.

Once the pesticides are infiltrated from the surface crust, they enter the soil layer. SEHR-ECHO calculates evaporation from the soil moisture. The fluxes infiltration, I, and leaching, L are therefore not equal. It is argued that the pesticides are very little volatile, and are therefore not lost with evaporation fluxes. Hence, the concentration increases in the active soil layer (as long as I=0 and Tr>0). However, it could be imagined that chemical degradation and uptake by plants play a major role in this layer. Therefore, a combination of the two degradation processes is introduced, and the total degraded mass in the soil layer is given as:

$$M_{deg,soil}[kg] = k_{deg,soil} * MS_{soil} * \delta t \tag{3.19}$$

where $k_{deg,soil}$ is the degradation rate [1/s] in the soil. This can be calibrated using the half life, which is the calibration parameter, of the substance:

$$k_{deg,soil}[\frac{1}{s}] = \frac{log(2)}{DT_{50} * 24 * 3600} \tag{3.20}$$

The mass leached is calculated based on the concentration in the soil layer. This time, the soil moisture is used, instead of having a fully saturated soil layer. The thickness of the active soil layer is given by the calibration parameter Zr [mm]. The concentration is given as:

$$C_{soil,dis}\frac{kg}{l}] = \frac{M_{soil,dis}}{Zr * s * A * \rho} \tag{3.21}$$

where ρ is the porosity of the soil layer and A the surface area of the catchment. As stated previously, the model uses the well-mixed assumption. This signifies that the total (mobile) mass in a given reservoir is dissolved in the total volume of available water in the reservoir. Here, the total amount of water is corresponding to $Zr*s*A*\rho$. It has to be noted that there is no fractioning in the soil layer, i.e. the mass remains entirely in the liquid phase.

The mass of pesticides leached towards the subsurface is then given as:

$$M_{leak}[kg] = C_{soil,dis} * L * 1000 * A * \delta t \tag{3.22}$$

The factor 1000 converts the leaching from mm/s to m/s.
With this, the remaining mass in the soil layer can be calculated:

$$MS_{soil}(t+1) = MS_{soil}(t) + M_{inf}(t) - M_{leak}(t) - M_{deg,soil}(t) \tag{3.23}$$

In the case of two reservoirs in parallel, the mass leached is split into two different fluxes, one into each reservoir. The split is done according the ϕ-method used for dividing the water fluxes into the deep and the subsurface reservoirs.

$$M_{leak,sub}[kg] = M_{leak}\frac{L_{sub}}{L} \tag{3.24}$$

and

$$M_{leak,prof}[kg] = M_{leak}\frac{L_{prof}}{L} \tag{3.25}$$

For two reservoirs in series, the leached mass from the soil layer is directly flowing into the subsurface reservoir. In both reservoirs, the pesticides are retained and leached towards the river according to following equations.

$$QM_{sub}[kg] = \frac{Q_{sub,NR} * MS_{sub}}{S_{sub} * A} \tag{3.26}$$

where $\check{M_{sub}}$ is the total mass of pesticides in the subsurface reservoir and S_{sub}*A the total volume of water in the subsurface reservoir. Again,it has to be noted that there is no immobile fraction in the subsurface reservoir, i.e. the totality of pesticides remain in the liquid fraction and are not adsorbed onto the soil. This is equal to a retardation factor of 1, i.e. the pesticides move at the same speed as the water. The pesticides undergo a chemical degradation, with a rate constant that can be different from the rate constant in the surface crust.

The remaining mass can therefore be calculated as (for reservoirs in parallel):

$$MS_{sub}(t+1) = MS_{sub}(t) + M_{leak}(t) - k_{deg,sub} * MS_{sub}(t) * \delta t - QM_{sub}(t) * \delta t \tag{3.27}$$

The same principles are used for the slow reservoir, with

$$QM_{prof}[\frac{kg}{s}] = \frac{Q_{prof,NR} * MS_{prof}}{S_{prof} * A} \tag{3.28}$$

Just as in the soil layer, no partitioning onto soil particles occurs in the reservoirs. Furthermore, the well-mixed assumption remains the same.

Lastly, the three mass fluxes towards the river are routed according to the river network. As the transport in the river can be assumed to be orders of magnitude faster than the transport trough the soil, the routing consists in a simple addition of the three contributing mass fluxes.

$$QM_{tot}[\frac{kg}{s}] = QM_{sup} + QM_{sub} + QM_{prof} \tag{3.29}$$

Numercial scheme

A simple explicit numerical implementation has been chosen. This allows to study the behaviour of the two different models during this early phase of the model development without loosing much time on the numerical implementation.

Algorithmic implementation

The model developed by Bertuzzo and al. has been written for Matlab. Several adaptations have been made in order to connect the transport model with the existing SEHR-model. The connection of the simple pesticide transport model with the SEHR-model is displayed in Fig. 3.13. The implementation of this conceptual model is done using three newly written Matlab functions. These Matlab functions can be easily adapted if necessary and are fully functional with the existing SEHR-model. As they are solely calculating the transport of pesticides, they require the fluxes and discharges calculated by the SEHR-model as inputs. They could also be directly included in the code of the SEHR-model, which reduces the number of auxiliary functions to be called. However, they could be adjusted with less ease, and changes to SEHR would have to be adapted accordingly.

1. *surface_pest.m:* In this function, the concept of the surface crust is retained. A given mass of pesticide is applied[2] onto the surface crust, where it is split into a mobile (dissolved) as well as an immobile (adsorbed) phase. This partitioning is done using the K_D of the specific pesticide. The K_D can be calibrated, if no viable values are available. The crusts thickness is currently fixed to 0.01 meter. This thickness is used to calculate the total volume of water in the surface crust, and therefore directly influencing the concentration of the pesticide in the water of the crust layer. The mobile fraction of the pesticide can be leached towards subsurface reservoirs and/or be washed off by surface runoff as it is done in the model by Bertuzzo and al. [Bertuzzo et al., 2013]. It is furthermore assumed that the surface crust is fully saturated at all times. This signifies that surface runoff (which is calculated using Dunne's model in the SEHR-model) has always the concentration of the mobile phase (hence the importance of the thickness of the surface crust). This shall reflect the importance of the first rainfalls after an application of pesticides. This importance has been pointed out by several studies (e.g. [Leu et al., 2004a]). Furthermore, the pesticide undergoes chemical degradation. This degradation is linked to a calibration parameter, $D_{50,crust}$, representing the half life of the given pesticide in the surface crust.

[2] As of now, the source is estimated based on the work of Stalder [Stalder, 2012], i.e. a file is created which reflects a time series of instantaneous application of one pesticide with a given mass in kg

2. *subsurface.m* The subsurface reservoir receives the leaching water from the surface crust. The infiltration (I) calculated by SEHR-ECHO is used as input, in addition to the concentration of pesticide calculated previously in the surface crust. In the subsurface reservoir, the pesticide is retained and leached towards the river based on the discharge of this specific reservoir. The pesticides undergo chemical degradation, with a half life $D_{50,subsurface}$ that may differ from the half life in the surface crust. This second half life can be calibrated separately from the previous one. Ultimately, the water released from the subsurface reservoir aliments the river directly and has the calculated concentration in pesticides. The deep reservoir is linked to the slow response of the hydrological model. In the transport of pesticides, this reservoir can have multiple behaviours/significations. Firstly, it could act as a sink for pesticides. This could be achieved using a very rapid degradation of the substance in this reservoir. Although this is physically not correct, it prevents the introduction of an additional parameter (that would represent the rate at which pesticides are released from the reservoir). Secondly, the deep reservoir could act as a source of pesticides; in the case of Atrazine, for example, it can be expected that some leftover mass is still present in the environment. The application of Atrazine is prohibited in Switzerland since summer 2011, but remaining Atrazine may be leaching towards rivers and groundwaters. This process could be modelled using an initial mass (that could be calibrated or known) and a leaching factor.

3. *pest_ norouting.m* The previous two functions calculate the transport of pesticides per subcatchment of the study area. The resulting mass flows have to be routed, in order to get a total mass flow at the control section. This is done using the same principles as used in SEHR, which is using no routing at all. The mass flows are simply added up in order to get the total mass flow. This may seem simplistic, but the residence times of pesticides in the river channel are negligibly small compared to the residence times in the subsurface storages. The routing function can be easily adapted if there is any need to do so.

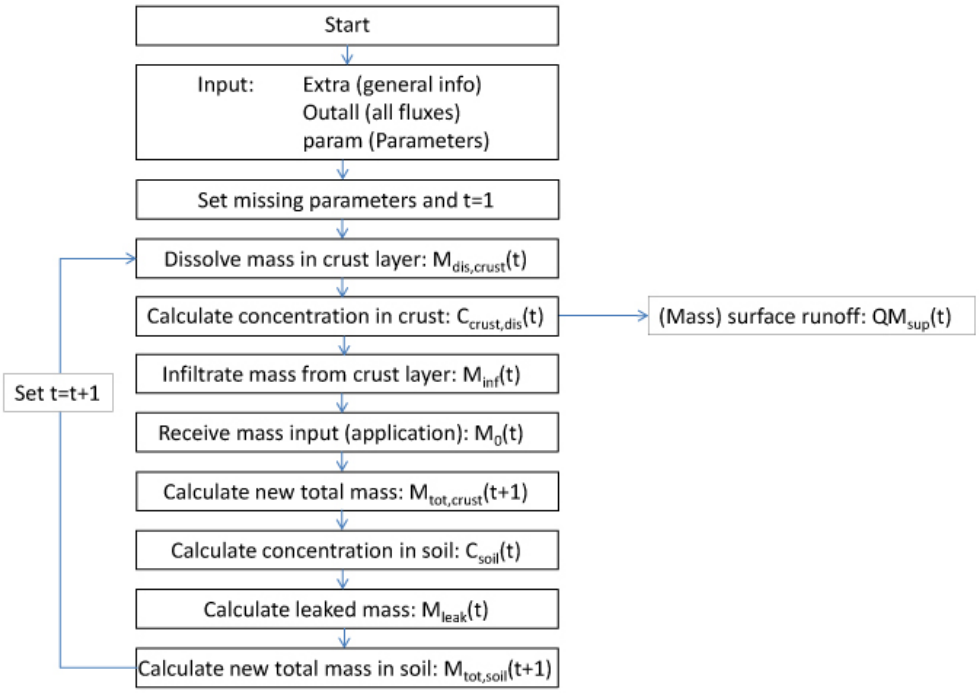

Figure 3.14: Workflow of the surface crust module

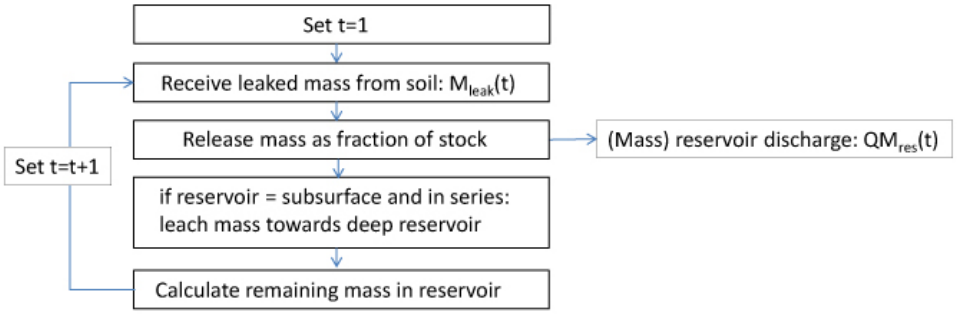

Figure 3.15: Workflow of the reservoirs modules

3.2.3 Complex model: Using water age

Mathematical concept

The opposite of the assumption of having completely mixed reservoirs is having a plug-flow reservoir. This signifies that the mass is not mixed in the total volume of the specific reservoir, but only within the volume of water that entered at the same time as the mass. The water leaving the reservoir therefore corresponds to the oldest water in the reservoir. Accordingly, mass is taken that has entered the reservoir at the same time as the water that has to be removed. When a fraction

of a given water parcel is removed, the corresponding fraction of the total mass is removed:

$$M_{out} = M_{tot} \frac{V_{w,out}}{V_{w,tot}} \tag{3.30}$$

The concept of the mobile and immobile fractions of mass are hence not retained. Apart from the change in this routing within a reservoir, the mathematics remain the same as for the simple model. Degradation and volatilization (if any) occur at the reservoir step for each parcel of mass as previously. The numerical scheme for the complex model is also the same as the simple model, using an explicit numerical implementation.

Algorithmic implementation

The major change is how to track the water age along the simulation. The computation of the water age is done using a new function (*wateragetimeV01.m*, see appendix F.3). Fig. 3.16 illustrates the concept behind the implementation.

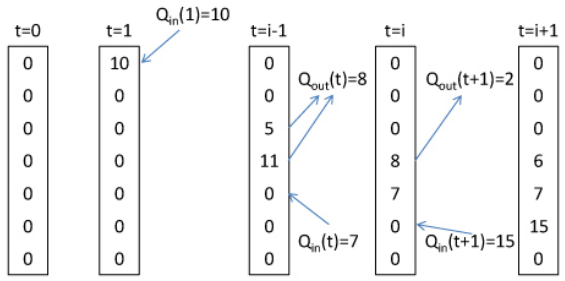

Figure 3.16: Numerical example of the implementation of the water age

At first, the volume flowing into the reservoir is stored at position i=t. The oldest water leaves the reservoir first, hence in order to compute the new water age vector, one has to remove water from the top (at first position where there is water). Both leaching and evaporation is taken from the oldest water. The uptake of pesticides in the evapotranspirational fluxes can be adjusted according to the volatilization of the pesticide. During this project, this volatilization is equal to zero. Evapotranspiration therefore concentrates the pesticides. Once the first position is emptied, the next can be emptied and so on.

Accordingly, pesticide mass is kept track of in a separate vector. Incoming mass is stored at i=t, and outgoing mass is computed according to the positions where water is leaving the reservoir.

3.3 Calibration process

The calibration of the parameters described in section 3.1.2 is done automatically using different external optimizers. The goal of this operation is to achieve a

close match between the observed and the simulated discharge, by adapting the parameters accordingly. The simulation should in other words be both precise and accurate. The first one signifies that the simulated and observed values are close, whereas the second signifies a low variability. During this project, only hydrological data has been available. Therefore, the pesticide transport models will not be calibrated, as measurements of concentrations are not yet available.

3.3.1 External optimizers

Three different algorithms have been used during the optimization procedure. These are the shuffled complex evolution metropolis (SCE [Duan et al., 1992], and as an optimized version SCEM [Vrugt et al., 2003]) as well as the differential evolution adaptive metropolis (DREAM) method [Vrugt et al., 2009].

SCE The shuffled complex evolution algorithm uses multiple chains in order to find the global optimum of the possible parameter sets. To do so, each chain starts at a random location in the feasible space of parameters and evolves towards an optimum; in order to not only find local optima, the chains share information (by mixing the population), so that each chain tends towards the global optimum [Duan et al., 1992].

SCEM The SCEM-UA algorithm is an optimized version of the SCE. The authors point out the importance of the shape and size of the proposal distribution (whether a new point is accepted as being better or not), and the influence of this distribution on the speed of conversion. They also state that the previously developed SCE algorithm posses a small chance to tend towards a local optimum. In order to prevent this from happening, the SCEM-UA algorithm uses a metropolis annealing covariance based offspring approach [Vrugt et al., 2003]. A second change to the original algorithm should prevent that the search is terminated in a localised optimum. This furthermore allows to know the a posteriori distribution of the parameters.

DREAM The DREAM algorithm also uses multiple Markov Chains. However, the shape and orientation of the proposal distribution can be adapted at each step. This increases the diversity in candidate points, which ultimately renders the algorithm more efficient and effective that the previously mentioned algorithms. Furthermore, outliers in the proposal candidates are removed in order to have a faster convergence [Vrugt et al., 2009].

3.3.2 Performance criteria

Each simulation has to be evaluated on how well it matches the observation data. This evaluation is done using different performance criteria. Various performance criteria exist, each with their respective advantage and disadvantages. An overview of several criteria is given by Reusser et al. [Reusser et al., 2009].

Common criteria are the sum of square error (SSE), the coefficient of determination (r^2), and the root mean square error ($RSME$), which are explained in more detail in appendix B.

For hydrological models however, the performance criteria called *Nash-Suttcliffe efficiency, NSE* is often used [Nash and Sutcliffe, 1970]. This criteria indicates the goodness of fit by comparing the simulation to the mean of the observation:

$$NSE = 1 - \frac{\sum_{i=1}^{t}(Q_{obs}^{i} - Q_{sim}^{i})^2}{\sum_{i=1}^{t}(Q_{obs}^{i} - \overline{Q_{obs}})^2} \tag{3.31}$$

where Q_{obs} is the observation and Q_{sim} the corresponding simulated value. The NSE can range from -∞ to 1, where 1 is a perfect match. Values bigger than 0 can be expected to be acceptable simulations, although 0 signifies that the mean is an equally good prediction as the simulation. For values below 0, the mean of the observation is a better prediction than the actual simulation. Furthermore, the Nash log can be used, which is calculated using the logarithmic values of the observation and simulation:

$$NSElog = 1 - \frac{\sum_{i=1}^{t}(log(Q_{obs}^{i}) - log(Q_{sim}^{i}))^2}{\sum_{i=1}^{t}(log(Q_{obs}^{i}) - \overline{log(Q_{obs})})^2} \tag{3.32}$$

This criteria reduces the sensibility to extreme values. In other words, taking the logarithm reduces the peaks, whereas low flows remain more or less at the same level. This increases the influence of the low flow levels, which allows to detect a constant model over- or underestimation [Krause et al., 2005].

Lastly, the bias of the simulation is calculated using

$$bias(\%) = \frac{\sum_{i=1}^{t}(Q_{sim}^{i} - Q_{obs}^{i})}{\sum_{i=1}^{t} Q_{obs}} * 100 \tag{3.33}$$

The bias also allows to detect a constant model over- or underestimation. The closer the bias to 0, the lesser it is over- or underestimated. Values below zero indicate an underestimation, whereas values above zero indicate an overestimation.

Altogether, these performance criteria indicate a goodness of fit for the complete simulation period, it is a global appreciation of the simulation. High NSE values can therefore represent a bad simulation at a small scale, whereas lower values could be representing a more useful simulation. This issue has been discussed by various authors (e.g. [Jain and Sudheer, 2008]). The behaviour and fit at a small scale is often not strongly influencing the chosen performance criterion. As the calibration period for the Petite Chamberonne covers only 9 months, single precipitation events however play an important role in the simulation. The

NSE cannot indicate the goodness of fit for these single events. In order to encounter this issue, visual observation and evaluation of the simulations have been done. This observation has been facilitated by using a newly written function that allows to plot all the different output variables of SEHR-ECHO (on DVD).

3.3.3 Parameters to be calibrated

Finally, not all of the parameters of the model have to be calibrated. Several parameters may be known or have only little impact on the result. Especially snow parameter, which are of lesser importance for this catchment due to it short winter period, can be fixed before calibration. Fixing several parameters, the number of remaining parameters that have to be calibrated is decreased and the calibration process accelerated.

Following parameters are hence not required:

1. c_{stm}: constant winter melt at soil/snow interface, mm/day
2. $a_{ice,scal}$: scaling parameter for ice degree-day factor (aice=an*aicescal)
3. t_{ice}: mean residence time in hours of glacier melt linear reservoir [h]
4. spatial variance of liq. snow water content, Wn, mm^2

Following parameters are fixed:

1. a_n, the degree-day melt factor, fixed at 3 mm/°C/day
2. θ_{cr}, snowpack retention capacity, fixed at 0.01

This leaves hydrology parameters to be calibrated, as follows:

1. Kc, in a range of [0.03 to 360] mm/h
2. c, [3.3 to 30]
3. Zr, [50 to 2000] mm
4. t_s, [1 to 250] h
5. $s*$, [0.2 to 0.8]
6. R_{sw}, [0.01 to 0.99] (in previous versions calibrated as s_w)
7. ϕ, [0 to 20] mm/h
8. $t_{d,scal}$, [1 to 2000] h

The two newly introduced parameters will also be calibrated:

1. SS, [1 to 2]. This represents a surface scaling parameter, that allows to increase the area of the subcatchment. This reduces issues linked to uncertainty in the delimitation of the subcatchement.
2. α, [1 to 25], the exponent of the Horton's mode of infiltration.

3.3.4 Calibration period

the calibration period corresponds to the longest available data time series. Discharge data measurements have started only on the 01-May-2012. The data have been gathered and made available on the first of February 2013. Therefore, the calibration is done using this period (01-May-2012 to 01-Feb-2013, 9 months). As has been shown in a previous study [Stalder, 2012], the main application of pesticides are taking placing during the month of April of each year. The application of pesticides and the respective transport can therefore only be studied qualitatively.

Chapter 4

Results

4.1 Results of the hydrological simulations

N°	Infiltration	Reservoir setup	Reservoir empty-fct	Snow module	Calibration	NSE
1	Horton	parallel	linear	on	SCE	0.59
2	Horton	parallel	linear	off		
3	Horton	parallel	non-linear	on	SCE	-2.14
4	Horton	parallel	non-linear	off		
5	Horton	series	linear	on	SCE	0.71
6	Horton	series	linear	off	SCE	0.77
7	Horton	series	non-linear	on	SCE	0.14
8	Horton	series	non-linear	off	SCE	0.70
9	Dunne	parallel	linear	on		
10	Dunne	parallel	linear	off		
11	Dunne	parallel	non-linear	on	SCE	-1.87
12	Dunne	parallel	non-linear	off		
13	Dunne	series	linear	on	SCE	0.70
14	Dunne	series	linear	off		
15	Dunne	series	non-linear	on		
16	Dunne	series	non-linear	off		

Table 4.1: Summary of all combinations. NSE is indicated for the calibrated combinations

In order to explore the different combinations mentioned in section 3.1.3, each of the four on/off options is evaluated with a standard set of parameters (which is not changed between simulations, see table 3.1). Based on this first comparison, a selection of combinations is calibrated using an automatic optimizer (section 4.1.5). Table 4.1 shows the numbering of every possible combination. The Nash-Sutcliffe efficiency reported in table 4.1 above is the result of the calibration procedure using the mentioned optimizer. A complete list of the different cali-

bration runs and with more performance indicators can be found in the appendix I.

4.1.1 Comparison: Snow module on/off

Deactivating the snow module is by far the simplest change to the SEHR model; instead of calculating an equivalent precipitation and a corresponding snow height, it can be assumed that there is no formation of snow and that all of the precipitation is in liquid form. In other words, precipitation is always directly corresponding to the equivalent precipitation[1]. On the other hand, with the snow module activated, a certain amount of precipitation is retained and released only after melting occurs. A shift in discharge can therefore be expected. The results shown below are simulations correspondingly with and without snow, using Horton's equation for infiltration as well as parallel and linear subsurface reservoirs (corresponding to N° 1 and 2). Fig. 4.1 shows a zoom on the period where significant changes can be observed. A figure of the complete simulated period can be found in appendix F.4.

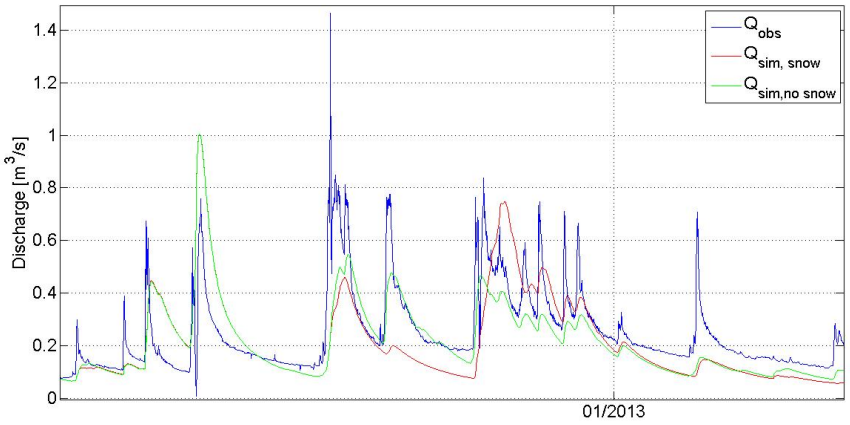

Figure 4.1: Result 1, snow on and off. With snow, the discharge is smaller during the first days of December, and bigger for the weeks thereafter.

Using the standard parameter set, the simulation is visually better when the snow is deactivated. It can be argued that the transformation of snow is done too quickly and too much snow is produced. Looking at the snow storage, a maximum height of roughly 60 mm is achieved by the end of December 2012 (see Fig. 4.2). This seems a lot, especially in Lausanne. However, it has to be pointed out that the winter 2012/2013 happened to be a winter where it snowed abundantly. It is however questionable whether 60 mm where achieved.

[1]The code for this operation can be found in appendix F.4

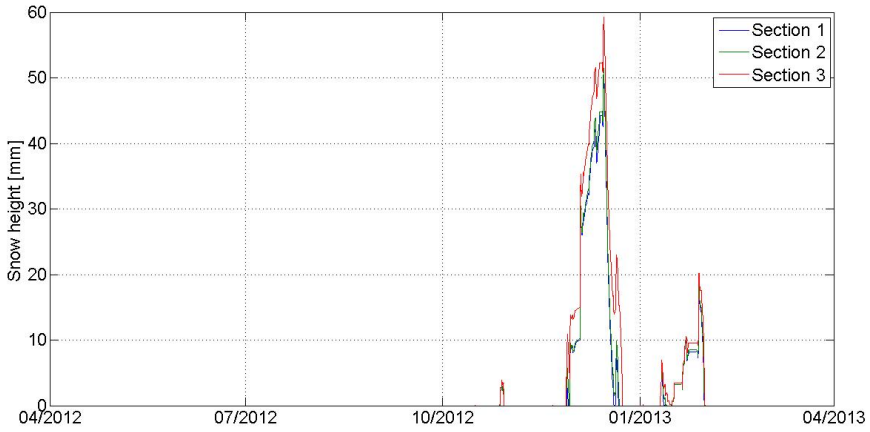

Figure 4.2: Snow storage corresponding to result 1

Snow module	NSE	Nash log	Nash bias
On	0.5109	0.6361	-0.0655
Off	0.6224	0.7104	-0.0531

Table 4.2: Performance statistics of snow module comparison

4.1.2 Comparison: Linear or non-linear empty-function

The second step consists in adapting the empty function of the reservoirs as described previously. When the empty function is made non-linear, the given reservoir can empty quicker when it has a big storage and slower when there is little storage. This should allow to simulate the fast recession after a rainfall event as observed in the data. The figure below shows the two simulations, using Horton infiltration, an active snow module and parallel reservoirs, plotted with the observed discharge. In order to be able to distinguish the two simulations, this figure shows a zoom on two rainfall events. The complete figure can be found in appendix H.2. Furthermore, the standard parameter set has been used for both simulations.

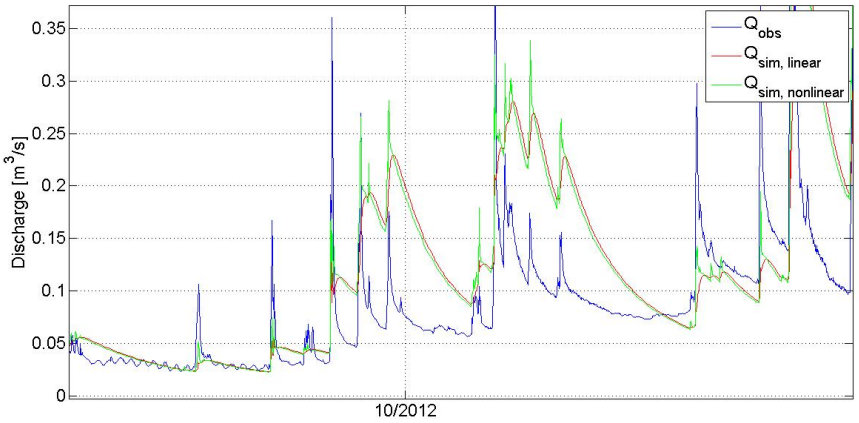

Figure 4.3: Results 2, linear or non-linear empty function. Only minor differences for the two simulations can be observed.

The difference between the two simulations is smaller than expected. Only at the peaks, the behaviour of the two simulations differs. This is mainly due to the storage in each reservoir, which influences directly the subsurface and deep discharge respectively. When exploring the storage over time, it first of all can be observed to be very small. Therefore, the corresponding flux will be equally small, and changing the empty function does not change drastically the simulated discharge. It can also be observed that the sum of both storages is similar in both (linear and non-linear) cases.

Computing the performance statistics, a minor difference can be observed. It seems that the linear empty function has a minor advantage over the non-linear function. The difference being only little, it will have to be explored when each combination is calibrated.

Empty-fct	NSE	Nash log	Nash bias
Linear	0.5109	0.6361	-0.0655
Non-linear	0.5066	0.6373	-0.0658

Table 4.3: Performance statistics for the modes of the empty function

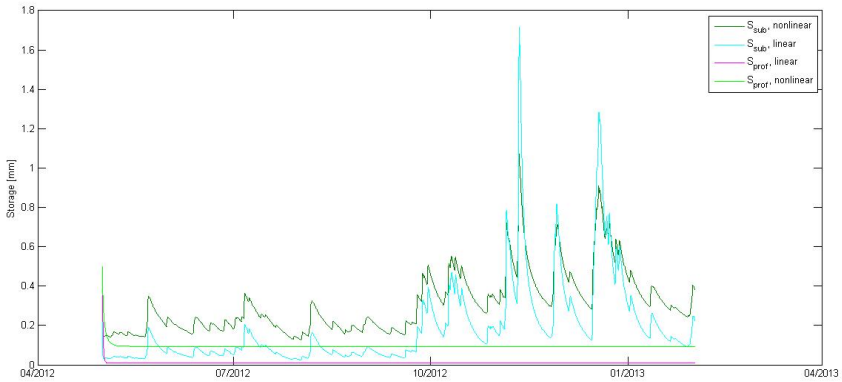

Figure 4.4: The storage in each reservoir, with corresponding linear or non-linear empty functions.

4.1.3 Comparison: Reservoirs in parallel or series

As explained previously, the disposition of the reservoirs can be changed. From the original state, where the two reservoirs are in parallel, it can be changed in order to have them in series. The upper storage leaches then into the deeper reservoir. This adaptation can change the behaviour of the two reservoirs.

Using the standard parameter set, there is no difference between the two simulated discharges. The storages of the two reservoirs show the same behaviour for both simulations. This is also confirmed when the performance statistics are computed.

Reservoir setup	NSE	Nash log	Nash bias
Series	0.5109	0.6361	-0.0655
Parallel	0.5099	0.6343	-0.0653

Table 4.4: Performance statistics with two different reservoir dispositions

This finding is justified, as the parameter ϕ removes a constant fraction of the leaching water and deviates it towards the deep, slow reservoir. Whether this is done before or during the emptying of the subsurface reservoir does not matter, as long as it is independent of the storage in the subsurface reservoir. Different results are to be expected with the calibration, when the parameters are adjusted to the specific setup of the reservoirs.

4.1.4 Comparison: Mode of infiltration

The mode of infiltration seems to be of major importance. In the original version of the model, Dunne's equation has been used. With this mode, runoff starts only after the soil has been saturated completely. In other words, the first water of a precipitation event does infiltrate and produce no run-off at all. This is

a clear disadvantage; precipitation events lead to immediate responses, as has been observed previously. A more direct runoff-generation function is given by Horton's equation. Using this mode, runoff is always produced, even when the soil is not fully saturated. With the exponent α, which can be calibrated, the threshold can be adjusted according to the models requirements.

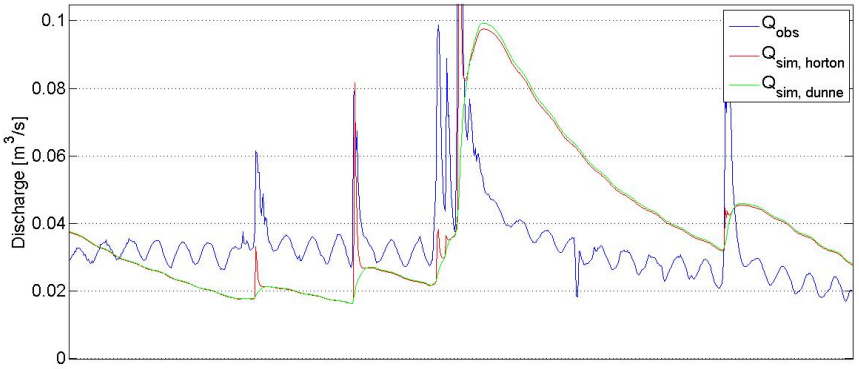

Figure 4.5: Result 4: Difference in simulations using Horton or Dunne for the calculation of the infiltration. A direct response to the forcing can be observed for Horton's mode.

Using the standard parameter set, the total differences are only small. When examining single events, the different behaviours of the two modes become evident. As predicted, Horton's mode produces a immediate response to a rainfall event, whereas Dunne's mode lags behind the event. When we compare the two simulations with the observation, it furthermore shows that the observation is modelled more precisely using Horton's equation. The performance statistics confirm this finding. While the simulation using Dunne shows a poor fit, it is improved by singly changing the mode of infiltration.

Infiltration	NSE	Nash log	Nash bias
Dunne	0.4616	0.5876	-0.0687
Horton	0.5109	0.6361	-0.0655

Table 4.5: Performance statistics with two different infiltration modes

4.1.5 Calibration of SEHR-ECHO

Every combination is calibrated using an automatic optimizer. Here, a short comment on each resulting parameter set is given. Based on these results, the best variant of SEHR-ECHO will be selected. As the previous comparison shows, the two possibilities of having snow or no snow as well as a linear or a non-linear empty function do not influence drastically the result of the simulation. Furthermore, due to the time-consuming process of the calibration, only a selection of

combinations have been calibrated. Therefore, groups of similar combinations have been made and commented together. These groups are the following:

1. Horton runoff and parallel reservoirs
2. Horton runoff and reservoirs in series
3. Dunne runoff

N° 1 - 4: Horton runoff and parallel reservoirs

N°	Kc	c	Zr	t_s	$s*$	R_{sw}	ϕ	$t_{d,scal}$	SS	α
1	358.93	13.84	89.68	6.63	0.32	0.50	14.07	106.43	1.23	14.93
3	358.93	13.84	89.68	6.63	0.32	0.50	14.07	106.43	1.23	14.93

Table 4.6: Parameters after calibration for combinations N°1 and 3

N°	NSE	NSE log	NSE bias	Global error	Issues
1	0.59	0.71	0.04	0.63%	no convergence
3	-2.14	-1.53	0.14	0.56%	no convergence

Table 4.7: Performance criteria of combinations with Horton runoff and parallel reservoirs

It has been observed that combinations with reservoirs in series perform better, and furthermore that the deactivation of the snow module is not necessary or even advised. Therefore, for this group, only N°1 and N°3 have been calibrated. It has to be noted that no convergence has been achieved, and that the two calibrations resulted in the same parameter set.

The linear (standard) empty function results in a simulation of medium quality, with a NSE of 0.59. The simulation fits small discharges better, which is pointed out by the nash log being higher (0.71). On the other hand, the non-linear empty function, with the same parameter set, overestimates drastically the peak discharges during summer and winter. Interestingly, the discharge is mainly composed of deep discharge, without any superficial flow. This finding can be linked to the high deep storage (initialized at 40m), which leads to a high deep discharge. The subsurface storage receives only 3 impulses of water over the whole calibration period (see Appendix H Fig. H.4). This is due to the high calibration parameter ϕ, which attributes almost all leaching water to the deep storage. The same observation can be made for the linear empty function.

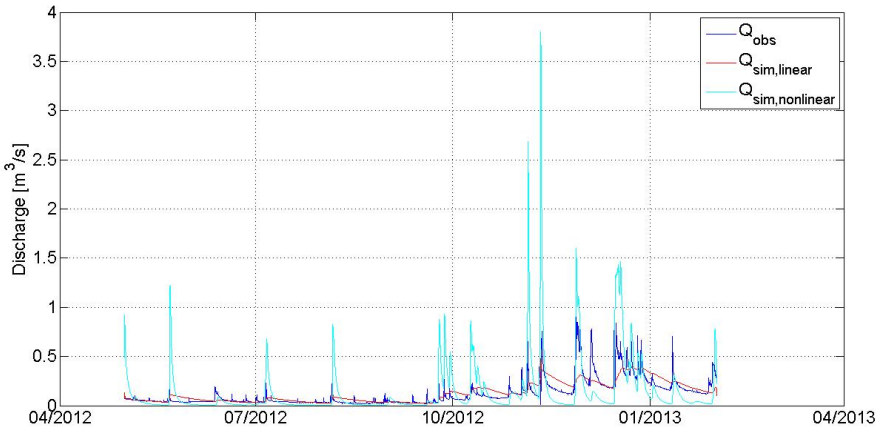

Figure 4.6: Simulated discharge for N°1 and 3. The nonlinear response function overestimates the peaks after a rainfall event. In both cases, the majority of the discharge is constituted of the deep discharge.

A calibration using DREAM has been evaluated. The algorithm did not converge; the parameters are therefore not as one could expect normally distributed around the best fitting parameter (see Fig. H.5, Appendix H). It can however be observed that the response times of both reservoirs tend to be as small as possible, which is consistent with the previously made observations. The scaling paramater SS is however estimated to be higher (1.69). As no convergence has been achieved, the a posteriori distribution showed in figure H.5 is questionable.

N°5 - 8: Horton runoff and reservoirs in series

N°	Kc	c	Zr	t_s	$s*$	R_{sw}	ϕ	$t_{d,scal}$	SS	α
5	257.37	13.95	1035.70	3.01	0.58	0.38	8.67	488.97	1.40	4.57
6	359.94	14.37	1305.90	1.91	0.55	0.45	5.48	991.50	1.48	4.66
7	334.42	21.52	115.83	66.90	0.67	0.01	14.97	1997.10	1.24	5.91
8	333.95	21.37	115.17	62.19	0.50	0.34	5.16	1984.90	1.26	6.52

Table 4.8: Parameters after calibration for combinations N°5 - 8

N°	NSE	NSE log	NSE bias	Global error	Issues
5	0.71	0.84	-0.03	0.51%	S_{sub} is negative (@t=1)
6	0.77	0.82	-0.03	0.53%	S_{sub} is negative (@t=1,2)
7	0.65	0.42	-0.65%	0.76%	S_{sub} is negative (@t=1)
8	0.70	0.46	-0.05	0.69%	

Table 4.9: Performance criteria of combinations with Horton runoff and reservoirs in series

N° 5 and N° 6 can be clearly distinguished from N° 7 and N° 8 when looking at the two parameters Zr and $t_{d,scal}$. Zr takes medium values for combinations using a linear empty function, opposed to the values at the lower level for the nonlinear empty function. This seems to be counterbalanced by the second parameter, $t_{d,scal}$. Additionally, combinations 7 and 8 seem to balance the very thin active soil layer with a larger residence time in the subsurface reservoir and a bigger volume that can be stored in the soil layer.

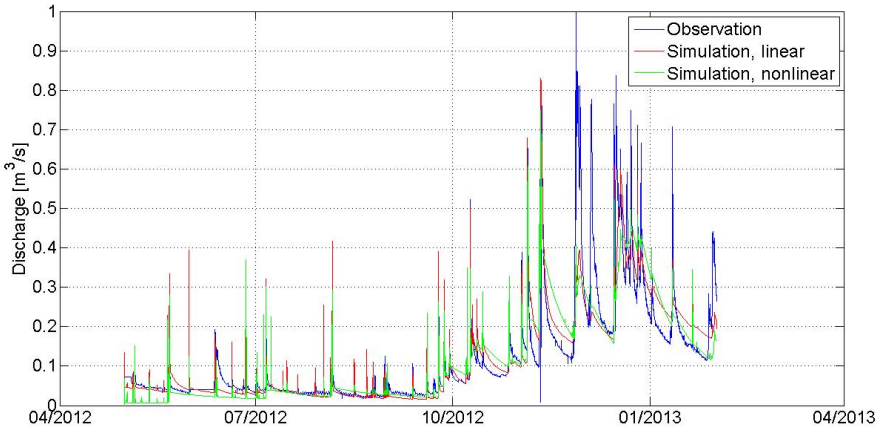

Figure 4.7: Discharge simulation (N° 5 and 7). With a nonlinear empty function, a faster, but less accurate decline after peaks can be observed.

Furthermore, small discharges are simulated more precisely using a linear empty function, as is confirmed by the nash log. In the case of a linear empty function, the discharge is composed of the three different discharges. The deep reservoir delivers a seasonal baseflow (high during winter, low during summer), whereas the subsurface reservoir is responsible for the recession after a peak. The peak itself is mostly due to surface runoff. In contrast to this observation, the discharge of combinations with nonlinear empty functions is composed mainly of deep reservoir discharge, with several minor peaks from the subsurface reservoir and superficial flow. The subsurface reservoir does not at all act in the same way as in the previous case, which is physically unreasonable.

N°9 - 16: Dunne runoff

N°	Kc	c	Zr	t_s	$s*$	R_{sw}	ϕ	$t_{d,scal}$	SS	α
11	358.99	23.74	124.79	18.17	0.41	0.84	9.02	47.95	1.29	2.51
13	2.20	3.33	187.38	4.46	0.20	0.06	12.68	370.83	1.42	12.83

Table 4.10: Parameters after calibration for combinations N°11 and 13

N°	NSE	NSE log	NSE bias	Global error	Issues
11	-1.87	-1.93	0.12	0.58%	no convergence Q_{sup}=0
13	0.70	0.83	0.02	0.57%	no convergence Q_{sup}=0

Table 4.11: Performance criteria of combinations with Dunne's mechanism runoff

For Dunne's mechanism of surface runoff, only two calibrations have been made. Both confirm the observation made in the initial stage; the major issue of the simulations are the surface runoff which cannot be represented correctly. In both cases (N° 11 and N° 13), no surface runoff is produced at all. The discharge is simulated with an adequate precision for N° 13, but without any surface runoff. The residence time in the subsurface reservoir is small (t_s=4h), and a thin active soil layer. This allows the fast response to rainfall, and the peaks can - even without surface runoff - be simulated correctly. N°11 furthermore overestimates the peaks after rainfalls and has thus a very poor NSE (worse than mean).

It has however to be noted that no convergence has been achieved for the two calibrations. It could therefore be that when one repeats the operation, other results are obtained - to the better or worse. All in all, if a simulation shows that one flux is zero, such as surface runoff in this case, one should reject the parameter set.

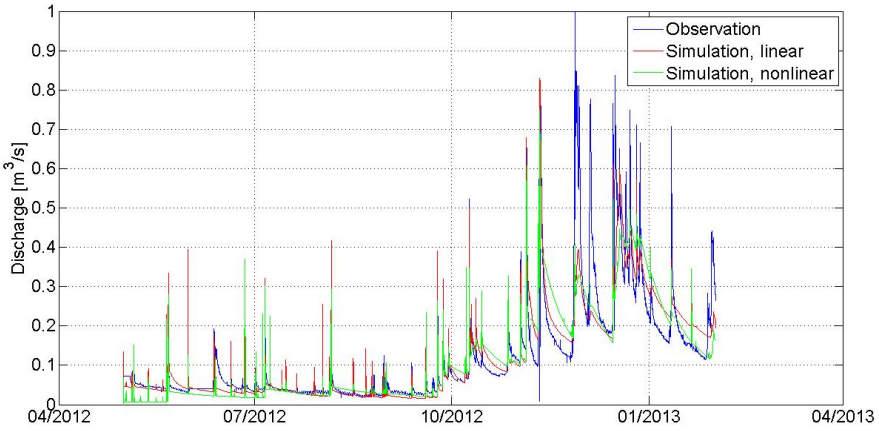

Figure 4.8: Discharge simulation (N° 11 and N° 13) with Dunne's mechanism.

4.1.6 New workflow

The new workflow has been calibrated several times, but no convergence has been achieved. Ultimately, the standard parameter set resulted in better results than any of the calibrations. A Monte-Carlo simulation was launched but only 7500 simulations could be evaluated in 14 hours, and the operation has been aborted. Using the standard parameter set, and an additional parameter RL_c=0.5, follow-

ing results are obtained.

NSE	NSE log	NSE bias	Global error	Issues
0.58	0.74	-0.09	0.12	0.46%

Table 4.12: Performance criteria of the new workflow, using the standard parameter set

The simulation fits the observation adequately, even without calibration of the parameters. The general behaviour of the simulation is also adequate. Especially during the winter, the simulation reflects the observation very well. The recession after peaks is modelled at a correct rate of decay. During the summer, the simulation fits less the observation than during winter. Especially high peaks during summer are underestimated.

The discharge is composed of all three discharges 4.10. During winter, the deep discharge dictates the order of magnitude and especially the peaks of discharge. As the reservoir is almost empty during summer, the deep discharge cannot contribute to peaks during the summer, which is consistent with the previous observation. The deep reservoir is hence not acting as the slow response using this parameter set, and releases the leaching water directly to the river.

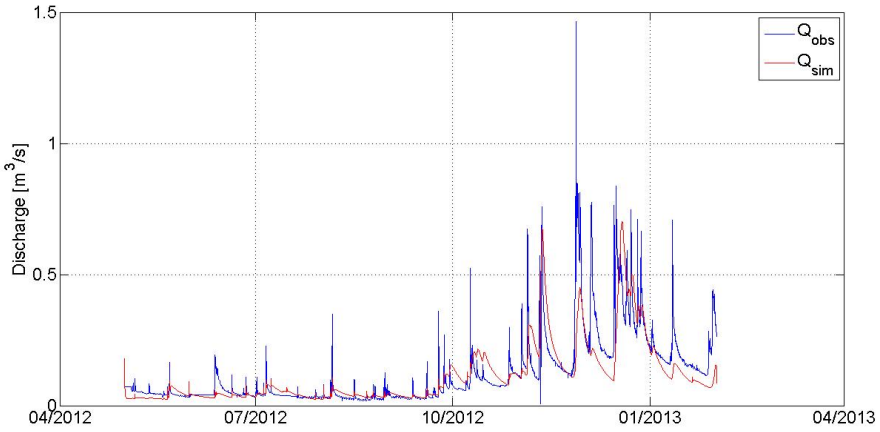

Figure 4.9: Discharge simulation of the new workflow, using the standard parameter set

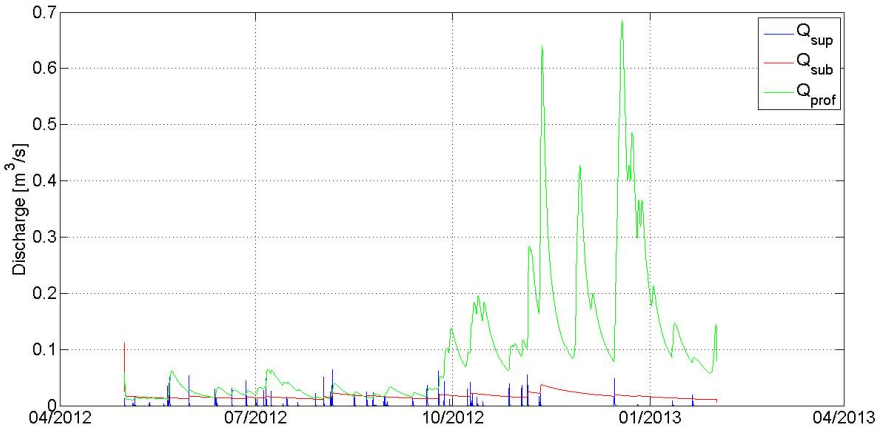

Figure 4.10: Contribution of each reservoir and superficial flow to the total discharge

4.1.7 Application of the Aabach-Model

In order to evaluate the global performance of SEHR-ECHO, another hydrological model has been applied to the catchment of the Petite Chamberonne. The model used for this comparison is the model developed by Bertuzzo et al. [Bertuzzo et al., 2013] for the catchment of the Aabach. The lumped, conceptual model is using an explicit numerical scheme and no surface runoff nor routing along the network for the discharge simulation (see Appendix G for a more detailed explanation). Using a Monte-Carlo simulation (150'000 simulations, 9 parameters), the best fit for the model was found to be 0.62. This could likely be improved using more simulations. The simulation represents the discharge using only the subsurface and deep reservoir, i.e. it lacks overland flow. For pesticide transport, it has been shown that a major fraction of the pesticides are lost after precipitation events with surface runoff. Furthermore, the model lacks the ability to applied pesticides on only a selection of subcatchments.

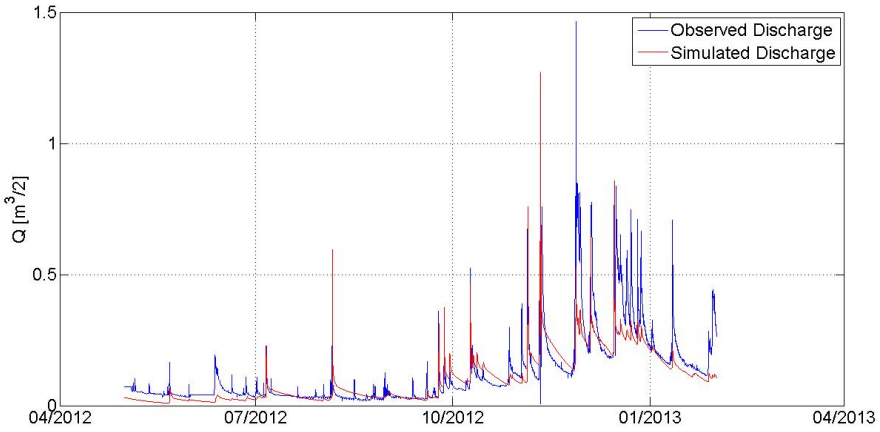

Figure 4.11: Results of simulation using the Aabach model

4.2 Results of the pesticide transport model

In order to calibrate and evaluated the models' performance, they should be compared to measured data. In this case, concentrations of different pesticides have been measured, but the data are only available towards the end of the project (too late to be taken into account). In order to evaluate the performance of the pesticide transport models, three case studies have been chosen. Each case study studies the behaviour of an abundantly used pesticide: Isoproturon, Mecoprop and Atrazine. Whilst the first two have been chosen due their widespread use, Atrazine has been chosen in order to take into account a different set of chemical properties.

All three pesticides are applied at equal amounts and the same date. The applications are the following:

- Application 1: On 15.06.2012 at 12:00, 0.75 kg/ha are applied to section 1 of the catchment.
- Application 2: On 25.06.2012 at 12:00, 1 kg/ha are applied to section 2 and 3 of the catchment.

It has been shown that major applications occur during the month of April. As hydrological data are available only starting in May 2012, the fictive applications have been shifted to June, in order to be able to study the behaviour.

The pesticide transport model is linked to the hydrological model, using combination N° 5, which proved to be the combination with be best overall performance.

Table 4.13 summarizes the chemical properties of the three pesticides. Using these values, the behaviour of the different model variants and their response to different chemical properties will be studied. Furthermore, they serve here as a proof-of-concept for the different variants of the model.

Pesticide	Molar mass [g/mol]	K_D	DT_{50}	Log K_{ow}
Isoproturon	206.29	0.06 to 1.27 L/kg [a]	6 - 28 days 22 - 42 days [b]	2.5 (20°C) [c]
Mecoprop	214.65	3.57	12 days (< 30 cm depth) 84 days (depth 80-80cm) [d]	3.13 [e]
Atrazine	215.69	2.34 [f]	13 to 261 days	2.75 [g]

[a] [Cooke et al., 2004]
[b] [Perrin-Ganiera et al., 1996]
[c] [IFA, 2013]
[d] [de Lipthay J.R. et al., 2007]
[e] [Rodríguez-Cruz et al., 2009]
[f] [Coquet, 2003]
[g] [EPA, 2006]

Table 4.13: Summary of chemical properties for selected case-studies

Isoproturon Isoproturon is an urea herbicide, which is mainly applied on cereal cultures. It is rather short lived in the environment, due to its low adsorption onto soil. The pesticide is easily desorbed from the soil and is often found in surface waters, as studies have shown (e.g [Cooke et al., 2004]). The half life can therefore vary from 6 days in controlled conditions up to 42 days in field conditions [Perrin-Ganiera et al., 1996].

Mecoprop This herbicide is widely applied against broad-leaf pest plants. It has a slightly higher half life than Isoproturon, and leaches similarly into subsurface water. It can also be found in groundwater [Rodríguez-Cruz et al., 2009].

Atrazine The organic herbicide is applied against broad-leaf and grassy weeds pests. Its application is controversial, as it is persistent in the environment and can be found in groundwaters. Its application in Switzerland has been limited to large corn cultures in 1987, before being completely banned in 2005 (SR 916.161). It has been chosen due to its popularity as well for its long half life, to see whether the models show different behaviours for this type of chemical.

4.2.1 Simple model: well mixed

Case study 1: Isoproturon

The case study has been evaluated using a half life of 6 days and a partition coefficient of 0.06 l/kg. One can observe that the relatively short half life of the pesticide dictates the output and concentration in the river. It can be observed that the major fraction of the pesticide is degrading in the surface crust (Fig.

4.12). The same observation can be made in the subsurface and deep storages, where the pesticide undergoes a degradation with the same rate constant.

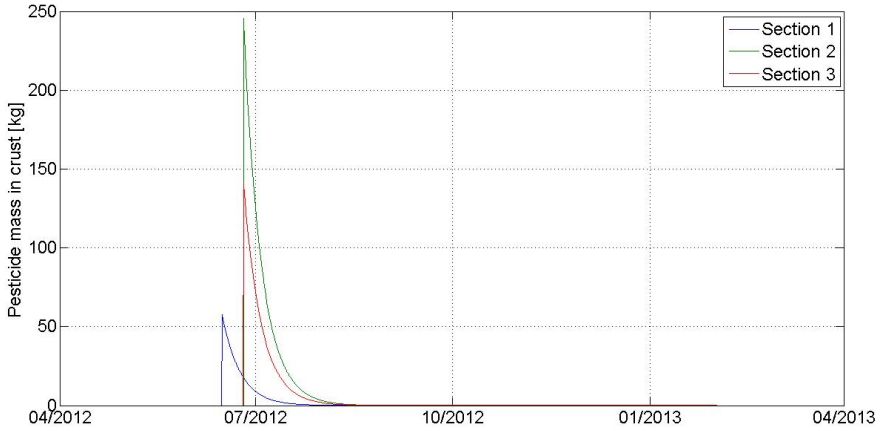

Figure 4.12: Total mass in crust layer

The maximum simulated mass in the river is 0.13 kg, yielding to a maximum concentration of 0.137 mg/l. The maximum of total mass and concentration occur during the same rainfall event. As Fig. 4.13 illustrates, the major fraction of the pesticide is released after a major rainfall event succeeding the second application. The concentration in the river (Fig. 4.14) is following the trend of the degradation in each reservoir, with peaks occurring at each precipitation event. The last releases of pesticides into the river can be observed in the first half of August, only 8 weeks after their application.

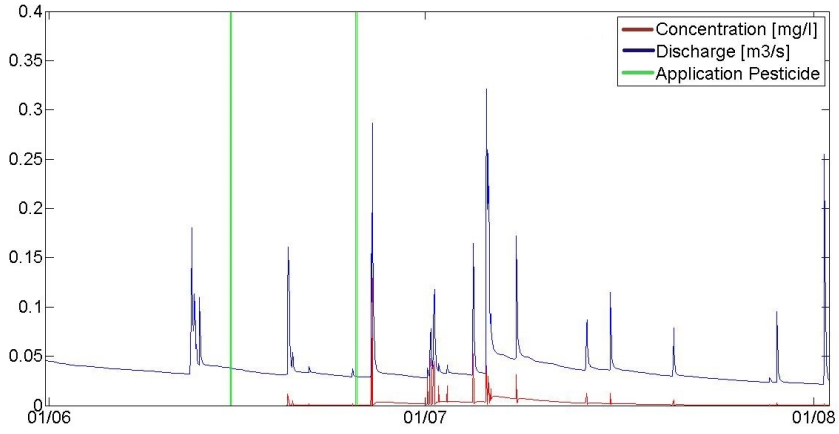

Figure 4.13: Peaks in concentration can be observed for applications preceding a precipitation event

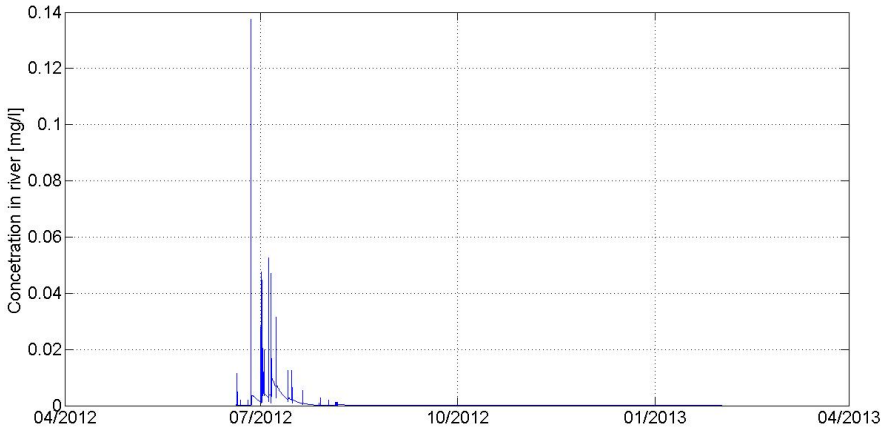

Figure 4.14: Concentration over time in river

Case study 2: Mecoprop

For this pesticide, a more favourable partitioning onto soil is chosen, with a K_D of 3.5 l/kg. Furthermore, the half life of the pesticide is higher than for the previous case. Furthermore, two different half lifes are chosen: 12 days in the surface crust and active soil layer, 60 days in the reservoirs [Rodríguez-Cruz et al., 2009] [de Lipthay J.R. et al., 2007].

The general behaviour of the total concentration in the river follows the same trends as in the previous case study. The fast degradation in the soil crust and active soil layer dictate the output of pesticides into the river. The effect is furthermore amplified, as the major fraction of the pesticide is fractioned onto soil particles (only 1/7000 of the total mass is in mobile). This prevents the infiltration of the pesticide towards lower soil layers and reservoirs, and hence also losses to the river.

It can be observed, just as in the previous case, that the maximum concentration occurs with the peak in runoff following a pesticide application (Fig. 4.15). The maximum concentration is 1000 times small than with the previous pesticide.

The mass in the two reservoirs show a similar behaviour, but the order of magnitude changes. Here, the total mass in the reservoirs is significantly lower than in the previous case study. Furthermore, pesticides appears in the reservoirs during January, more than 6 months after being applied to the surface. This is likely due to the higher partitioning coefficient. Mecoprop is retained and released more slowly than Isoproturon. The mass in the reservoirs however is not leaving them, as they are ultimately degraded in the reservoirs.

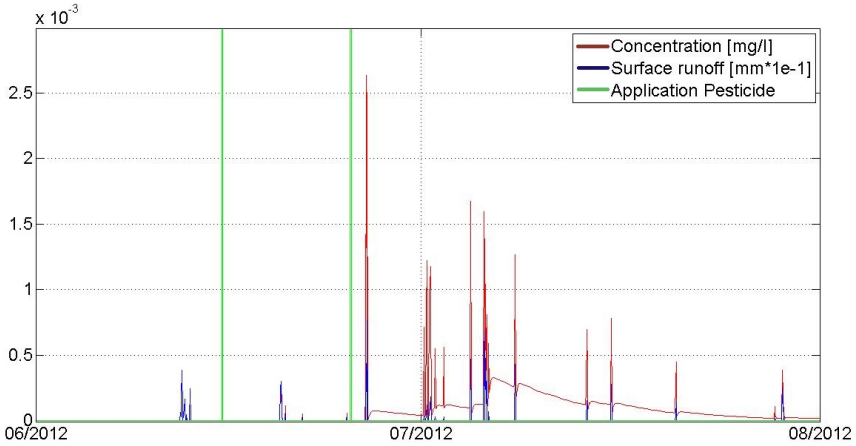

Figure 4.15: A peak in concentration can be observed for precipitation events following shortly after an application of pesticides

Case study 3: Atrazine

Atrazine is studied in order to test the behaviour of the model facing slow degradation rates. In consequence, a half life of 9 months (=270 days) in the crust layer and active soil layer and of 365 days in the reservoirs has been chosen. A partition coefficient of 2 is taken for the case study.

Contrary to the previous case studies, the degradation of Atrazine is small compared to the simulation period. This is confirmed by the simulation. The mass in the crust is released by both infiltration and superficial flow. Due to the relatively low solubility (only 1/4000 of total mass in mobile phase), the total mass decreases only very slowly. Furthermore, due to the slow degradation, the mass remains at a high level during the year. With the current parameter set, it can be expected that a major fraction of the applied pesticide remains in the soil until the next application. Accordingly, the pesticide accumulates in the soil layer (see Appendix H, Fig. H.7), and passes slowly towards the subsurface and even later towards the deep storages.

Interestingly, the contribution in terms of mass per flow shows a shift from surface runoff to the subsurface reservoirs (see Fig. 4.16). This correlates with the mass stored in each reservoir, and represents the fact that the pesticide is not degrading quickly. The concentration in the river is however not peaking in the same way: during summertime, less mass is released, but the discharge is tenfold lower than during winter. Therefore, the concentration is levelled out over one year

Concentration peaks after precipitation which follow an application can be observed just as in the previous case studies (Fig. H.8, Appendix H).

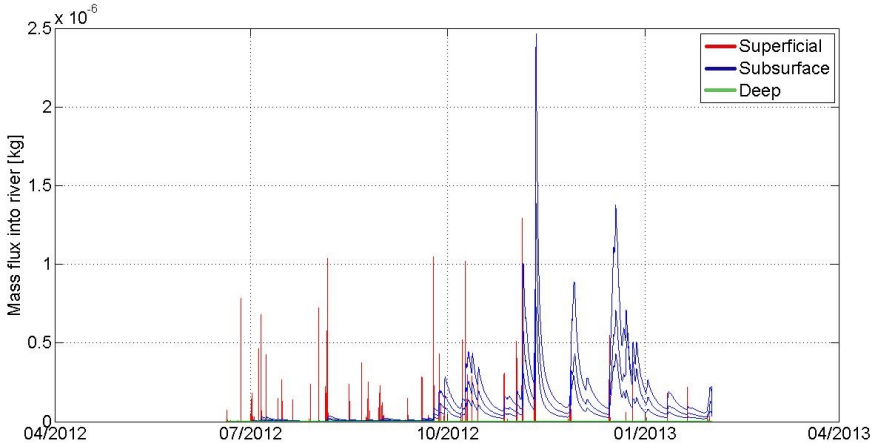

Figure 4.16: Contribution of each mass flux to total mass flux in river

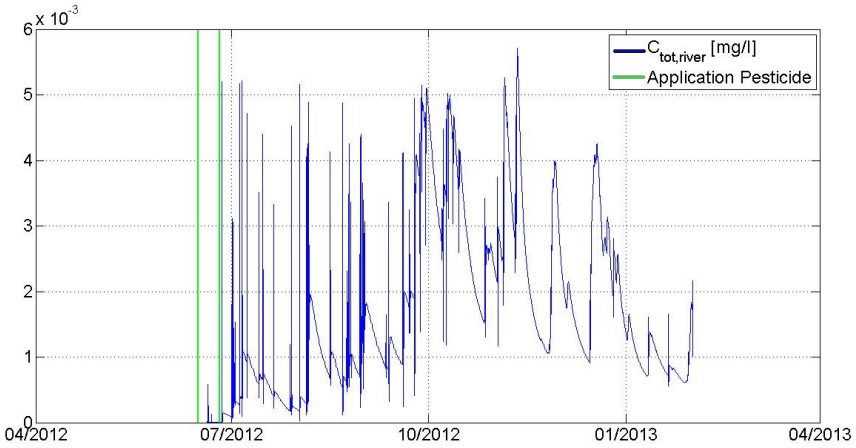

Figure 4.17: Resulting concentration in river

4.2.2 Complex model: water age

Case study 1: Isoproturon

The simulated concentration of Isoproturon is similar to the simulation using the simple model. The peaks in concentration can be observed when precipitation events follow shortly after an application of pesticides (Fig. 4.18).

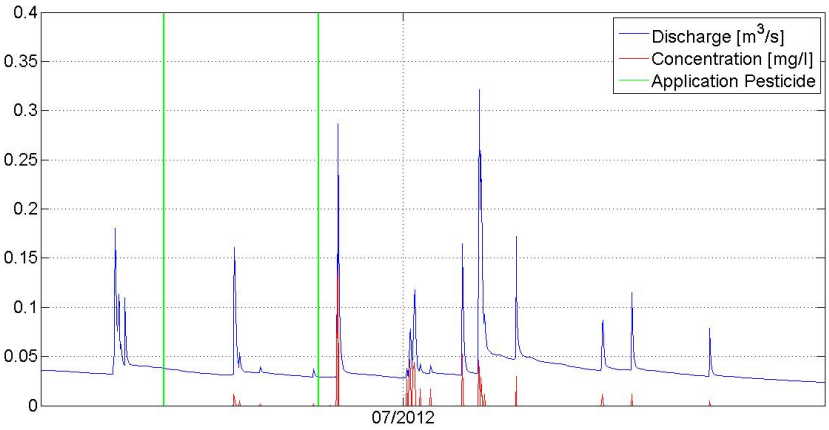

Figure 4.18: Results of the simulated concentration of Isoproturon in the river using the complex model

The recession of the concentration after such a peak is however different; the subsurface and deep reservoir do not contribute to the recession. As this model can be conceptualized as a plug flow, the substance has to travel through the complete active soil layer in order to reach the reservoirs. From the reservoirs itself, the substance can be released in the river. Substance enters the soil layer shortly after the application with the first infiltration flux, and exits the soil layer only several months later (Fig. 4.19). The water in the soil layer is completely replaced after 3 months (plug flow), thus mass leaches 3 months after having entered the soil layer. During that time, the chemical degradation of the substance takes place. Especially with a short half live of 6 days, only 0.09% of the initial mass remain after 60 days. This is reflected in the small amount of remaining mass that is leached towards the reservoirs in October.

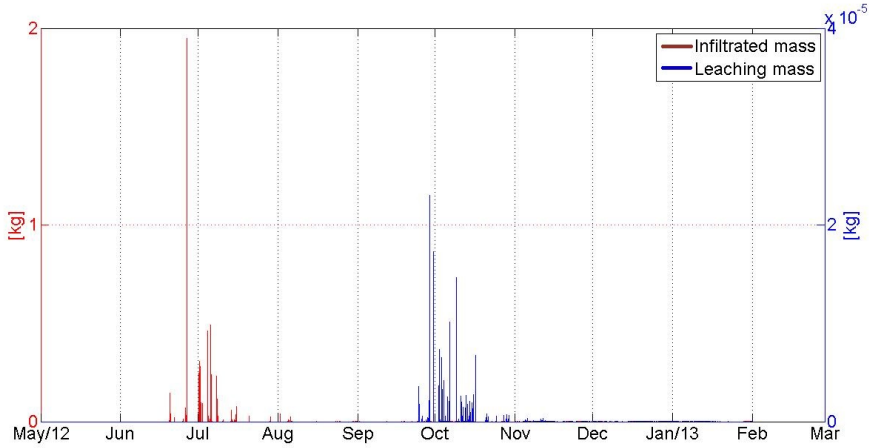

Figure 4.19: Infiltration of mass from the surface crust into the soil layer, and according leaching mass from the soil layer

Case study 2: Mecoprop

As the simulation using the simple model has shown, Mecoprop behaves similar to Isoproturon. This is confirmed using the complex model. Peaks in concentration are still obtained for precipitation events shortly after applications. Due to the higher partition coefficient, Mecoprop does not partition as easily into water. The concentration in the infiltration flux is therefore smaller than for the previous case. The travel time across the soil layer is not influenced by these properties, the water required still approximately 3 months to travel across the soil layer. The small degradation rate (or higher half life) influence the leaching mass: more mass remains after 3 months than for the previous case study. This influence is however small, and the overall concentration in the river resembles - both in variability and magnitude - the first case study.

Case study 3: Atrazine

The simulation using the complex model shows a different behaviour as the previous simulation using the simple model, especially the concentration in the river decreases more dominantly over the summer months. The pattern of infiltrating mass into the soil layer and leaching mass from the soil layer towards the reservoirs is the same as for the previous two case studies. In the case of Atrazine however, the degradation is much less important than for Isoproturon and Mecoprop. This is translated in the infiltrating mass and leaching mass being of the same order of magnitude; only the 3 months delay can be observed. The major difference happens on the level of the two reservoirs.

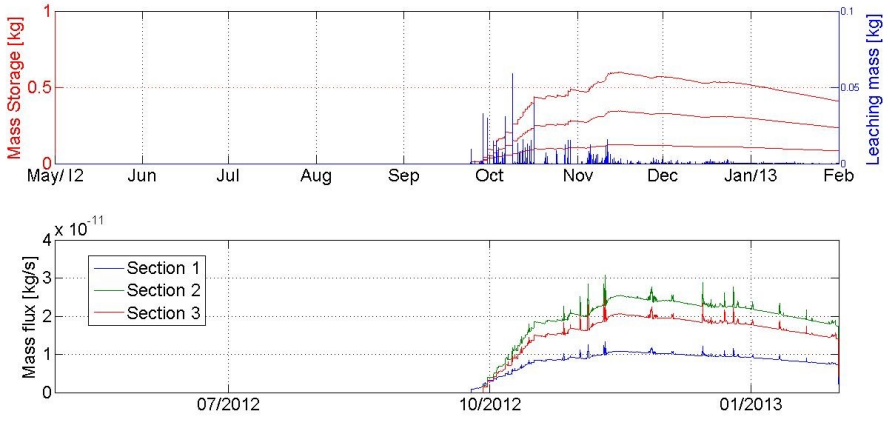

Figure 4.20: Top: Leaching mass into subsurface reservoir and subsurface mass storage. Bottom: Mass flux from subsurface reservoir to river

An increase of mass in both reservoirs during the months of October can be observed (Fig. 4.20 illustrated for subsurface reservoir). The peaks which are added to the general increase are due to the input from the soil layer. The soil layer releases the pesticides as they entered, only after a 3-months long

retardation period. In the reservoirs itself, the pesticides are well mixed, and therefore released immediately. Using these parameters, the driving flux of the total concentration is the mass flux related to the surface runoff. In fact, Atrazine sticks to soil particles and is only slowly released. During the same period, the chemical degradation is negligible. Therefore, even towards the end of the simulation period, the main input into the river is released from the surface crust.

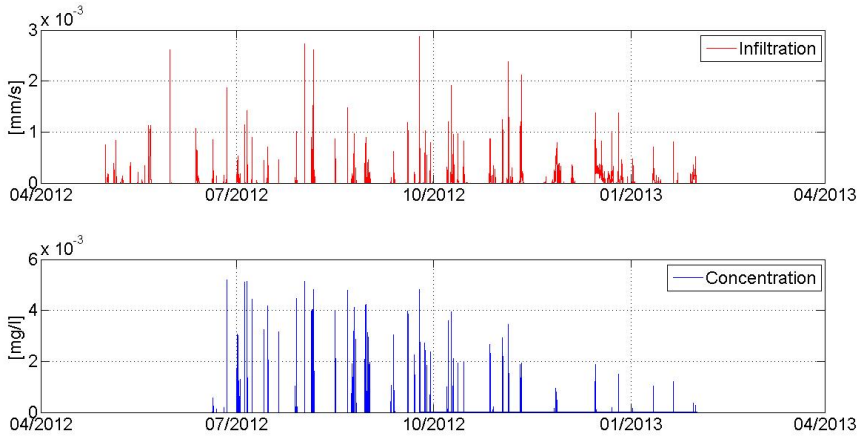

Figure 4.21: Top: Infiltrating water. Bottom: Total concentration in river.

Chapter 5

Discussion

5.1 Hydrological Model

Options for reservoirs The results show clearly that the optimal reservoir configuration are two reservoirs in series with a linear empty function. The non-linearity of the empty function not only slows down the calibration process, but yields to poor results. Emptying the reservoirs, when there is a considerable storage in the reservoir, is calibrated wrongly in the process. The question remains whether this is due to the calibration or due to the option itself. Further calibration and maybe Monte-Carlo-simulations would have to be done, in order to be able to fully conclude on the linearity of the empty function. It can however be stated that linear empty functions have been widely used in conceptual hydrological models, and it has been proven that they can represent the recession after discharge peaks well [Fenicia et al., 2006]. It would be hence advisable to keep the linear empty function.

Infiltration method During the calibration process, it has been observed that Horton's mechanism of surface runoff leads to better simulations. None of the calibration using Dunne's mechanism converged. Two observations explaining this can be made: Firstly, the catchment is mostly flat, agricultural fields with some small patches of forests. Secondly, these agricultural fields are highly influenced by human, as has been shown in a previous study [Stalder, 2012]. The main influence are drainage pipes flowing towards the river, and less importantly flatted terrain for agricultural use. In these cases, surface runoff is generated described by Horton's mechanism.

Horton overland flow can be described as a from top saturated soil layer, i.e. underlying soil layers may not be fully saturated when surface runoff is produced [Horton, 1940]. This physical approach is still widely applied nowadays and it is doubtful whether our understanding of infiltration has improved since [Beven, 2004]. On the other hand, Dunne's mechanism of infiltration requires a saturation of the soil layer from the bottom, i.e. surface runoff is produced once the water table reaches the surface [Dunne and Black, 1970]. A recent study [Mirus and Loague, 2013] investigated the different mechanisms of runoff using a physical-based hydrological model. Of special interested was, to delimit

the different surface runoff mechanisms based on several factors. Firstly, it has been observed that Dunne's mechanism starts at pits and ponds in gentle slopes. This is explained by the fact that the rising water table reaches the ground surface faster in such pits and ponds. Furthermore, highly permeable soils prevent Horton runoff, as the precipitation can easily be infiltrated. In other words, the dynamics of the soil moisture and the properties directly influencing the soil moisture are reflected in the type of overland flow. As soon as the rainfall intensity is bigger than the underlying hydraulic conductivity (infiltration capacity), Horton overland flow is produced.

Reflecting these findings with regard to the catchment of the Petite Chamberonne, one can easily see that the main mechanism producing surface runoff should be Horton's mechanism. The Petite Chamberonne is gently sloping and highly influenced by humans. Pits are filled and the topmost hydraulic conductivity is presumably much smaller (due to compaction from agricultural use) than the underlying hydraulic conductivity (drainages). The topmost layers can therefore be saturated, whereas the underlying layers are drained and therefore not fully saturated. It is therefore evident that the saturation front moves from top to bottom and that Horton overland flow is the prevailing mechanism producing surface runoff. It has to be noted that the two mechanisms are two extremes of a continuous scale. In the catchment, it is likely to observe both mechanisms, depending at the exact location of the observant. In addition to this, the fast subsurface flow - representing flow in the drainage system - is likely to be of importance.

Entry data, measurement errors and uncertainty The quality of the simulation not only depends on the model itself, but also on the quality of the input data. Several issues have been detected during the preparation of the input data (Section 3.1.1) and discussed. It is important to conclude on the important influences of the data on the simulation.

Firstly, rainfall have been reconstructed using a nearby weather station (Crissier). The analysis has shown that the used precipitation patterns are reasonably close to the gauging station at the Petite Chamberonne. The uncertainty introduced by the snow measurements remain. It has to be noted that only one winter season is measured, which increases the uncertainty of this season, as no other winters are available for comparison. The discharge data of the station at the Sorge showed an increased discharge during the winter 2012/2013 which does not resemble previous years. This raises suspicion on the validity of the calibration period for the Petite Chamberonne.

Secondly, this points out another important issue of the calibration: the calibration period. Only 9 months of data are available, therefore only 9 months can be calibrated. Furthermore, no additional data is available for a validation of the model. Particularities that occurred during these 9 months influence the calibration strongly, and can deteriorate the results. The calibration should be remade once more data is available, with at least 2 (the more the better) consecutive winter seasons.

Thirdly, the delimitation of the subcatchment remains still - to a certain

extent (approx. 20%) - uncertain. These 20% can influence the final result of the simulation. In the calibrations showed in chapter 4, this fact is reflected in a very low evapotranspiration over the 9 months period. Interestingly, the 20% error remains even after the correction of the channel network by P.Queloz. *SS* being constantly calibrated at 1.2 could also indicate a bias of the measuring station at the Petite Chamberonne, in other words, the station measures 20% excess discharge. This however is less likely to be the case. Another source of error could be the rating curves, as has been discussed in section 3.1.1. Lastly, it could indicate a source that is adding a constant discharge corresponding to 20% of the annual precipitation over the catchment. Sources from outside of the catchments delimitations have been explored by questioning experts from the cantonal agencies. Although there are some small sources in the catchment, their exact origin remains unknown and their discharge most likely negligible.

It could be interesting to simulate discharge with these uncertainties of the input data using a stochastic approach. With this, a bandwidth of discharges could be simulated and the parameters would also be given with a certain variability. This is partially done when using the optimizer DREAM; during the calibration process, no convergence has been achieved for any of the model combinations.

Snow module Whether the snow module should be deactivated or not during the calibration procedure is closely linked to the previous statements. At this stage of the project, it seems that the simulation fits better with a deactivated snow module. In reality however there is snow, and especially when taking into account the difficulties of snow measurements leading to an underestimation of the measured precipitation (as explained in section 3.1.1), the simulation with an activated snow module seems more realistic. This will however have to be confirmed with the next winter season's data. Taking a stochastic approach would show the influence of the uncertainty in snow measurement (or precipitation measurement in general), and the performance statistics would likely be improved.

One should on the other hand keep in mind that the goal of the calibration process is to be able to link the SEHR-model to a pesticide transport module. Pesticides are never applied on snow, but in April, only after the snow has melted. Modelling December and January (where most of the snow fall events occur) correctly is only of an importance in order to know the state of the subsurface reservoirs. These will then influence the behaviour of subsurface fluxes, which are important for the transport of pesticides. It does however not directly influence the discharge of the river during the month of May, where most of the pesticide transport is occurring.

Further improvements The Petite Chamberonne is only a small catchment of approximately 4.5 km^2. The total catchment of the Chamberonne is 10 times as big. Having measurement stations all over the catchment, one could combine these catchments, in order to improve the hydrological simulation (and lastly the simulation of pesticide transport). Each subcatchment could be calibrated separately, and the resulting parameter set combined in order to get a better

understanding of the total catchment (e.g. [Merz and Böschl, 2004]).

Having compared the results of SEHR-ECHO with the hydrological model used for the simulations of the Aabach, similar results for the hydrological response have been obtained. The lack of surface runoff in the Aabach model however lessens the utility of this model. The utilisation of SEHR-ECHO furthermore allows the simulation of spatially distributed applications of pesticides, whereas the Aabach-model is a lumped model. Having surface runoff plays a major role in the transport of pesticides, which is taken into account only by SEHR-ECHO. It is therefore advisable to use SEHR-ECHO instead of a simpler model, although the computational requirements are bigger. The newly tested workflow of SEHR-ECHO proved to give interesting results for the hydrological simulations. It is however more difficult linking a pesticide transport module to it; the pesticides would have to be separated amongst the two soil layers (fast and slow), and it is not yet clear how to do this separation.

5.2 Pesticide transport modelling

Behavioural studies Firstly, the possibilities of linking a pesticide transport model with SEHR-ECHO seem unlimited. It has been shown (and successfully tested) that different types of models for the simulation of pesticide transport can be developed for SEHR-ECHO. Using the fluxes provided by SEHR-ECHO, the simulation of the pesticide transport is facilitated.

The behavioural studies of the pesticide transport model has shown that the general expected behaviour can be achieved. Pesticides applied shortly before precipitation events are likely to result in higher losses than pesticides applied prior to a dry period. This finding has also been observed by Leu et al. [Leu et al., 2004a]. The degradation in the crust is mainly due to a chemical degradation, and no volatilization occurs. Furthermore, for pesticides having a slow degradation rate (e.g. Atrazine), a build-up of pesticides in the reservoirs can be expected. For the two models, the first peak of concentration arrives after approximately 110h (time until first precipitation event after first application) and the peak after the second application arrives after 50h (time until first precipitation after second application). Only in the long term, the behaviour of the concentration changes, which is especially visible for Atrazine due to its slow degradation. The concentration simulated using the complex model shows the plug flow behaviour, as each parsel of mass is released on its own, whilst the concentration reaches zero in between. This is not the case for the simple model, where the concentration is lower in general, but does not reach zero but decreases slowly until the next input of mass from the surface crust (re-)increases the concentration. The assumption of a perfect plug flow seems therefore questionable. This observation is especially true for pesticides having slow degradation rates. For pesticides degrading quickly, this difference is, though still present, less pronounced and therefore less important; especially in view of the main mass being lost to the first two rainfall events.

Moreover, these models require calibration in order to fully understand their utility. This will have to be done once measurements of pesticide concentration

are available. It could be useful to calibrate the hydrological model and the pesticide transport at the same time, as has been stated by Bertuzzo et al. [Bertuzzo et al., 2013]. In order to do so, gathering longer time series of hydrological data seems advisable.

Further improvements Although no calibration of the pesticide transport models has been done, some general ideas of improvement can be presented.

Firstly, one could use additional calibration parameters. Especially the thickness of the surface crust plays an important role, as it is used for the calculation of the concentration in the surface runoff. The thickness is currently fixed at 0.01m, but could easily be made a calibration parameter. The water content of the surface crust could also be calibrated, but it has the same impact as the thickness. It would therefore be advisable to calibrate only one of the two, fixing the other. Secondly, using the concepts of the water age, one could imagine preferential flow paths in the soil layer. As the water age concept is a pure plug flow and the fully mixed assumption the complete opposite of this, it could be interesting to test an intermediate version. This could be represented by a certain fraction of the water (and the pesticides it holds) percolating more directly through the soil layer than others. This leads to a more physically-like concept of the hydrological part of the model, and has been studied by Botter et al. [Botter et al., 2010] under the name of travel time distributions.

Chapter 6

Conclusion

The project consisted of two closely linked parts: hydrological modelling and pesticide transport modelling.

For the hydrological simulations, different models have been tested. The best model proved to be combination N°5. It uses Horton's mechanism for runoff generation and subsurface reservoirs in series instead of in parallel. It is noteworthy that this model has not shown the best NSE (0.71, best 0.77), but that the overall performance of the model proved to be better than any other model. For future models in the catchment of the Petite Chamberonne, Horton overland flow should be used, as Dunne overland flow does not appear to be importance in the said area. The disposition of the reservoirs is less conclusive; it has been shown that the performance of the hydrological model using reservoirs in series is better than in parallel. More importantly, reservoirs in series are used for pesticide transport modelling by Bertuzzo et al (2010), and it will have to be proven once the pesticide transport model can be calibrated. Deactivating the snow module has not proven to be relevant. A deactivated snow module allowed to improve the performance of the hydrological model in terms of a better NSE, but its physical significance is questionable. Especially as the calibration has been done using data of only one winter season, it is argued that the uncertainty is large, and that it therefore is better including the simulation of snow. Using these adaptations, the model SEHR-ECHO proved to be able to simulate the discharge of the small catchment of the Petite Chamberonne reasonably well. It has also been shown that it is advisable using the more complex model and spatially explicit model SEHR-ECHO instead of a simpler model, such as the model used for the Aabach.

As for the pesticide transport models, no definitive conclusion can be drawn due to the lack of measured data. No calibration has thus be done. It has been proven that it is technically feasible to connect different models for pesticide transport simulation to SEHR-ECHO. Two different types of models have been tested; firstly, a well mixed model, and secondly, a plug flow model. Both models showed reasonable and similar outputs during three different case studies. It can be argued that a third - intermediate - option, could be tested. The outcoming of these 3 different models, once calibrated, will have to be evaluated in a future step of the project Catch-Herb.

Bibliography

[ASCE, 1996] ASCE (1996). *Hydrology Handbook*. American Society of civil Engineers, 2 edition.

[Bertuzzo et al., 2013] Bertuzzo, E., Thomet, M., Botter, G., and Rinaldo, A. (2013). Catchment-scale herbicides transport: Theory and application. *Advances in Water Resouces*, 52:232–242.

[Beven, 2004] Beven, K. (2004). Robert e. horton's perceptual model of infiltration processes. *Hydrological processes*, 18:3447–3460.

[BFS, 2012] BFS (2012). Auswirkungen auf die umwelt - pflanzenschutzmittel. Technical report, Bundesamt für Statistik (BFS).

[Botter et al., 2010] Botter, G., Bertuzzo, E., and Rinaldo, A. (2010). Transport in the hydrologic response: Travel time distributions, soil moisture dynamics, and the old water paradox. *Water Resources Research*, 46:W03514, doi:10.1029/2009WR008371.

[Clapp and Hornberger, 1978] Clapp, R. and Hornberger, G. (1978). Empirical equations for some soil hydraulic properties. *Water Resources Research*, 14:4:601–604.

[Cooke et al., 2004] Cooke, C., Shaw, G., and Collins, C. (2004). Determination of solid–liquid partition coefficients (kd) for the herbicides isoproturon and trifluralin in five uk agricultural soils. *Environmental Pollution*, 132:541–552.

[Coquet, 2003] Coquet, Y. (2003). Sorption of pesticides atrazine, isoproturon, and metamitron in the vadose zone. *Vadose Zone Journal*, 2:40–51.

[Da Ronco, 2013] Da Ronco, P. (2013). Modeling the hydrologic response of snow-dominated alpine catchments: the role of sunlight exposure. Master's thesis, École polytechnique fédérale de Lausanne (EPFL).

[Daly et al., 1998] Daly, H., Doyen, J., and Purcell, A. I. (1998). *Introduction to insect biology and diversity*. Number 2. Oxford University Press.

[de Lipthay J.R. et al., 2007] de Lipthay J.R., Sørensen, S., and Aamand, J. (2007). Effect of herbicide concentration and organic and inorganic nutrient amendment on the mineralization of mecoprop, 2,4-d and 2,4,5-t in soil and aquifer samples. *Environmental Pollution*, 148:83–93.

[Domeneghetti et al., 2012] Domeneghetti, A., Castellarin, A., and Brath, A. (2012). Assessing rating-curve uncertainty and its effects on hydraulic model calibration. *Hydrology and Earth System Sciences*, 16:1191–1202.

[Duan et al., 1992] Duan, Q., Sorooshian, S., and Gupta, V. (1992). Effective and efficient global optimization for conceptual rainfall-runoff models. *Water Resources Research*, 28(4):1015–1031.

[Dunne and Black, 1970] Dunne, T. and Black, R. (1970). Partial area contributions to storm runoff in a small new england watershed. *Water Ressources Research*, 6(5):1296–1311.

[El Nemr et al., 2013] El Nemr, A., Moneer, A., Khaled, A., and El-Sikaily, A. (2013). Levels, distribution, and risk assessment of organochlorines in surficial sediments of the red sea coast, egypt. *Environmental Monitoring and Assessment*, 185(6):4835–4853.

[EPA, 2006] EPA (2006). Decision documents for atrazine. Technical report, Environmental Protection Agency (EPA), http://www.epa.gov/oppsrrd1/REDs/atrazine_combined_docs.pdf.

[EPA, 2011] EPA (2011). Ddt. Technical report, Environmental Protection Agency (EPA).

[Favre et al., 2010] Favre, G., Dugon, J., and Charles, R. (2010). Pratiques phytosanitaires en grandes cultures de 1992 à 2004. Technical report, AGRIDEA.

[Fenicia et al., 2006] Fenicia, F., Savenije, H., Matgen, P., and Pfister, L. (2006). Is the groundwater reservoir linear? learning from data in hydrological modelling. *Hydrology and Earth System Sciences*, 10:139–150.

[Horton, 1940] Horton, R. (1940). An approach towards physical interpretation of infiltration capacity. *Proceedings of the Soil Science Society of America*, 5:399–417.

[IFA, 2013] IFA (2013). Gestis-stoffdatenbank: Isoproturon. Technical report, IFA (Institut für Arbeitsschutz der Deutschen Gesetzlichen Unfallversicherung.

[Imfeld, 2011] Imfeld, C. (2011). Développement d'un modèle précipitation-débit géomorphologique pour les zones tempérées : Application au bassin versant de la chamberonne. Master's thesis, École polytechnique fédérale de Lausanne (EPFL).

[Jain and Sudheer, 2008] Jain, S. and Sudheer, K. (2008). Fitting of hydrologic models: A close look at the nash–sutcliffe index. *Journal of Hydrologic Engineering*, 13(10):981–986.

[Krause et al., 2005] Krause, P., Boyle, D. P., and Bäse, F. (2005). Comparison of different efficiency criteria for hydrological model assessment. *Advances in Geosciences*, 5:89–97.

[Larose et al., 2007] Larose, M., Heathman, G. C., Norton, L. D., and Engel, B. (2007). Hydrologic and atrazine simulation of the cedar creek watershed using the swat model. *Journal of Environmental Quality*, 36:521–531.

[Leu et al., 2005] Leu, C., Singer, H., Müller, S., Schwarzenbach, R., and Stamm, C. (2005). Comparison of atrazine losses in three small headwater catchments. *Journal of Environmental Quality*, 34(5):1873–1882.

[Leu et al., 2004a] Leu, C., Singer, H., Stamm, C., Müller, S., and Schwarzenbach, R. (2004a). Simultaneous assessment of sources, processes, and factors influencing herbicide losses to surface water in a small agricultural catchment. *Environmental Science and Technology*, 38:3827–3834.

[Leu et al., 2004b] Leu, C., Singer, H., Stamm, C., Müller, S., and Schwarzenbach, R. (2004b). Variability of herbicide losses from 13 fields to surface water within a small catchment after a controlled herbicide application. *Environmental Science and Technology*, 38:3835–3841.

[Merz and Böschl, 2004] Merz, R. and Böschl, G. (2004). Regionalisation of catchment model parameters. *Journal of Hydrology*, 287(1-4):95–123.

[Mirus and Loague, 2013] Mirus, B. and Loague, K. (2013). How runoff begins (and ends): Characterizing hydrologic response at the catchment scale. *Water Resources Research*, 49:1–20.

[Monteith, 1965] Monteith, J. (1965). Evaporation and environment. Symposium of the Society for Experimental Biology, The State and Movement of Water in Living Organisms, Vol. 19, Academic Press, Inc., NY.

[Nash and Sutcliffe, 1970] Nash, J. and Sutcliffe, J. (1970). River flow forecasting through conceptual models part i — a discussion of principles. *Journal of Hydrology*, 10(3):282–290.

[Neitsch et al., 2009] Neitsch, S., Arnold, J., Kiniry, N., and Williams, J. (2009). Soil and water assessment tool - theoretical documentation. report no. 406. Technical report, College of Agriculture and Life Sciences, Texas A&M University.

[Nicótina et al., 2008] Nicótina, L., Alessi Celegon, E., Rinaldo, A., and Marani, M. (2008). On the impact of rainfall patterns on the hydrologic response. *Water Resources Research*, 44:W12401, 10.1029/2007WR006654.

[Pechlivanidis et al., 2011] Pechlivanidis, I., Jackson, B., Mcintyre, N., and Wheater, H. (2011). Catchment scale hydrological modelling: a review of model types, calibration approaches and uncertainty analysis methods in the context of recent developments in technology and applications. *Global NEST Journal*, 13(3):192–214.

[Penman, 1948] Penman, H. (1948). Natural evaporation from open water, bare soil, and grass. *Proc. Roy. Soc*, A193:120–146.

[Perrin-Ganiera et al., 1996] Perrin-Ganiera, C., Breuzinb, C., Portala, J.-M., and Schiavona, M. (1996). Availability and persistence of isoproturon under field and laboratory conditions. *Ecotoxicology and Environmental Safety*, 35(3):226–230.

[Praskievicz and Chang, 2009] Praskievicz, S. and Chang, H. (2009). A review of hydrological modelling of basin-scale climate change and urban development impacts. *Progress in Physical Geography*, 33(5):650–671.

[Queloz, 2012] Queloz, P. (2012). Catchment-scale hydrologic transport of herbicides: theory, observations, ecological risk assessment. *Research Plan - PhD Thesis*.

[Reusser et al., 2009] Reusser, D. E., Blume, T., Schaefli, B., and Zehe, E. (2009). Analysing the temporal dynamics of model performance for hydrological models. *Hydrology and Earth System Sciences*, 13:999–1018.

[Rodríguez-Cruz et al., 2009] Rodríguez-Cruz, M., Baelum, J., Shaw, L., Sørensen, S., Shi, S., Aspray, T., Jacobsen, C., and Bending, G. (2009). Biodegradation of the herbicide mecoprop-p with soil depth and its relationship with class iii tfda genes. *Soil Biology & Biochemistry*, 42(1):32–39.

[Schaefli, 2013] Schaefli, B. (2013). *Comments in SEHR-ECHO m-codes*. École polytechnique fédérale de Lausanne (EPFL).

[Schleiss, 2012] Schleiss, A. (2012). Gestion du risque d'inondation dans un bassin versant urbanisé: Exemple de la mèbre-sorge. Technical report, École polytechnique fédérale de Lausanne (EPFL).

[Spreafico and Weingartner, 2005] Spreafico, M. and Weingartner, R. (2005). The hydrology of switzerland. Technical report, Federal Office for Water and Geology FOWG.

[Stalder, 2012] Stalder, P. (2012). Identification des sources de pesticides agricoles dans le bassin versant de la chamberonne. Projet SIE.

[SwissTopo, 2012] SwissTopo (2012). map.geo.admin.ch.

[Tarboton, 2013] Tarboton, D. (2013). Terrain analysis using digital elevation models (taudem).

[Tomkins, 2012] Tomkins, K. (2012). Uncertainty in streamflow rating curves: methods, controls and consequences. *Hydrological processes*, doi: 10.1002/hyp.9567.

[Vrugt et al., 2003] Vrugt, J., Gupta, H., Bouten, W., and Sorooshian, S. (2003). A shuffled complex evolution metropolis algorithm for optimization and uncertainty assessment of hydrologic model parameters. *Water Resources Research*, 39(8).

[Vrugt et al., 2009] Vrugt, J., Ter Braak, C., Diks, C., Robinson, B., Hyman, J., and Higdon, D. (2009). Accelerating markov chain monte carlo simulation by differential evolution with self-adaptive randomized subspace sampling. *Journal of Nonlinear Sciences & Numerical Simulation,*, 10(3):271–288.

[Wilson et al., 1990] Wilson, J., Conrad, S., Mason, W., Peplinski, W., and Hagan, E. (1990). Laboratory investigation of residual liquid organics. *United States Environmnental Protection Agency, EPA.*, 600/6-90/004.

[Yu et al., 2013] Yu, Y., Wang, B., Wang, X., Liu, W., Cao, J., Wong, M., and Tao, S. (2013). Temporal trends in daily dietary intakes of ddts and hchs in urban populations from beijing and shenyang, china. *Chemosphere*, 91(10):1395–1400.

[Zweifel and Sevruk, 2002] Zweifel, A. and Sevruk, B. (2002). Comparative accuracy of solid precipitation measurement using heated recording gauges in the alps. Workshop paper.

Appendix A

Appendix: Additional information on the Chamberonne catchment

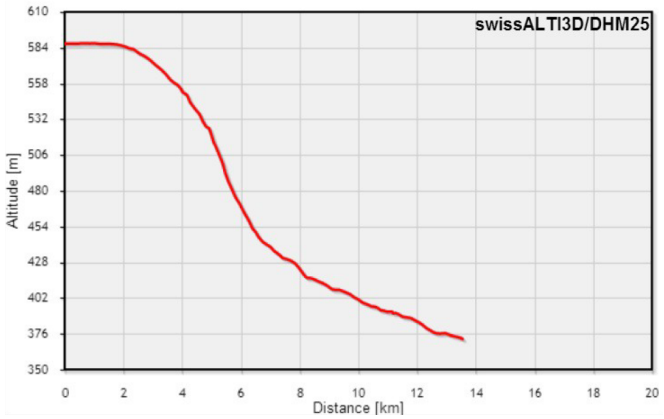

Figure A.1: Slope of the Sorge/Chamberonne river [SwissTopo, 2012]

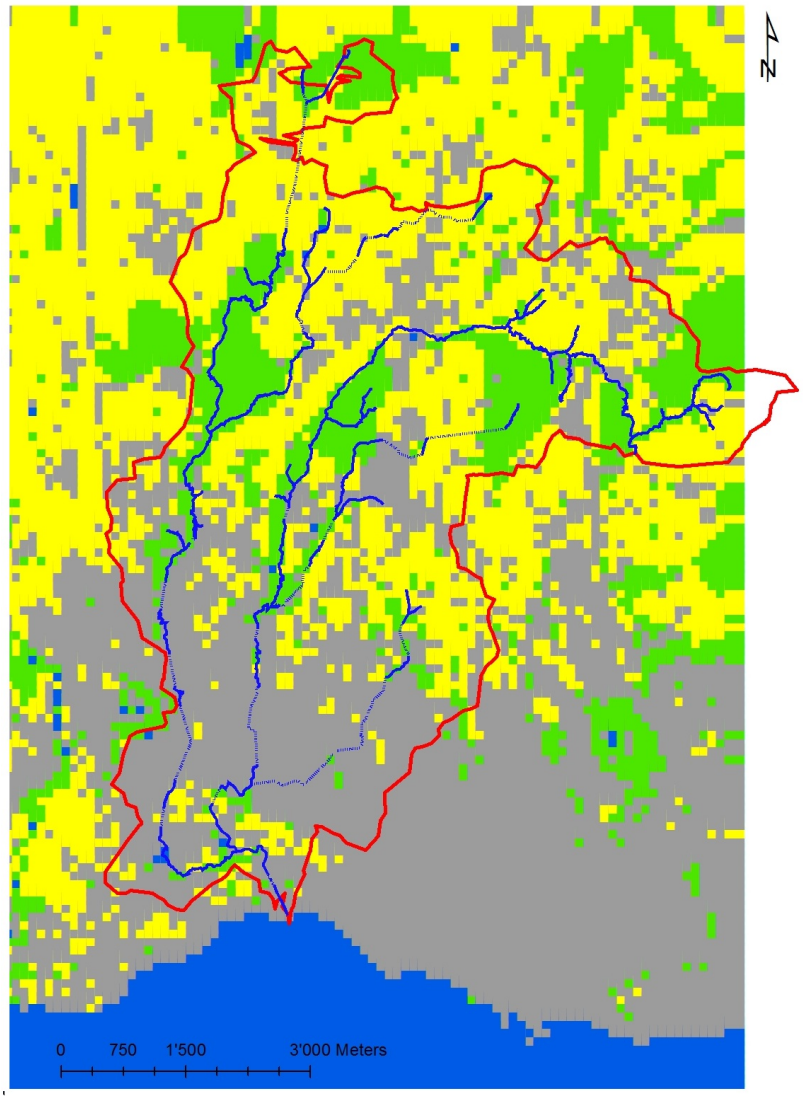

Figure A.2: Land use in the Chamberonne catchment

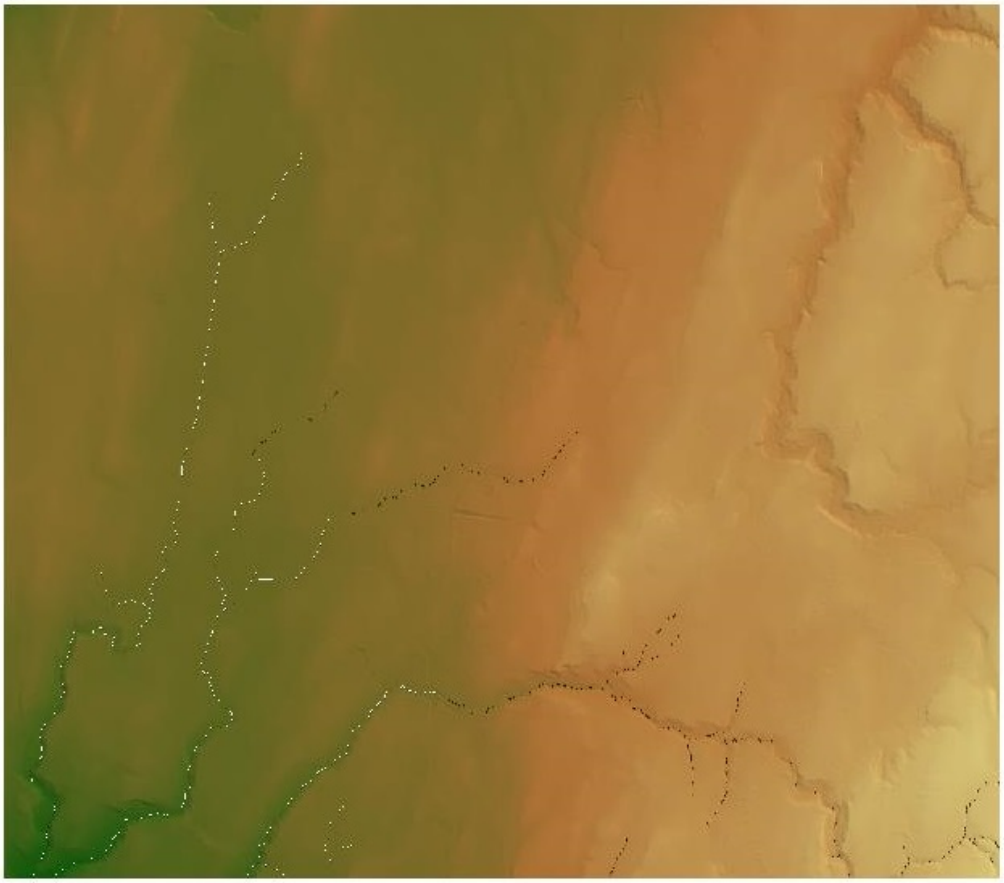

Figure A.3: The DEM with the burnt in channel network, used for delimiting the subcatchment of the Petite Chamberonne

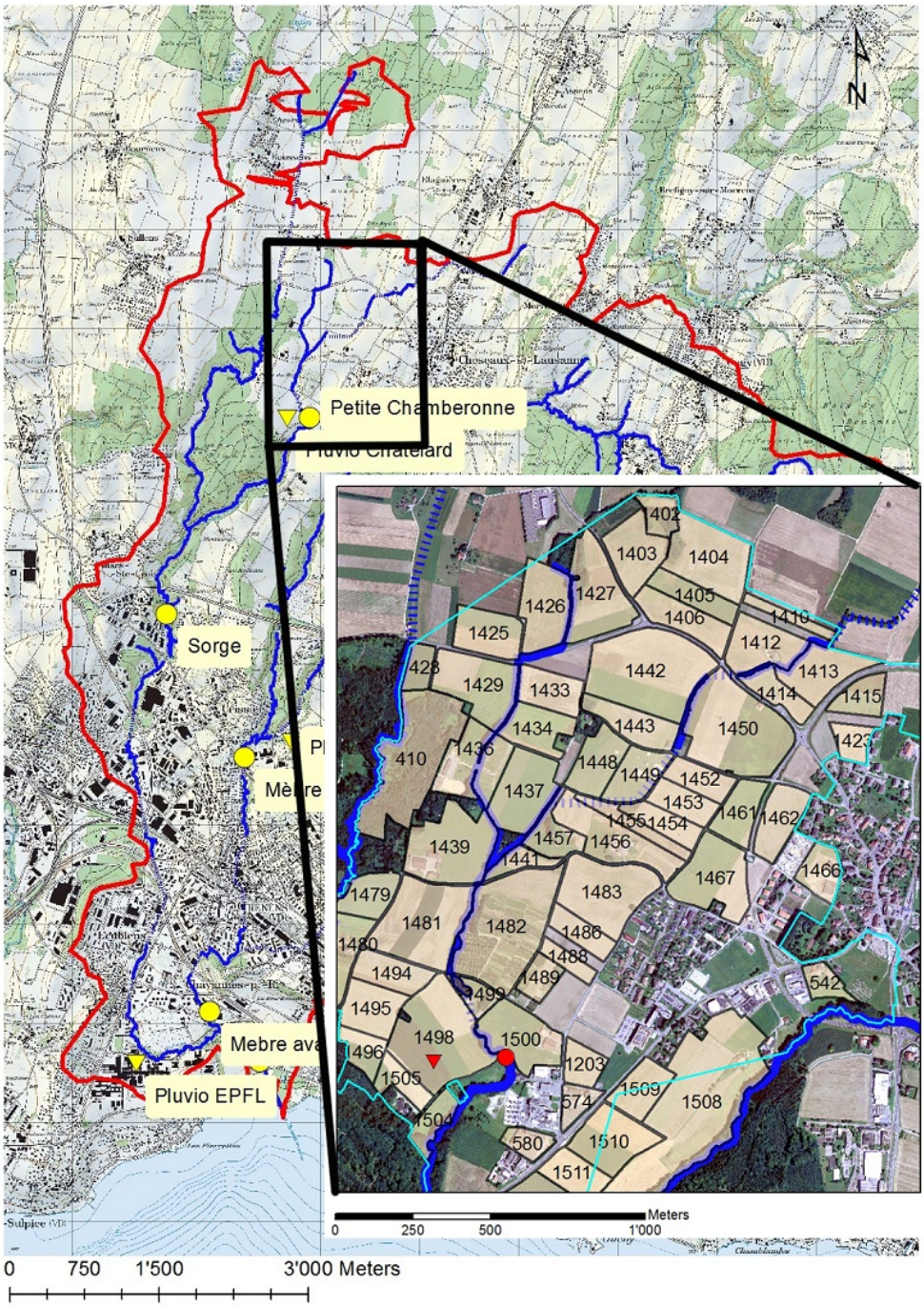

Figure A.4: The subcatchment of the Petite Chamberonne. Indicated are the location of the rain gauge and sampling stations, as well as the parcels investigated during the semester project [Stalder, 2012]

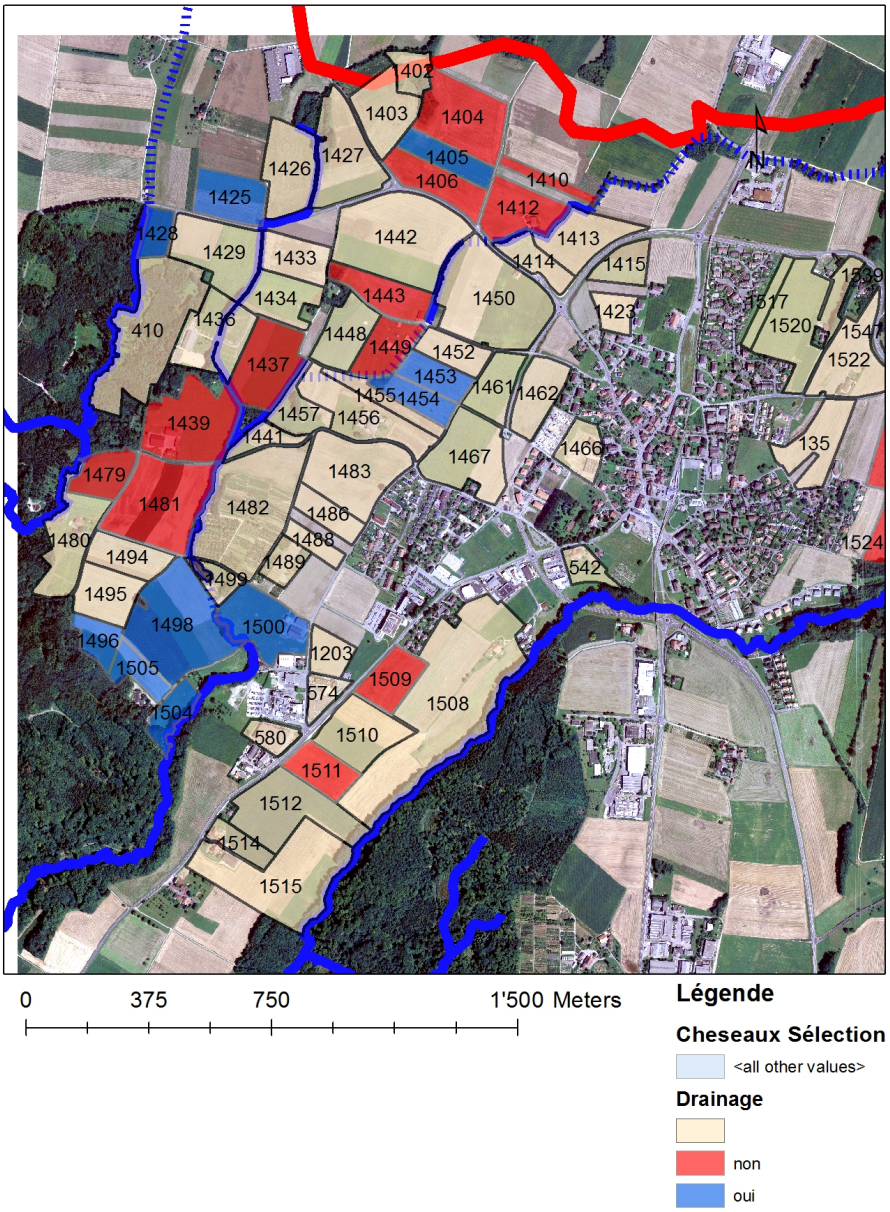

Figure A.5: Indications of drained areas according to the semester project 2012. It is assumed that most of the field having no informations are drained towards the Petite Chamberonne [Stalder, 2012]

Appendix B

Appendix: Rating curves for all stations

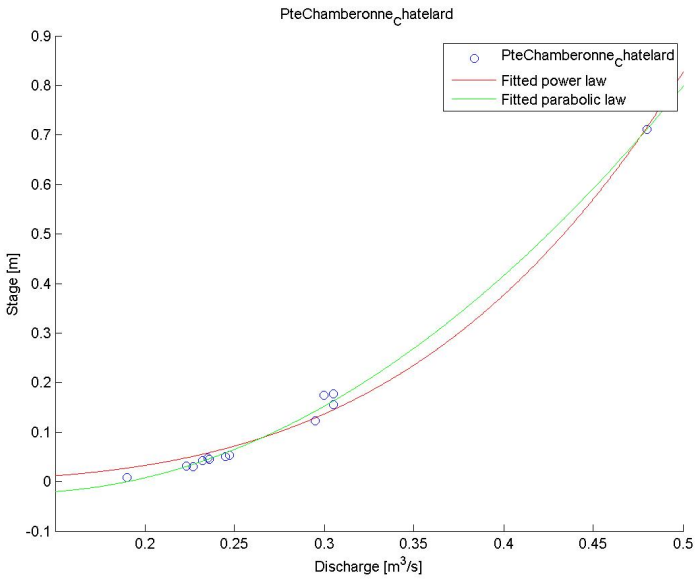

Figure B.1: Rating curve, Petite Chamberonne

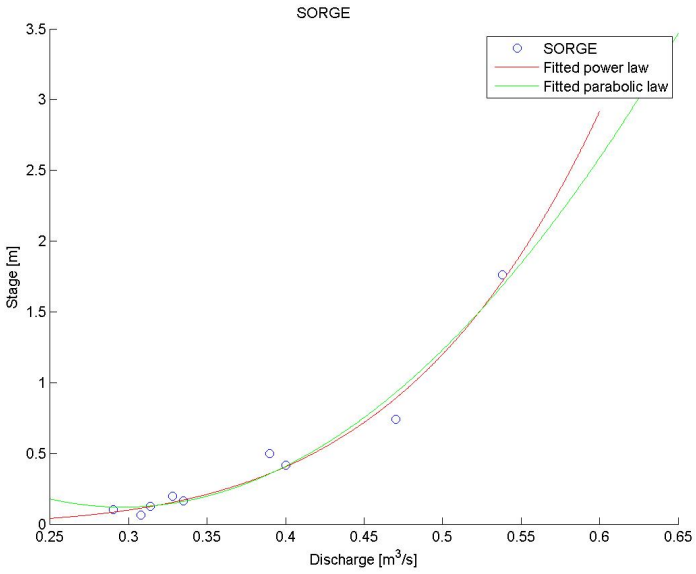

Figure B.2: Rating curve, Sorge

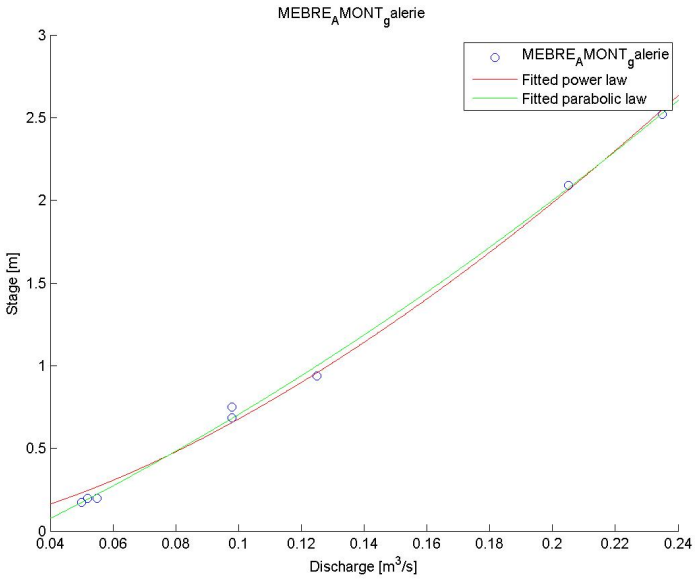

Figure B.3: Rating curve, Mèbre amont

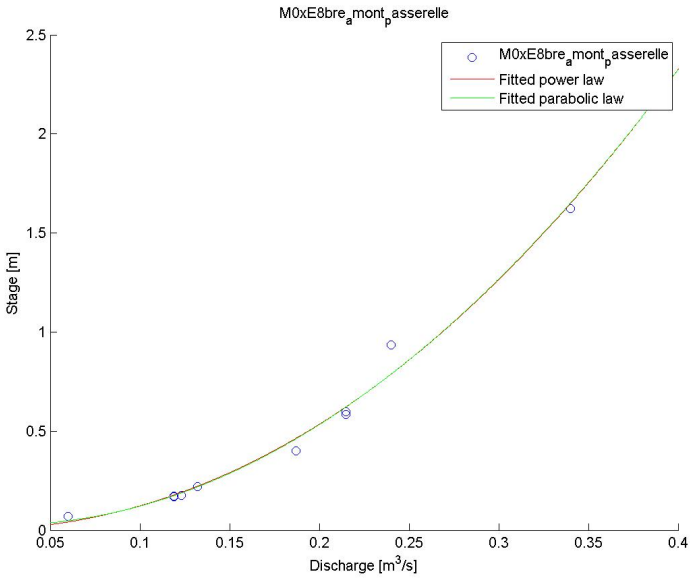

Figure B.4: Rating curve, Mèbre aval passerelle

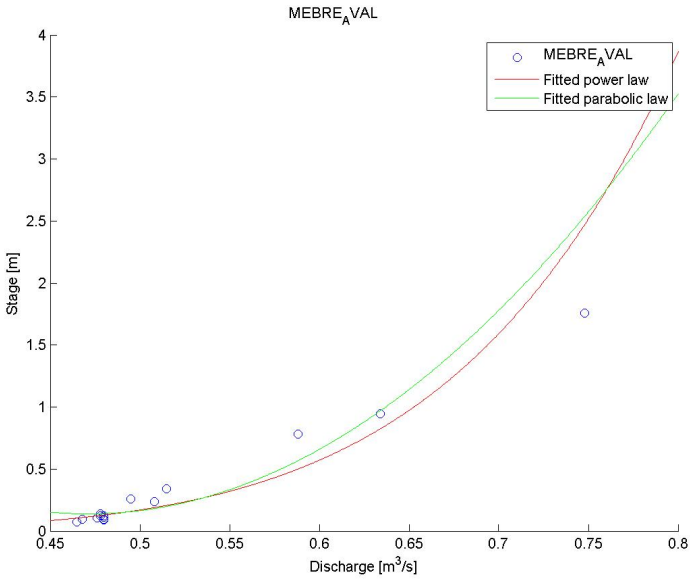

Figure B.5: Rating curve, Mèbre aval galerie

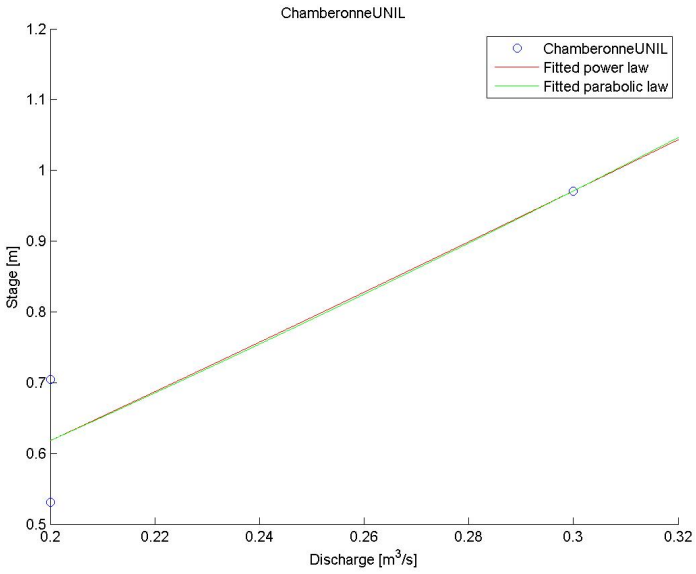

Figure B.6: Rating curve, Chamberonne

B.1 Coefficients of fitted laws

$$Q = a_1 * x^{a_2} \tag{B.1}$$

Station	a_1	a_2
Petite Chamberonne	9.5174	3.5239
Sorge	35.1091	4.8698
Mèbre amont, passerelle	16.2604	2.1216
Mèbre amont, galerie	24.0722	1.5505
Mèbre aval	17.044	6.6474
Chamberonne, UNIL	3.7145	1.1144

Table B.1: Coefficients of fitted power law

$$Q = b_1 * x^2 * b_2 * x + b_3 \tag{B.2}$$

Station	b_1	b_2	b_3
Petite Chamberonne	5.9412	-1.5239	0.074901
Sorge	26.7464	-15.8412	2.4663
Mèbre amont, passerelle	16.182	-0.7431	0.033947
Mèbre amont, galerie	15.4146	8.3257	-0.28154
Mèbre aval	31.3259	-29.5205	7.0936
Chamberonne, UNIL	1.4755	2.7922	0.00053099

Table B.2: Coefficients of fitted parabolic law

B.2 Goodness of fit measures

Station	SSE	R2	DFE	AdjSQU	RSME
Petite Chamberonne	0.0013686	0.99667	10	0.996	0.011699
Sorge	0.067273	0.97106	6	0.96142	0.10589
Mèbre amont, passerelle	0.029034	0.98593	7	0.98191	0.064403
Mèbre amont, galerie	0.0095721	0.99829	5	0.99761	0.043754
Mèbre aval	1.0673	0.92243	13	0.9105	0.28653
Chamberonne, UNIL	0.015138	0.84586	0	NaN	NaN

Table B.3: Goodness-of-fit indicators for fitted parabolic law

Station	SSE	R2	DFE	AdjSQU	RSME
Petite Chamberonne	0.004785	0.98836	11	0.9873	0.020857
Sorge	0.04775	0.97946	7	0.97653	0.082592
Mèbre amont, passerelle	0.029937	0.98549	8	0.98368	0.061173
Mèbre amont, galerie	0.021905	0.99609	6	0.99544	0.060422
Mèbre aval	0.85444	0.9379	14	0.93346	0.24705
Chamberonne, UNIL	0.015138	0.84586	1	0.69172	0.12304

Table B.4: Goodness of fit indicators for the fitted power law

SSE: sum of squares due to error
R2: coefficient of determination or R2
Adjusted R2: degree of freedom adjusted R2
RSME: root mean square error

Sum of squares due to error

$$SSE = \sum_{i=1}^{n} w - i(y_i - f_i)^2 \tag{B.3}$$

Where y_i is the observation and f_i the prediction. A weighting, W_i, can be applied to the data.

The closer to 0 the SSE gets, the smaller the error and therefore better predictions are achieved.

R-square R^2

$$R^2 = 1 - \frac{\sum_{i=1}^{n}(w_i(y_i - f_i)^2)}{\sum_{i=1}^{n}(w_i(y_i - y_{av})^2)} = 1 - \frac{SSE}{SST} \tag{B.4}$$

Here, additionally to the SSE, the total sum of squares (SST) comes into play. y_{av} being the mean of the observed data y_i, R^2 can take a value between 0 and 1. As an example, a R^2 of 0.8 means that the fit explains 80 % of the total variation in the data.

Degrees of Freedom & Adjusted R-Square The degree of freedom (v) is defined as the number of response values (n) minus the number of fitted coefficients (m). The higher the better.

The adjusted R^2 is then defined as

$$adjusted R^2 = 1 - \frac{SSE(n-1)}{SST(v)} \tag{B.5}$$

Root Mean Squared Error RMSE This estimate measures the standard deviation of the random component in the data. It is defined as

$$RMSE = \sqrt{MSE} = \sqrt{SSE/v} \tag{B.6}$$

B.3 Code used for fitting rating curves

```
%%%%% Construction of stage-discharge curves
%%%%% ----------------------------------------------------------------------
%%%%% based on measurements for given stations. A spreadsheat with Q-h
%%%%% relationships has to be available. As a result, plots of fitted
%%%%% curves are given and saved in the folder, goodness-of-fit indicators
%%%%% are stored in structures. Interpretation is up to you...

%%%%% Pascal Stalder (pascal.stalder@epfl.ch), 2013
%%%%% ----------------------------------------------------------------------

clear all
close all
addpath Jaugeages

manning=0;

%%% Import data from excel file
file=importdata('TARAGE_H_Q_pascal.xls');

%%% Definition of station names. New stations can be added without
%%% problems, e.g. S7 =Example_Station. In this case, the variable "stations"
%%% will have to be adjusted accordingly. Changing/adapting names is also
%%% possible, but have to correspond to the names in the excel spreadsheet.

S1='PteChamberonne_Chatelard';
S2='ChamberonneUNIL';
S3='SORGE123';
S4='MEBRE_AVAL';
S5='M0xE8bre_amont_passerelle';
S6='MEBRE_AMONT_galerie';

stations=char(S1,S2,S3,S4,S5,S6);
[rows, max_string]=size(stations);

%%% law that will be used for fitting the curves (can be adjusted, currently only fit1 and fit3 are working)
fit1 = fittype('a1*(x)^a2');
fit2 = fittype('a1*(x+a3)^a2','coeff',{'a1','a2','a3'});
fit3 = fittype('b1*x^2+b2*x+b3','coeff',{'b1','b2','b3'});

%% loop over rows, each row corresponding to a station

for i =1:rows
    i
    %%% read data and define variables discharge and stage
    read_station=getfield(file.data,stations(i,:))
    discharge_name=['Q', stations(i,1:8)];
    h_name=['h',stations(i,1:8)];

```

```
49      %%% save data in separate variables, Q and h per station
50      eval([discharge_name '= read_station(:, 2);']);
51      eval([h_name '= read_station(:, 1);']);
52
53      %%% eliminate NaN (usually first column, station name, but somehow
            not
54      %%% consistent)
55      eval(['sum(isnan(' discharge_name '))'])
56      eval(['sum(isnan(' h_name '))'])
57
58      eval([discharge_name ' = ' discharge_name '(isnan(' discharge_name
            ')==0);']);
59      eval([h_name ' = ' h_name '(isnan(' h_name ')==0);']);
60
61      %%% apply correction (20% error) to large water levels
62  %     eval([discharge_name '(' h_name '>0.4)=' discharge_name '('
        h_name '>0.4)*0.8;'])
63
64
65      %%% Applying Manning-Strickler at Petite Chamberonne
66      if i==1 && manning==1;
67          b=1.24;
68          j=0.01;
69
70          eval(['length_pcham=length( ' discharge_name ');']);
71
72          for k=1:length_pcham
73              eval(['K(k)=(' discharge_name '(k)* ((2*' h_name '(k)+b) .
                    ^(2/3)))/(sqrt(j)*((b*' h_name '(k) ).^(5/3)));'])
74              eval(['K(k)=(' discharge_name '(k)* ((2*' h_name '(k)+b) .
                    ^(2/3)))/(sqrt(j)*((b*' h_name '(k) ).^(5/3)));'])
75
76          end
77          coeff_strickler=50;
78
79          hPteChamb_new=0.48;
80          QPteChamb_new(end+1)=(mean(K)*sqrt(j)*((b*hPteChamb_new)^(5/3)
                ))/((2*hPteChamb_new+b)^(2/3)) ;
81      end
82
83
84      %%% power type of equation, fitting Q = c (h + a)^b (fit1)
85      powerfit_loop1=['pof1',stations(i,1:8)];
86      powerfit_loop2=['pof1',stations(i,1:8)];
87      goodpof1_loop=['goodpof1', stations(i,1:8)];
88
89      eval(['[' powerfit_loop1 ',' goodpof1_loop ']' '= fit(' h_name ','
            discharge_name ',fit1);']);
90
91          %     not yet working ??!! -> complex numbers...? (fit2)
92          %     powerfit_loop1=['pof2',stations(i,1:8)];
93          %     eval([powerfit_loop2 '= fit(' discharge_name ',' h_name
                ',fit2);']);
94
95      %%% parabolic type of equation, fitting  Q= b1*x^2+b2*x+b3 (fit3)
96      parabolic_loop=['paf',stations(i,1:8)];
97      goodpaf_loop=['goodpaf', stations(i,1:8)];
```

```
98      eval(['[' parabolic_loop ',' goodpaf_loop ']'  '= fit(' h_name ','
            discharge_name  ',fit3);']);
99
100     %%% plotting results, fitted curves
101     if true
102         figure(i)
103         hold on
104         eval(['title(''' stations(i,:) ''')']);
105         eval(['plot(' h_name ',' discharge_name ',''o'')']);
106         eval(['plot(' powerfit_loop1 ', ''r'')' ]);
107         eval(['plot(' parabolic_loop ', ''g'')' ]);
108         eval(['legend(''' stations(i,:) ''',''Fitted power law'', ''
                Fitted parabolic law'')' ])
109         xlabel('Stage [m]')
110         ylabel('Discharge [m^3/s]')
111         print(['tarage' stations(i,1:8)], '-djpeg')
112     end
113
114     clear read_station
115
116     eval(['goodpaf_tex=[' goodpaf_loop '.sse ;' goodpaf_loop '.rsquare
            ;' goodpaf_loop '.dfe;' goodpaf_loop '.adjrsquare;'
            goodpaf_loop '.rmse];'])
117     eval(['goodpof_tex=[' goodpof1_loop '.sse ;' goodpof1_loop '
            .rsquare;' goodpof1_loop '.dfe;' goodpof1_loop '.adjrsquare;'
            goodpof1_loop '.rmse];'])
118
119
120     %write variables in latex format, requires function var2tex,
            output can
121     %then be directly imported into latex document
122     if i==1
123
124         eval(['var2tex(''fittedpof.txt'',''w'',''aa' stations(i,1:8) '
                '', ' powerfit_loop1 '.a1);'])
125         eval(['var2tex(''fittedpof.txt'',''a'',''ab' stations(i,1:8) '
                '',' powerfit_loop1 '.a2);'])
126         eval(['var2tex(''fittedpaf.txt'',''w'',''ba' stations(i,1:8) '
                '',' parabolic_loop '.b1);'])
127         eval(['var2tex(''fittedpaf.txt'',''a'',''bb' stations(i,1:8) '
                '',' parabolic_loop '.b2);'])
128         eval(['var2tex(''fittedpaf.txt'',''a'',''bc' stations(i,1:8) '
                '',' parabolic_loop '.b3);'])
129
130         eval(['var2tex(''goodnessoffitpaf.txt'',''w'', ''paf-sse-'
                stations(i,1:8) ''', goodpaf_tex(1) );']);
131         eval(['var2tex(''goodnessoffitpaf.txt'',''a'', ''paf-rsquare-'
                 stations(i,1:8) ''', goodpaf_tex(2) );']);
132         eval(['var2tex(''goodnessoffitpaf.txt'',''a'', ''paf-dfe-'
                stations(i,1:8) ''', goodpaf_tex(3) );']);
133         eval(['var2tex(''goodnessoffitpaf.txt'',''a'', ''paf-adjrsquar
                -' stations(i,1:8) ''', goodpaf_tex(4) );']);
134         eval(['var2tex(''goodnessoffitpaf.txt'',''a'', ''paf-rmse-'
                stations(i,1:8) ''', goodpaf_tex(5) );']);
135
136         eval(['var2tex(''goodnessoffitpof.txt'',''w'', ''pof-sse-'
                stations(i,1:8) ''', goodpof_tex(1) );']);
```

```
137         eval(['var2tex(''goodnessoffitpof.txt'',''a'', ''pof-rsquare-'
                stations(i,1:8) ''', goodpof_tex(2) );']);
138         eval(['var2tex(''goodnessoffitpof.txt'',''a'', ''pof-dfe-'
                stations(i,1:8) ''', goodpof_tex(3) );']);
139         eval(['var2tex(''goodnessoffitpof.txt'',''a'', ''pof-
                adjrsquare-' stations(i,1:8) ''', goodpof_tex(4) );']);
140         eval(['var2tex(''goodnessoffitpof.txt'',''a'', ''pof-rmse-'
                stations(i,1:8) ''', goodpof_tex(5) );']);
141
142     else
143
144         eval(['var2tex(''fittedpof.txt'',''a'',''aa' stations(i,1:8) '
                '', ' powerfit_loop1 '.a1);'])
145         eval(['var2tex(''fittedpof.txt'',''a'',''ab' stations(i,1:8) '
                '',' powerfit_loop1 '.a2);'])
146         eval(['var2tex(''fittedpaf.txt'',''a'',''ba' stations(i,1:8) '
                '',' parabolic_loop '.b1);'])
147         eval(['var2tex(''fittedpaf.txt'',''a'',''bb' stations(i,1:8) '
                '',' parabolic_loop '.b2);'])
148         eval(['var2tex(''fittedpaf.txt'',''a'',''bc' stations(i,1:8) '
                '',' parabolic_loop '.b3);'])
149
150
151         eval(['var2tex(''goodnessoffitpaf.txt'',''a'', ''paf-sse_'
                stations(i,1:8) ''', goodpaf_tex(1) );']);
152         eval(['var2tex(''goodnessoffitpaf.txt'',''a'', ''paf-rsquare_'
                stations(i,1:8) ''', goodpaf_tex(2) );']);
153         eval(['var2tex(''goodnessoffitpaf.txt'',''a'', ''paf-dfe_'
                stations(i,1:8) ''', goodpaf_tex(3) );']);
154         eval(['var2tex(''goodnessoffitpaf.txt'',''a'', ''paf-
                adjrsquare_' stations(i,1:8) ''', goodpaf_tex(4) );']);
155         eval(['var2tex(''goodnessoffitpaf.txt'',''a'', ''paf-rmse_'
                stations(i,1:8) ''', goodpaf_tex(5) );']);
156
157         eval(['var2tex(''goodnessoffitpof.txt'',''a'', ''pof-sse-'
                stations(i,1:8) ''', goodpof_tex(1) );']);
158         eval(['var2tex(''goodnessoffitpof.txt'',''a'', ''pof-rsquare-'
                stations(i,1:8) ''', goodpof_tex(2) );']);
159         eval(['var2tex(''goodnessoffitpof.txt'',''a'', ''pof-dfe-'
                stations(i,1:8) ''', goodpof_tex(3) );']);
160         eval(['var2tex(''goodnessoffitpof.txt'',''a'', ''pof-
                adjrsquare-' stations(i,1:8) ''', goodpof_tex(4) );']);
161         eval(['var2tex(''goodnessoffitpof.txt'',''a'', ''pof-rmse-'
                stations(i,1:8) ''', goodpof_tex(5) );']);
162     end
163     eval(['clear  ' goodpof1_loop '  ' goodpaf_loop '   rows'])
164
165 end
166
167
168 %%end of script
```

B.4 Code used for interpolation

```
%%%% Interpolation of discharge based on stage measurements
%%%% Requires stage_discharge to be launched previously

%%%% Pascal Stalder, (pascal.stalder@epfl.ch), 2013

addpath(genpath('C:\Users\Pascal\Documents\EPFL\Unterricht\PDM'))

close all

edit_stage=1;
edit_tarage=0;
edit_mean=0;
%% Part ONE, should be improved (xlsread takes over a minute...)

'importing data, may take some minutes'

S1='PteChamberonne_Chatelard';
S2='ChamberonneUNIL';
S3='SORGE123';
S4='MEBRE_AVAL';
S5='M0xE8bre_amont_passerelle';
S6='MEBRE_AMONT_galerie';

stations=char(S1,S2,S3,S4,S5,S6);
[rows, max_string]=size(stations);
%
Mamont_gal2009=xlsread('MAMONT_galerie\Mamont_2009.xlsx');
Mamont_gal2010=xlsread('MAMONT_galerie\Mamont_2010.xlsx');
Mamont_gal2011=xlsread('MAMONT_galerie\Mamont_2011.xlsx');
Mamont_gal2012=xlsread('MAMONT_galerie\Mamont_2012.xlsx');
Mamont_gal2013=xlsread('MAMONT_galerie\Mamont_2013.xlsx');

eval(['data.' stations(6,1:8) '=[Mamont_gal2009(:,1:2);Mamont_gal2010
    (:,1:2);Mamont_gal2011(:,1:2);Mamont_gal2012(:,1:2);Mamont_gal2013
    (:,1:2)];']);

Mamont_pass2012=xlsread('MAMONT_passerelle\
    MAMONT_passerellel_2012.xlsx');
Mamont_pass2013=xlsread('MAMONT_passerelle\
    MAMONT_passerellel_2013.xlsx');

eval(['data.' stations(5,1:8) '=[Mamont_pass2012(:,1:2);
    Mamont_pass2013(:,1:2)];']);

Maval2009=xlsread('MAVAL\MAval_2009.xlsx');
Maval2010=xlsread('MAVAL\MAval_2010.xlsx');
Maval2011=xlsread('MAVAL\MAval_2011.xlsx');
Maval2012=xlsread('MAVAL\MAval_2012.xlsx');
Maval2013=xlsread('MAVAL\MAval_2013.xlsx');

eval(['data.' stations(4,1:8) '=[Maval2009(:,1:2);Maval2010(:,1:2);
    Maval2011(:,1:2);Maval2012(:,1:2);Maval2013(:,1:2)];']);

```

```
48 PChamb2012=xlsread('Petite_CHAMBERONNE\Pte_Chamberonne_2012.xlsx');
49 PChamb2013=xlsread('Petite_CHAMBERONNE\Pte_Chamberonne_2013.xlsx');
50
51 eval(['data.' stations(1,1:8) '=[PChamb2012(2:end,1:2);PChamb2013(2:
       end,1:2)];']);
52
53 Sor2009=xlsread('SOR\Sor_2009.xlsx');
54 Sor2010=xlsread('SOR\Sor_2010.xlsx');
55 Sor2011=xlsread('SOR\Sor_2011.xlsx');
56 Sor2012=xlsread('SOR\Sor_2012.xlsx');
57 Sor2013=xlsread('SOR\Sor_2013.xlsx');
58
59 eval(['data.' stations(3,1:8) '=[Sor2009(:,1:2);Sor2010(:,1:2);Sor2011
       (:,1:2);Sor2012(:,1:2);Sor2013(:,1:2)];']);
60
61 eval(['data.' stations(2,1:8) '= zeros(100,2);']);
62
63 clear Sor2009 Sor2010 Sor2011 Sor2012 Sor2013
64 clear PChamb2012 PChamb2013
65 clear Maval2009 Maval2010 Maval2011 Maval2012 Maval2013
66 clear Mamont_gal2009 Mamont_gal2010 Mamont_gal2011 Mamont_gal2012
       Mamont_gal2013
67 clear Mamont_pass2012 Mamont_pass2013
68 %% Part Two
69
70
71 for i=1:rows
72
73     ['calculating station: '  stations(i,:)]
74
75     %%% correction factor for strange date format
76     %%% data correction (due to issue on computer where script has
           been
77     %%% written: openoffice only, hence read data from xls is
           erroneous.
78     %%% sadly, has to be done manually. Eventually can be removed if
           issue
79     %%% resolved, check manually!
80     eval(['date_wrong=data.' stations(i,1:8) '(1,1);']);
81
82     if strcmp(stations(i,1:8),'PteChamb')
83         date_right=datenum(2012,04,30,11,10,00);
84     elseif strcmp(stations(i,1:8),'SORGE123')
85         date_right=datenum(2009,12,8,12,55,03);
86     elseif strcmp(stations(i,1:8),'MEBRE_AV')
87         date_right=datenum(2009,12,11,13,15,00);
88     elseif strcmp(stations(i,1:8),'M0xE8bre')
89         date_right=datenum(2012,04,27,12,05,00);
90     elseif strcmp(stations(i,1:8),'MEBRE_AM')
91         date_right=datenum(2009,12,15,12,45,03);
92     else
93         'no date correction'
94     end
95
96     correction=date_right-date_wrong
97
```

```
98      eval(['data.' stations(i,1:8) '(:,1)=data.' stations(i,1:8) '(:,1)
            +correction;']);
99
100     %%remove NaN at first position (header). Replace with value at
            second
101     %%position (not really nice, could be adapted).
102     if eval(['isnan(data.' stations(i,1:8) '(1,1)) == 1 '] )
103         eval(['data.' stations(i,1:8) '(1,:)=data.' stations(i,1:8) '
                (2,:);']);
104     end
105
106 %     %% apply correction factor to large water levels (large= bigger
    than
107 %     %% 0.55m), cap at 0.55m or 20% error
108 %
109 %     eval(['n=length(data. ' stations(i,1:8) '(:,1));']);
110 %
111 %     for m=1:n
112 %
113 %         if eval(['data.' stations(i,1:8) '(m,2)>0.55;'])
114 %             eval(['data.' stations(i,1:8) '(m,2)=max(0.55, (0.8*
    data.' stations(i,1:8) '(m,2)))']);
115 %         end
116 %     end
117
118
119     %%% Apply power law (fit1 from script stage_discharge)
120     eval(['coeff_a1=pof1' stations(i,1:8) '.a1;']);
121     eval(['coeff_a2=pof1' stations(i,1:8) '.a2;']);
122     %%% INTERPOLATION takes place here
123     eval(['data.' stations(i,1:8) '(:,3)= coeff_a1*data.' stations(i
            ,1:8) '(:,2).^coeff_a2;']);
124
125     %%% Apply parabolic law (fit3 from script stage_discharge)
126     eval(['coeff_b1=paf' stations(i,1:8) '.b1;']);
127     eval(['coeff_b2=paf' stations(i,1:8) '.b2;']);
128     eval(['coeff_b3=paf' stations(i,1:8) '.b3;']);
129     %%% INTERPOLATION takes place here
130     eval(['data.' stations(i,1:8) '(:,4)= coeff_b1*data.' stations(i
            ,1:8) '(:,2).^2 + coeff_b2*data.' stations(i,1:8) '(:,2)+
            coeff_b3;']);
131
132
133     %%% Calculate hourly mean (measurements are every 5 minutes)
134
135     eval(['hourly_date.' stations(i,1:8) '= (round(1+24*data.'
            stations(i,1:8) '(1,1))/24): 1/24 : ((round(24*data.' stations
            (i,1:8) '(end,1))/24));'])
136     eval(['length_hour=length(hourly_date.' stations(i,1:8) ');'])
137
138     eval(['hourly_meanQ.' stations(i,1:8) '_pow=zeros(1,length_hour-1)
            ;'])
139     eval(['hourly_meanQ.' stations(i,1:8) '_par=zeros(1,length_hour-1)
            ;'])
140
141     for k=1:(length_hour-1)
```

```
142         eval(['idx_inf=min(find(data.' stations(i,1:8) '(:,1) >
                hourly_date.' stations(i,1:8) '(k)));'])
143         eval(['idx_sup=max(find(data.' stations(i,1:8) '(:,1) ≤
                hourly_date.' stations(i,1:8) '(k+1)));'])
144
145         eval(['hourly_meanQ.' stations(i,1:8) '_pow(k)=mean(data.'
                stations(i,1:8) '(idx_inf:idx_sup,3));' ])
146         eval(['hourly_meanQ.' stations(i,1:8) '_par(k)=mean(data.'
                stations(i,1:8) '(idx_inf:idx_sup,4));' ])
147     end
148
149     eval(['hourly_meanQ.' stations(i,1:8) '_par=hourly_meanQ.'
            stations(i,1:8) '_par'';'])
150     eval(['hourly_meanQ.' stations(i,1:8) '_pow=hourly_meanQ.'
            stations(i,1:8) '_pow'';'])
151
152     eval(['hourly_date.' stations(i,1:8) '= hourly_date.' stations(i
            ,1:8) '(1:(end-1));'])
153     eval(['hourly_date.' stations(i,1:8) '=hourly_date.' stations(i
            ,1:8) ''';'])
154
155
156
157     %%% storing data in format adapted to model input
158     if eval(['exist(''hourly_meanQ.' stations(i,1:8) '_par'')']) &&
            eval(['exist(''hourly_meanQ.' stations(i,1:8) '_pow'')'])
159
160         eval(['dummy.dateQobs=hourly_date.' stations(i,1:8) ';'])
161
162         eval(['dummy.Qobs=hourly_meanQ.' stations(i,1:8) '_pow;'])
163         eval(['save(''' stations(i,1:8) 'pow.mat'', ''-struct'',''
                dummy'')'])
164
165         eval(['dummy.Qobs=hourly_meanQ.' stations(i,1:8) '_par'])
166         eval(['save(''' stations(i,1:8) 'par.mat'', ''-struct'',''
                dummy'')'])
167     end
168
169     %%%% plot the fitted time series, each station
170     if edit_stage
171         figure()
172         hold on
173         grid on
174         eval(['plot(data.' stations(i,1:8) '(:,1),data.' stations(i
                ,1:8) '(:,2), data.' stations(i,1:8) '(:,1),data.'
                stations(i,1:8) '(:,3),''r'')']);
175         eval(['plot(data.' stations(i,1:8) '(:,1),data.' stations(i
                ,1:8) '(:,4),''g'')']);
176         legend('Stage','Power law fitted discharge', 'Parabolic law
                fitted discharge')
177         eval(['title(''' stations(i,:) ''')']);
178         xlabel('Date')
179         datetick('x','mm/yyyy')
180         print(['interpolated' stations(i,1:8)], '-djpeg')
181     end
182
183     if 1
```

```
184         figure()
185         hold on
186         grid on
187         eval(['plot(data.' stations(i,1:8) '(:,2),data.' stations(i
                ,1:8) '(:,3), ''*'') ']);
188         eval(['plot(data.' stations(i,1:8) '(:,2),data.' stations(i
                ,1:8) '(:,4), ''*r'')']);
189         legend('Fitted power law', 'Fitted parabolic law')
190         eval(['title(''Recreated stage-discharge curve: ' stations(i
                ,:) ''')']);
191         xlabel('Stage [m]')
192         ylabel('Discharge [m]')
193         print(['recreatedtarage' stations(i,1:8)], '-djpeg')
194     end
195
196
197
198     if edit_mean && eval(['exist(''hourly_meanQ_' stations(i,1:8) '
            _par'')']) && eval(['exist(''hourly_meanQ_' stations(i,1:8) '
            _pow'')'])
199         figure()
200         hold on
201         grid on
202         eval(['plot(data.' stations(i,1:8) '(:,1),data.' stations(i
                ,1:8) '(:,3)) ']);
203         eval(['plot(hourly_date_' stations(i,1:8) ', hourly_meanQ_'
                stations(i,1:8) '_pow, ''r'')']);
204         legend('Measurements: 5min', 'Converted: 1h')
205         eval(['title(''Conversion to hourly mean discharge (power law)
                : ' stations(i,:) ''')']);
206         xlabel('time')
207         ylabel('Discharge [m^3/s]')
208         datetick('x','mm/yyyy')
209         print(['convertedhourlymean_pow_' stations(i,1:8)], '-djpeg')
210
211         figure()
212         hold on
213         grid on
214         eval(['plot(data.' stations(i,1:8) '(:,1),data.' stations(i
                ,1:8) '(:,4)) ']);
215         eval(['plot(hourly_date_' stations(i,1:8) ',hourly_meanQ_'
                stations(i,1:8) '_par, ''r'')']);
216         legend('Measurements: 5min', 'Converted: 1h')
217         eval(['title(''Conversion to hourly mean discharge (parabolic
                law): ' stations(i,:) ''')']);
218         xlabel('time')
219         ylabel('Discharge [m^3/s]')
220         print(['convertedhourlymean_par_' stations(i,1:8)], '-djpeg')
221     end
222
223     i
224 end
225
226 %%% extract raw data
227
228 save('5min_allstations.mat', '-struct','data');
229
```

```
230
231 %end of script
```

Appendix C

Appendix: Rain

C.1 Code: Comparison of different rain gauges at 4 locations(EPFL, Crissier, Pully & Chatelard)

```
%%% rain comparaison of pluvio Chatelard, EPFL, Crissier and Pully

%%% Pascal Stalder, 2013 (pascal.stalder@epfl.ch)

clear all
close all

addpath(genpath(cd))

%% Part ONE: read input data
rain_chat=[xlsread('Chatelard_PLUVIO_2012.xlsx');  xlsread('
    Chatelard_PLUVIO_2013.xlsx')];
rain_epfl=[xlsread('METEO_2011.xlsx');xlsread('METEO_2012.xlsx');
    xlsread('METEO_2013.xlsx')];
read_pully=importdata('EPFLMebreSorge\order20005\order_20005_data.txt'
    );
load('rainCrissier.mat')

%replace NaN by the rain occuring the previous/next year
for i=1:length(rainCrissier)
     if isnan(rainCrissier(i))==1 && (i+24*365)< numel(rainCrissier)
         rainCrissier(i)=rainCrissier(i+24*365);
     elseif isnan(rainCrissier(i))==1 && (i+24*365) > numel(
         rainCrissier)
         rainCrissier(i)=rainCrissier(i-24*365);
     end
end

% rain_crissier=xlsread('rain_crissier.xls');
%% Part TWO: correct dates

%%% date correction chatelard
date_wrong=rain_chat(1,1);
date_right=datenum('05-01-2012 23:16');
```

```
31 correction=date_right-date_wrong;
32
33 rain_chat(:,1)=rain_chat(:,1)+correction;
34
35 %%% define new date, 1h time step
36 new_date_chat=(round(rain_chat(1,1)):(1/24):round(rain_chat(end,1)))';
37
38 %%% date correction epfl
39 date_wrong=rain_epfl(1,1);
40 date_right=datenum('01-01-2011');
41 correction=date_right-date_wrong;
42
43 rain_epfl(:,1)=rain_epfl(:,1)+correction;
44
45 new_date_epfl=(round(rain_epfl(1,1)):(1/24):round(rain_epfl(end,1)))';
46
47 v_date_epfl=datevec(new_date_epfl);
48 v_date_chat=datevec(new_date_chat);
49 v_date_Crissier=datevec(dateCrissier);
50 %% Part THREE: reshape Pully input data
51
52 rain_pully=read_pully.data(:,2);
53 rain_pully=rain_pully./24;
54 date_pully=read_pully.data(:,1);
55 string_date=num2str(date_pully);
56 year_pully=string_date(:,1:4);
57 month1_pully=string_date(:,5:6);
58 day_pully=string_date(:,7:8);
59 hour_pully=string_date(:,9:10);
60 for i=1:length(month1_pully)
61     date_string(i,:)=[year_pully(i,:), '/', month1_pully(i,:) ,'/',
          day_pully(i,:), '  ', hour_pully(i,:),':00'];
62 end
63 date_pully=datenum(date_string);
64
65 v_date_pully=datevec(date_pully);
66
67 %% Part FOUR: new method, counting rainfall events per one hour
68 new_rain_chat=zeros(length(new_date_chat),1);
69 new_rain_epfl=zeros(length(new_date_epfl),1);
70
71 for i=1:length(new_date_chat)-1
72     idx_sup=min(find(rain_chat(:,1)>new_date_chat(i)));
73     idx_inf=max(find(rain_chat(:,1)≤new_date_chat(i+1)));
74     new_rain_chat(i)=sum(rain_chat(idx_sup:idx_inf,2));
75 end
76
77 for i=1:length(new_date_epfl)-1
78     idx_sup=min(find(rain_epfl(:,1)>new_date_epfl(i)));
79     idx_inf=max(find(rain_epfl(:,1)≤new_date_epfl(i+1)));
80     new_rain_epfl(i)=sum(rain_epfl(idx_sup:idx_inf,2));
81 end
82
83 %% Part FIVE: daily statistics
84 daily_date_pully=min(date_pully):max(date_pully)-1;
85 daily_date_chat=min(new_date_chat):max(new_date_chat)-1;
86 daily_date_epfl=min(new_date_epfl):max(new_date_epfl)-1;
```

```
87  daily_date_Crissier=round(min(dateCrissier)):round(max(dateCrissier))
        -1;
88
89  for i=1:length(daily_date_pully);
90      daily_rain_pully(i)=sum(rain_pully((1+(i-1)*24:24+(i-1)*24)));
91  end
92
93  for i=1:length(daily_date_epfl);
94      daily_rain_epfl(i)=sum(new_rain_epfl((1+(i-1)*24:24+(i-1)*24)));
95  end
96
97  for i=1:length(daily_date_chat);
98      daily_rain_chat(i)=sum(new_rain_chat((1+(i-1)*24:24+(i-1)*24)));
99  end
100 for i=1:length(daily_date_Crissier);
101     daily_rain_Crissier(i)=sum(rainCrissier((1+(i-1)*24:24+(i-1)*24)))
            ;
102 end
103
104 %% Part SIX: monthly statistics
105
106 month_pully(1)=v_date_pully(1,2);
107 month_epfl(1)=v_date_epfl(1,2);
108 month_chat(1)=v_date_chat(1,2);
109 month_Crissier(1)=v_date_Crissier(1,2);
110
111 k=1;
112 monthly_rain_pully(1)=0;
113 for i=1:length(v_date_pully(:,2))
114     if v_date_pully(i,2)==month_pully(k)
115         monthly_rain_pully(k)=monthly_rain_pully(k)+rain_pully(i);
116     elseif v_date_pully(i,2)≠month_pully(k)
117
118         if month_pully(k)<12
119             month_pully(k+1)=month_pully(k)+1;
120         elseif month_pully(k)==12
121             month_pully(k+1)=1;
122         end
123
124         k=k+1;
125         monthly_rain_pully(k)=rain_pully(i);
126     end
127 end
128
129 k=1;
130 monthly_rain_chat(1)=0;
131
132 for i=1:length(v_date_chat(:,2))
133     if v_date_chat(i,2)==month_chat(k)
134         monthly_rain_chat(k)=monthly_rain_chat(k)+new_rain_chat(i);
135     elseif v_date_chat(i,2)≠month_chat(k)
136
137         if month_chat(k)<12
138             month_chat(k+1)=month_chat(k)+1;
139         elseif month_chat(k)==12
140             month_chat(k+1)=1;
141         end
```

```
142
143         k=k+1;
144         monthly_rain_chat(k)=new_rain_chat(i);
145     end
146 end
147
148 k=1;
149 monthly_rain_epfl(1)=0;
150
151 for i=1:length(v_date_epfl(:,2))
152     if v_date_epfl(i,2)==month_epfl(k)
153         monthly_rain_epfl(k)=monthly_rain_epfl(k)+new_rain_epfl(i);
154     elseif v_date_epfl(i,2)≠month_epfl(k)
155
156         if month_epfl(k)<12
157             month_epfl(k+1)=month_epfl(k)+1;
158         elseif month_epfl(k)==12
159             month_epfl(k+1)=1;
160         end
161
162         k=k+1;
163         monthly_rain_epfl(k)=new_rain_epfl(i);
164     end
165 end
166
167 k=1;
168 monthly_rain_Crissier(1)=0;
169 for i=1:length(v_date_Crissier(:,2))
170     if v_date_Crissier(i,2)==month_Crissier(k)
171         monthly_rain_Crissier(k)=monthly_rain_Crissier(k)+rainCrissier
                (i);
172     elseif v_date_Crissier(i,2)≠month_Crissier(k)
173
174         if month_Crissier(k)<12
175             month_Crissier(k+1)=month_Crissier(k)+1;
176         elseif month_Crissier(k)==12
177             month_Crissier(k+1)=1;
178         end
179
180         k=k+1;
181         monthly_rain_Crissier(k)=rainCrissier(i);
182     end
183 end
184
185 %% Part SEVEN: Cumulative dist
186
187 common_date=max([min(daily_date_chat),min(daily_date_epfl),min(
        daily_date_pully),min(daily_date_Crissier)]'):min([max(
        daily_date_Crissier),max(daily_date_chat),max(daily_date_epfl),max
        (daily_date_pully)]');
188
189
190 cum_rain_epfl=cumsum(daily_rain_epfl(find(daily_date_epfl==common_date
        (1)):find(daily_date_epfl==common_date(end))));
191 cum_rain_chat=cumsum(daily_rain_chat(find(daily_date_chat==common_date
        (1)):find(daily_date_chat==common_date(end))));
```

```
192 cum_rain_pully=cumsum(daily_rain_pully(find(daily_date_pully==
        common_date(1)):find(daily_date_pully==common_date(end))));
193 cum_rain_Crissier=cumsum(daily_rain_Crissier(find(daily_date_Crissier
        ==common_date(1)):find(daily_date_Crissier==common_date(end))));
194
195
196 %% Part Eight: plot and compare, use for recreation of rain
197 %
198 figure(1)
199 hold on
200 plot(daily_date_chat,daily_rain_chat)
201 plot(daily_date_epfl,daily_rain_epfl,'r')
202 % plot(daily_date_pully,daily_rain_pully,'g')
203 plot(daily_date_Crissier,daily_rain_Crissier,'m')
204 xlabel('Date')
205 datetick('x','dd/mm/yyyy')
206 ylabel('Rainfall [mm/day]')
207 legend('Chatelard','EPFL','Crissier')
208
209 figure(2)
210 hold on
211 plot(common_date,cum_rain_chat)
212 plot(common_date,cum_rain_epfl, 'r')
213 plot(common_date,cum_rain_pully, 'g')
214 plot(common_date,cum_rain_Crissier,'m')
215 legend('Chatelard','EPFL','Pully','Crissier')
216 xlabel('Date')
217 datetick('x','dd/mm/yyyy')
218 ylabel('Cumulative Rainfall [mm]')
219
220
221 figure(3)
222 hold on
223 plot(month_chat,monthly_rain_chat, 'linestyle','o')
224 plot(month_epfl,monthly_rain_epfl, 'linestyle','o', 'color', 'r')
225 plot(month_pully,monthly_rain_pully, 'linestyle','o', 'color','g')
226 plot(month_Crissier,monthly_rain_Crissier, 'linestyle','o','color','m'
        )
227 legend('Chatelard','EPFL','Pully','Crissier')
228 xlabel('Date')
229 ylabel('Monthly rainfall [mm/month]')
230
231
232 %% Part NINE: Recreation of reasonnable rain pattern at chatelard
233
234 %%% find point where it seems normal (around end of summer 2012)
235 %%% endpoint of longest sequence of zeros:¬  2100
236
237 tail_rain_chat=new_rain_chat(2100:end);
238 date_stop=new_date_chat(2100);
239 % index_stop=find(new_date_epfl==date_stop);
240 % front_rain_chat=new_rain_epfl(1:index_stop);
241 %
242 % index_stop=find(dateCrissier==date_stop);
243 % front_rain_chat_Crissier=rainCrissier(1:index_stop);
244
245 index_stop=find(dateCrissier==date_stop);
```

```
246 front_rain_chat_Crissier=rainCrissier(1:index_stop);
247
248 rec_rain=[front_rain_chat_Crissier;tail_rain_chat];
249
250
251 %% Part TEN: redo daily & monthly statistics for reconstructed data
        and all the other stuff
252 rec_date=daily_date_Crissier(1):(1/24):new_date_chat(end);
253 day_rec=daily_date_Crissier(1):new_date_chat(end)-1;
254 v_date_rec=datevec(rec_date);
255
256 % v_date_rec=v_date_rec(1:length(rec_date), :);
257
258 for i=1:length(day_rec)
259     daily_rec_rain(i)=sum(rec_rain((1+(i-1)*24:24+(i-1)*24)));
260 end
261
262
263 monthly_rain_rec(1)=0;
264 month_rec(1)=v_date_rec(1,2);
265 k=1;
266 for i=1:length(v_date_rec(:,2))-1
267     if v_date_rec(i,2)==month_rec(k)
268         monthly_rain_rec(k)=monthly_rain_rec(k)+rec_rain(i);
269     elseif v_date_rec(i,2)~=month_rec(k)
270
271         if month_rec(k)<12
272             month_rec(k+1)=month_rec(k)+1;
273         elseif month_rec(k)==12
274             month_rec(k+1)=1;
275         end
276
277         k=k+1;
278         monthly_rain_rec(k)=rec_rain(i);
279     end
280 end
281
282 common_date_rec=max([min(daily_date_Crissier) min(day_rec),min(
        daily_date_epfl),min(daily_date_pully)]):min([max(
        daily_date_Crissier) max(day_rec),max(daily_date_epfl),max(
        daily_date_pully)]);
283
284
285 cum_rain_epfl=cumsum(daily_rain_epfl(find(daily_date_epfl==
        common_date_rec(1)):find(daily_date_epfl==common_date_rec(end))));
286 cum_rec=cumsum(daily_rec_rain(find(day_rec==common_date_rec(1)):find(
        day_rec==common_date_rec(end))));
287 cum_rain_pully=cumsum(daily_rain_pully(find(daily_date_pully==
        common_date_rec(1)):find(daily_date_pully==common_date_rec(end))))
        ;
288 cum_rain_Crissier=cumsum(daily_rain_Crissier(find(daily_date_Crissier
        ==common_date_rec(1)):find(daily_date_Crissier==common_date_rec(
        end))));
289
290 %% Plot results
291
292 figure()
```

```
293 plot(rec_date(1:end-1), rec_rain)
294 legend('Reconstructed Rainfall')
295 ylabel('Rainfall mm/h')
296 xlabel('Date')
297 datetick('x','mm/yyyy')
298
299
300
301 figure()
302 hold on
303 plot(common_date_rec,cum_rec)
304 plot(common_date_rec,cum_rain_epfl, 'r')
305 plot(common_date_rec,cum_rain_pully, 'g')
306 plot(common_date_rec,cum_rain_Crissier, 'm')
307 legend('Reconstructed','EPFL','Pully', 'Crissier')
308 xlabel('Date')
309 datetick('x','dd/mm/yyyy')
310 ylabel('Cumulative Rainfall [mm]')
311
312 %% Save results
313 % Constructed_prec_dt1h.J=rec_rain;
314 % Constructed_prec_dt1h.dateJ=rec_date;
315 % Constructed_prec_dt1h.dtJ=3600;
316
317 modrainCrissier.J=rainCrissier;
318 modrainCrissier.dtJ=3600;
319 modrainCrissier.dateJ=dateCrissier;
320
321
322 save('modrainCrissier.mat','-struct','modrainCrissier')
```

C.2 Additional figures for recreated rainfall

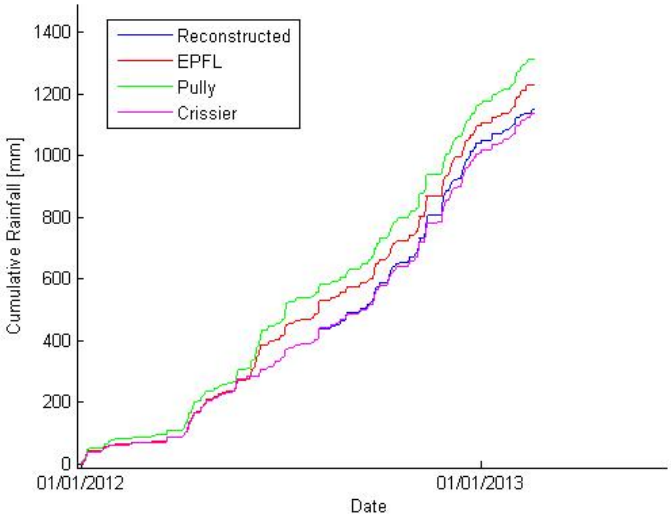

Figure C.1: Cumulative rainfall of all four stations, as well as the reconstructed rainfall series

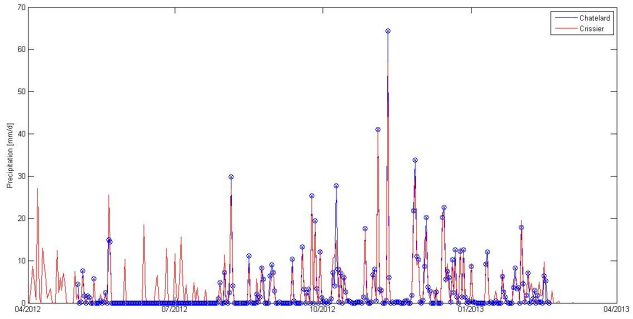

Figure C.2: Overlay of daily rainfall at Chatelard and Crissier. An extremely good match can be observed, except for the period where the gauge at Chatelard has not been working properly.

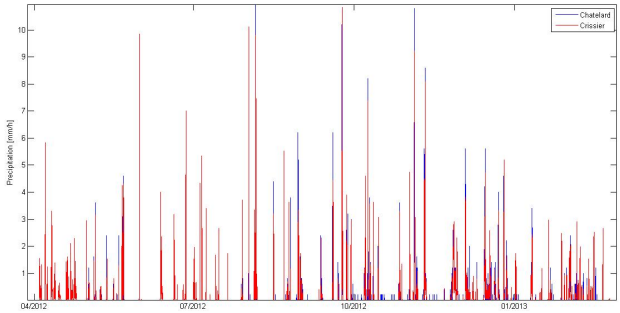

Figure C.3: Hourly rainfall at Crissier and Chatelard. Even at an hourly timestep, a good match can be observed.

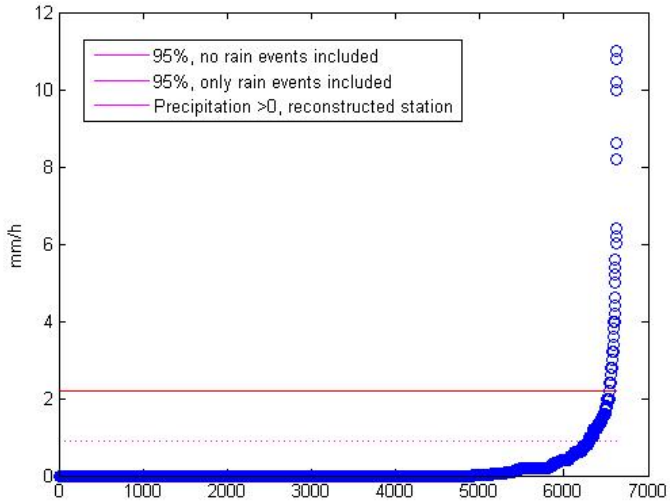

Figure C.4: Sorted reconstructed rainfall and indications of 95 percentiles.

Appendix D

Appendix: Potential Evapotranspiration

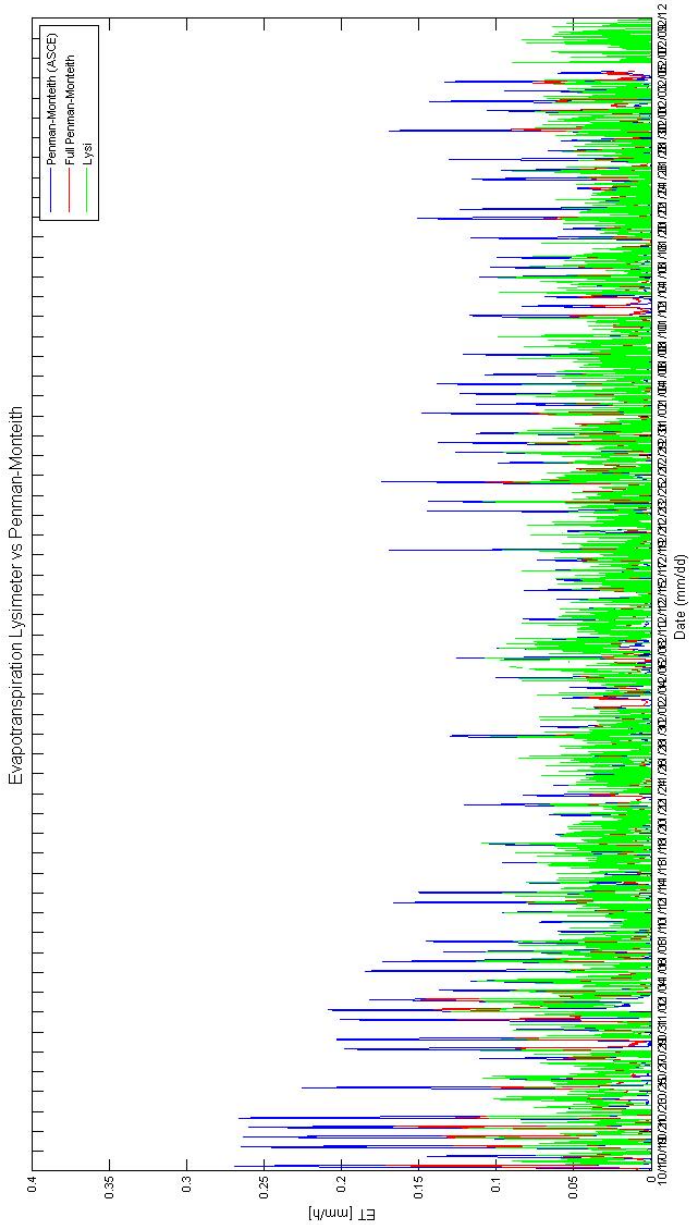

Appendix E

Appendix: Additional and/or new Matlab functions

E.1 Computation of storage fluxes

```
function [Q, L]=estSTOREflux(S,k,param, Extra)

%read variables and required parameter
nl=Extra.nonlinear;
dt=Extra.dt;
phi=param(Extra.paramind.phi);
series=Extra.series;

%Compute corresponding storage flux
%-------------------------------------

if nl==0
    Q(1,:)=k.*S(1,:);
end

if nl==1
    Q(1,:)=k.*S(1,:).^2;
end


%Compute L, if reservoir setup = in series, and this is Ssub
%-------------------------------------
if series==1
    L=min(S/dt,phi);
end

if series==0
    L=0;
end
```

E.2 Estimation of soil layer fluxes

```
function [Rs,I,ET,L]=estSEHRfluxesV02(s,Tpot,Peq,Ksat,c,rho,Zr,s1,sw,
    smax,A,Aimp,dt, alpha, Extra)


 L(1,:)= Ksat.*s.^c;   % mm/s

if Extra.horton==0
    % DUNNE INFILTRATION
    % available space for infiltration
    % attention:
    % check with formulation where the available space accounts for
        water that is leaving through
    % leaching during the same time step

    infspace(1,:)=rho*Zr*(smax-s); % infiltration space

    RsA(1,:)=max(0,Peq(1,:)-infspace/dt-L);
    RsAimp= Peq(1,:).*Aimp./A; % mm/s
    Rs=RsA+RsAimp;

    I(1,:)=Peq(1,:).*(1+Aimp./A)-Rs; % [mm/s]
    %comb: infiltration with respect to entire area, including
    %impervious
elseif Extra.horton==1
    % HORTON INFILTRATION

    RsA(1,:)=max(0,((s./smax).^alpha).*Peq-L);
    RsAimp= Peq(1,:).*Aimp./A;
    Rs=RsA+RsAimp;

    I(1,:)=Peq(1,:).*(1+Aimp./A)-Rs;
end

ET(1,:)=max(0,min(Tpot,Tpot.*((s-sw)/(s1-sw)))); % mm/s

% the checks for physical constraints should probably not be done in
    here but in the
% main algorithm, which proposes an s that is used in this function


% 1st correction for leaching: leaching cannot be bigger than
    available water in soil
L(1,:)=min(((smax-s)*Zr*rho)/dt,L); % mm/s
waterdef=max(-min(L),0); % positive if there is a deficit
L(waterdef>0)=L(waterdef>0)+waterdef;
ET(waterdef>0)=ET(waterdef>0)-waterdef;

% 2n correction s cannot be bigger smax
sproj=((s*Zr*rho)/dt+I-L-ET)/(Zr*rho)*dt;
waterexceed=max(0,(sproj-smax)*Zr*rho);
I(waterexceed>0)=I(waterexceed>0)-waterexceed(waterexceed>0);
Rs(waterexceed>0)=Rs(waterexceed>0)+waterexceed(waterexceed>0);

```

```
% 3rdn correction s cannot be smaller than 0
sproj=((s*Zr*rho)/dt+I-L-ET)/(Zr*rho)*dt;
waterdef=max(0,(0-sproj)*Zr*rho);
ET(waterdef>0)=ET(waterdef>0)-waterdef(waterdef>0);
```

E.3 Function for the computation of the water age and pesticide mass output

```
function [Wage Mout Mage]=sehrechoV07(Lh, param,Extra, t, Minf)
% %%%%%%%%%%%%%%%%%%%%%%%%%%%%%%%%%%%%%%%%%%%%%%%%%%%%%%%%%%%%%%%%%%%%%%%%%%
% This code is part of the Spatially-Explicit Hydrologic Response (SEHR)
% model of the ECHO laboratory, EPFL; see MainSEHR for details.
% %%%%%%%%%%%%%%%%%%%%%%%%%%%%%%%%%%%%%%%%%%%%%%%%%%%%%%%%%%%%%%%%%%%%%%%%%%

% this is the time based water age calculation (see Master thesis Stalder,
% 2013) and corresponding mass output from the active soil layer

% 1. initialize variables
% 2. fill water age vector at the bottom with Ih
% 3. remove water (Vout=ETh+Lh) at the top, until Vout is achieved
% 4. keep track of indices where water has been removed (index corresponds
% to "time of entrance" of water
% 5. remove corresponding mass from mass age vector
% 6. generate mass output vector

N=Extra.N;
Nsc=Extra.Nsc;

% 1. initialize variables
Wage=zeros(N,Nsc);
Mout=zeros(N,Nsc);
Mage=zeros(N,Nsc);
Vouttest=zeros(1,Nsc);

% 2. fill water age and mass input at i=t;
Wage(t,:)=Ih;
Mage(t,:)=Minf;

% 3. remove water from bottom
Vouttot=ETh+Lh;

i=1;
while Vouttest(1,:)<Vouttot
    Vouttest(1,:)=Vouttest(1,:)+Wage(i,:);
    i=i+1;
end

```

```
Vouttest=sum(Wage(1:i-1,:));
Vremaining=Vouttot-Vouttest;
Wage(i,:)=Wage(i,:)-Vremaining;

if any(Wage)<0
    display('Water age vector below zero')
end
```

E.4 No snow module

```
function [Peq,Hn,Wn,rain,Qice,Mn,Mngr,balcheck]=nosnow(Extra,snowpar)
%%%%%%%%%%%%%%%%%%%%%%%%%%%%%%%%%%%%%%%%%%%%%%%%%%%%%%%%%%%%%%%%%%%%%%%%%%%
% This code is part of the Spatially-Explicit Hydrologic Response (SEHR)
% model of the ECHO laboratory, EPFL; see MainSEHR for details.
%%%%%%%%%%%%%%%%%%%%%%%%%%%%%%%%%%%%%%%%%%%%%%%%%%%%%%%%%%%%%%%%%%%%%%%%%%%

% input: an: degree-day factor for snowmelt in mm/C/day("n" stands for neige)
% units:
% Peq: mm/s
% Hn, Wn etc: mm
% This script is written in order to simulate a no-snow event. Used and written
% during the master thesis of Pascal Stalder, 2013. Instead of calling
% snowmod, replace name by nosnow, but keep same structure.

Nsc=Extra.Nsc;
nsteps=Extra.N; % attention: in this function, N stands for snowfall (french: neige)
dt=Extra.dt;

altstat=Extra.altstat; % in [m.a.s.l]


%% short curcuit rain, no ice nor snow and give rain as output

rain=Extra.Preal; % in mm/s
Peq=rain;
Qice=zeros(nsteps,Nsc);

Wn=zeros(nsteps,Nsc); % initial liquid snow store [mm]
Hn=Wn;% inital solid snow store [mm]
Mn=Wn;
Mngr=Wn;


% Test water balance
balind=1;
warmup=1;
balflux=[warmup+1:length(Peq)];
```

```
38 state1=warmup+0;
39 state2=length(Peq);
40 %comb 30.10.2012: attention:Mnh is in mm and not in mm/time step
41
42 balHn =0;
43 balWn =0;
44 balglob=0;
45 balcheck=[balHn,balWn,balglob]*3600*24;
```

Appendix F

Appendix: The Aabach model

F.1 Workflow

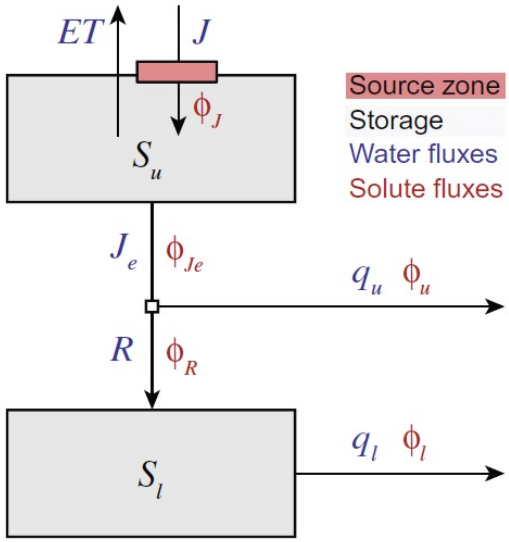

Figure F.1: Workflow of the Aabach model (taken from [Bertuzzo et al., 2013])

F.2 Adapted function of the Aabach model used during Monte-Carlo simulation

```
function [QtotS] = hydmod_PST(J, pet, par, dt)

N=length(J);
S=4641801; %surface of the basin [m2]

%------ parameters for soil moisture dynamics
------------------------------------
n=par(1);       %porosity
```

```
8  Z=1;      %[m]
9  s1=par(2);    %above sw plant evaporates at potential ET
10 % s1=0.59;
11 sw=s1*par(3);     %wilting point
12 Ksat=par(4)/3600;   %[m/s] hydraulic conductivity at saturation
13 % Ksat=360/3600;
14 % k =1/(0.1*24*3600); %discharge rate [1/s] (parameter of the
       exponential IUH, mean IUH equal to 1/k)
15 k=1/(par(5)*3600);
16 % kgw= 1/(100*24*3600); %[1/s]
17 kgw=1/(par(6)*3600);
18 % c=par(4);     %Clapp exponent
19 c=par(7);
20 Kc=par(8); %cultural coefficient
21 Recharge=par(9); %[m/s]
22
23 pet=Kc*pet;
24
25 %
       ********************************************************************************
26 % Numerical Simulation --> Soil moisture dynamics
27 %
       ********************************************************************************
28 %NB! no surface runoff is taken in account
29
30 %------ fluxes
31 Je=zeros(N,1);  %percolation (as in the paper)
32 ET=zeros(N,1);  %evapotranspiration
33 Qsub=zeros(N,1);   %discharge
34 R=zeros(N,1); %groundwater recharge
35 Qgw=zeros(N,1); %groundwater
36
37 %------ storage
38 s=zeros(N,1);   %soil moisture [-]
39 ST=zeros(N,1);  %storage nel subsurface [m3/m2]
40 Sgw=zeros(N,1); %groundwater storage [m3/m2]
41
42 s(1)=0.1;       %initial soil moisture value
43 Sgw(1)=0.01;
44
45 %------ Numerical Simulation
       ------------------------------------------------
46 tic
47 for t=1:N  %for loop on the number of timesteps
48     %upper storage
49     ET(t)=max(0,min(pet(t),pet(t)*((s(t)-sw)/(s1-sw)))); %[m/s]
50     Je(t)=Ksat*s(t)^c; %[m/s] alimente le "subsurface reservoir" Lsub
51
52     s(t+1)=min(1,s(t)+(J(t)-ET(t)-Je(t))*dt/(n*Z));  %soil moisture
           cannot exceeds one
53
54     %subsurface reservoir
55     R(t)=min(ST(t)/dt,Recharge);
56     Qsub(t)=k*ST(t); %[m/s]=[m3/m2/s]
57
```

```
58      ST(t+1)=ST(t)+(Je(t)-Qsub(t)-R(t))*dt;
59
60      %lower storage
61      Qgw(t)=kgw*Sgw(t);
62
63      Sgw(t+1)=Sgw(t)+(R(t)-Qgw(t))*dt;
64  end
65
66  Qtot=Qsub+Qgw; %[m3/m2]
67  QtotS=Qtot*S;
```

Appendix G

Appendix: Additional figures to results

G.1 Hydrological model

G.1.1 Comparison

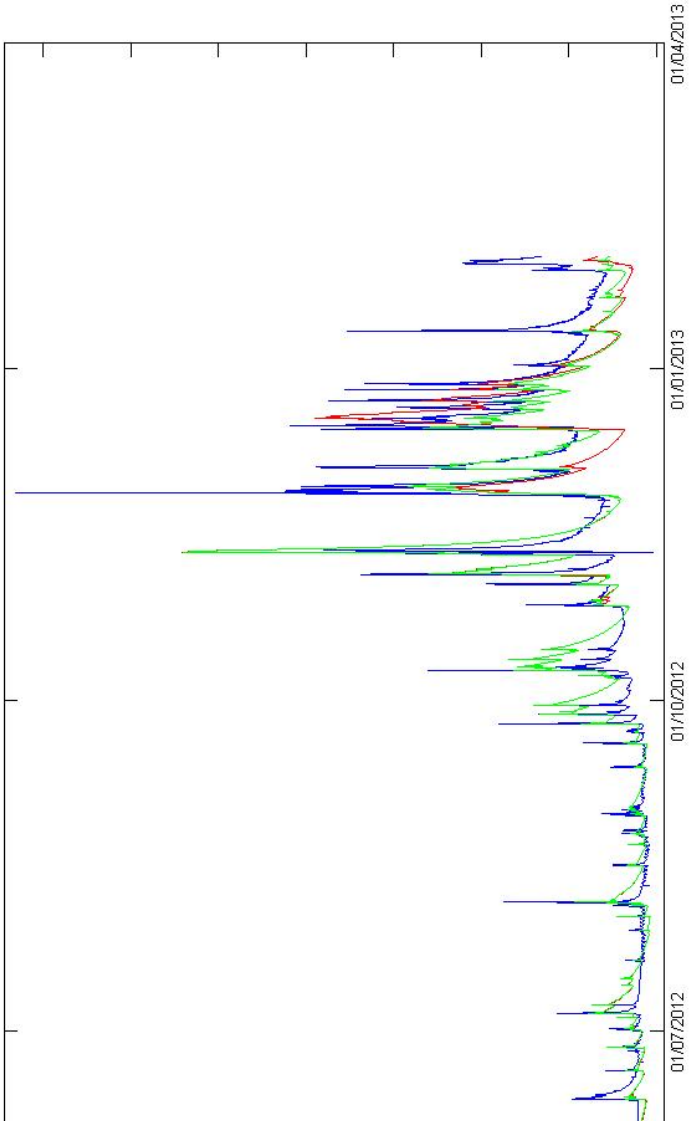

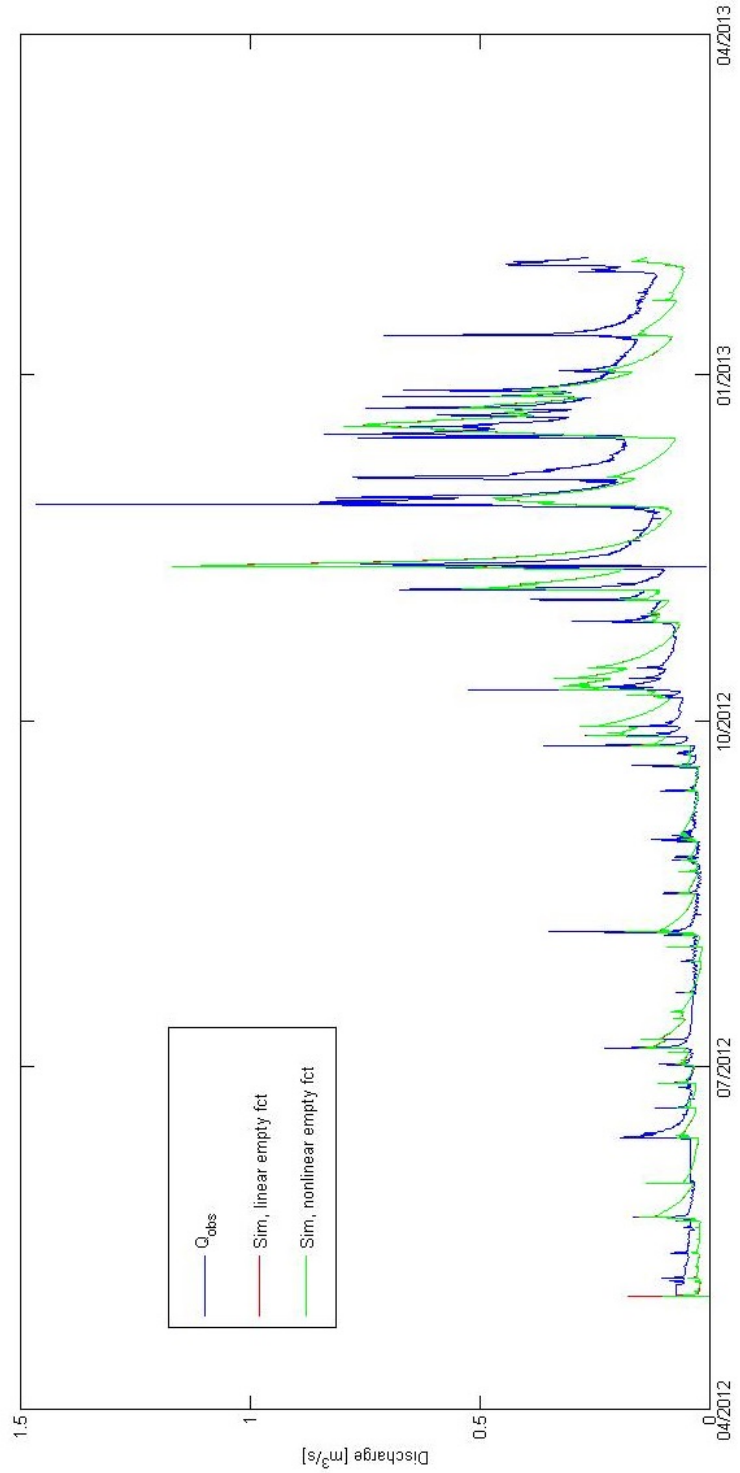

Figure G.2: Result 2: Simulation with linear and non-linear empty functions.

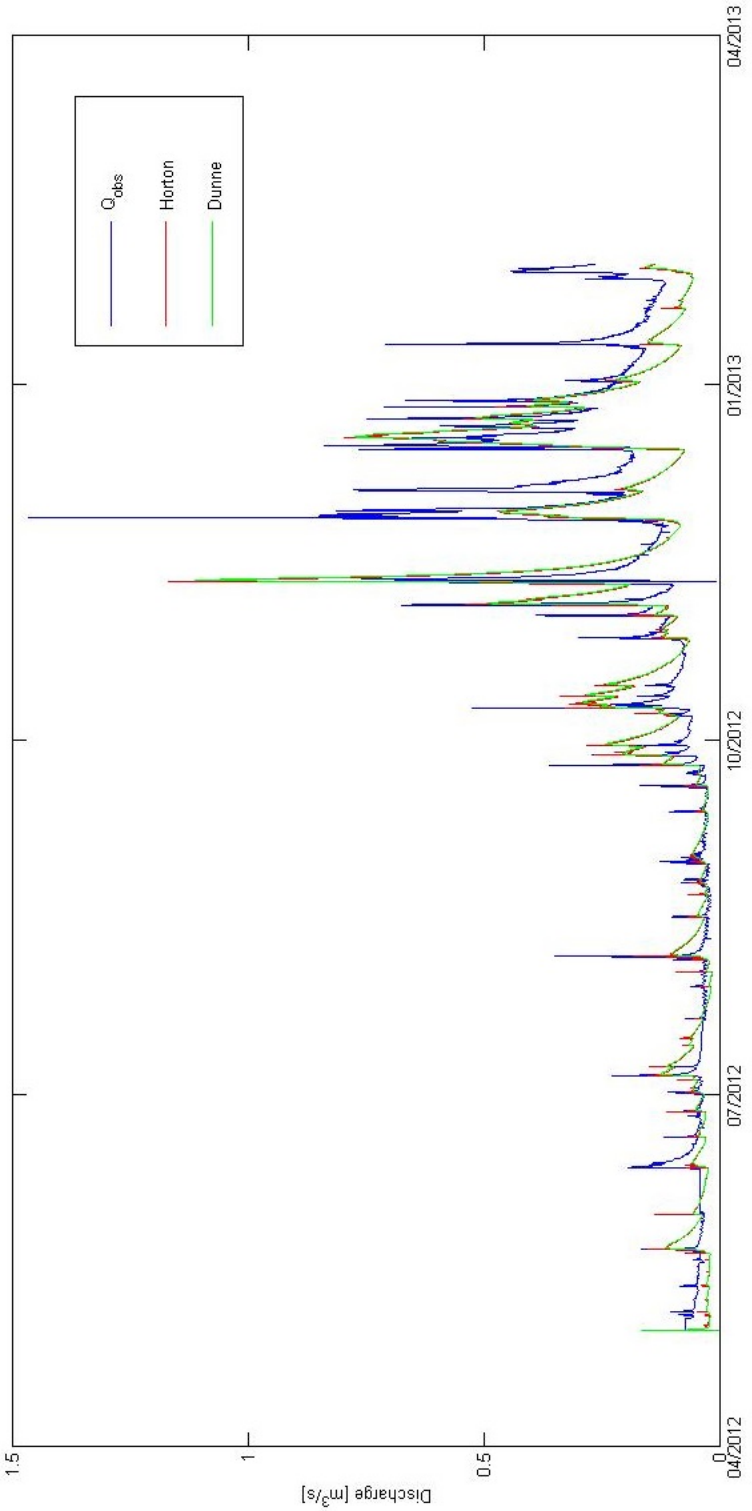

Figure G.3: Results 4: Complete simulation period with two modes of infiltration

G.1.2 Additional figures to combinations

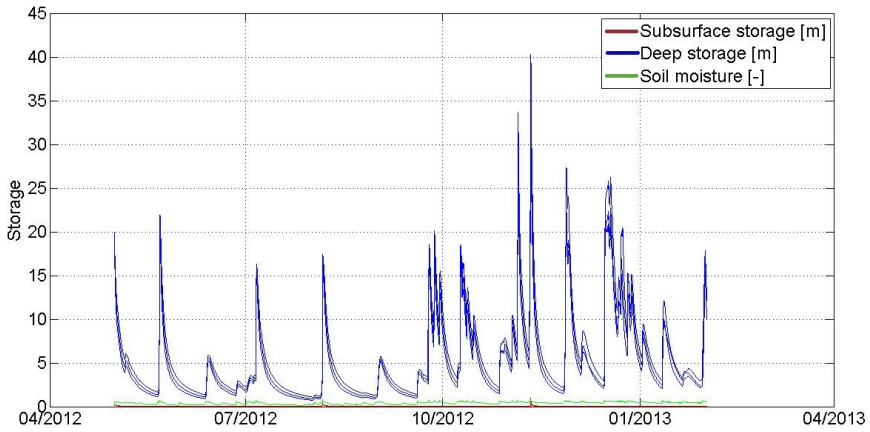

Figure G.4: Storage for nonlinear empty function and parameter set N°3. 3 impulses into the subsurface storage can be observed, the majority of the discharge is due to the deep storage.

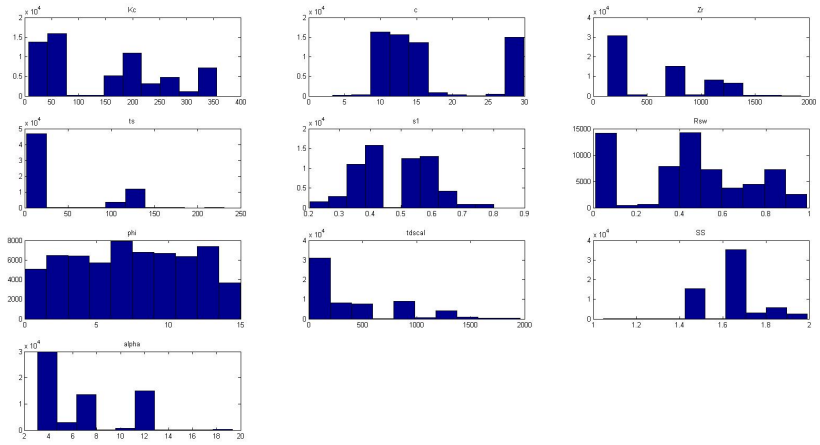

Figure G.5: Results of calibration using DREAM, combination N°5

G.2 Pesticide modelling

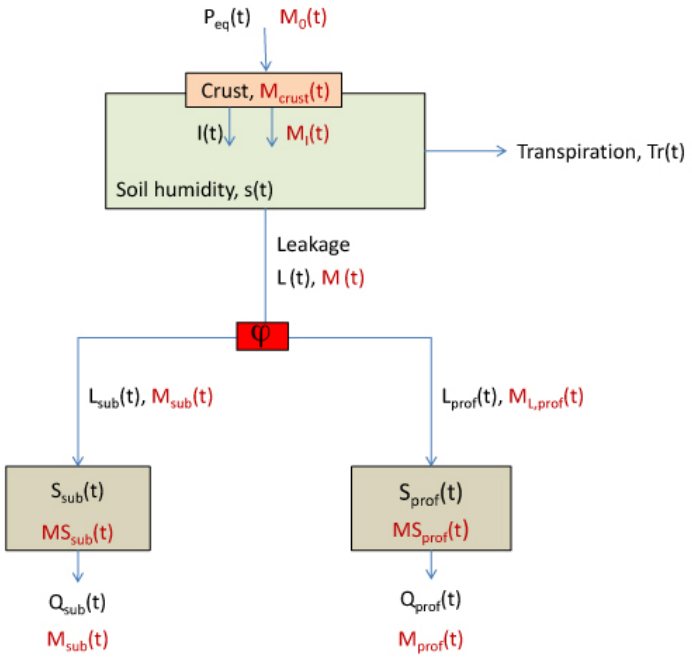

Figure G.6: Workflow of the simple pesticide transport model in case of parallel reservoirs

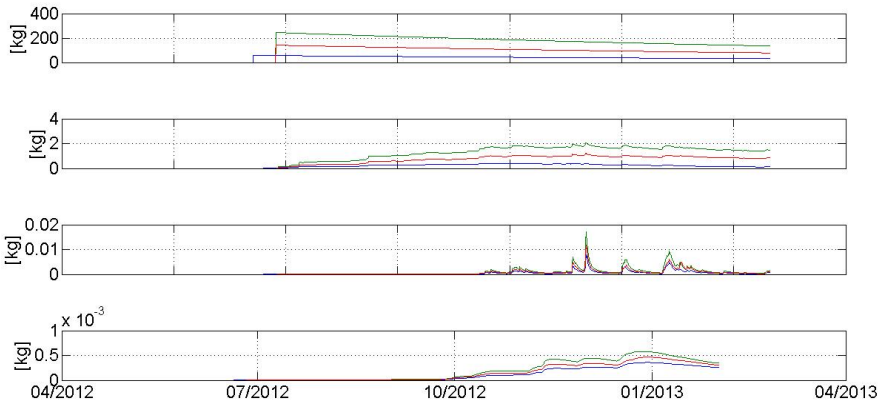

Figure G.7: Mass storage of Atrazine, using the simple model. From top to bottom: Total mass in crust, total mass in soil, total mass in subsurface reservoir, total mass in deep reservoir.

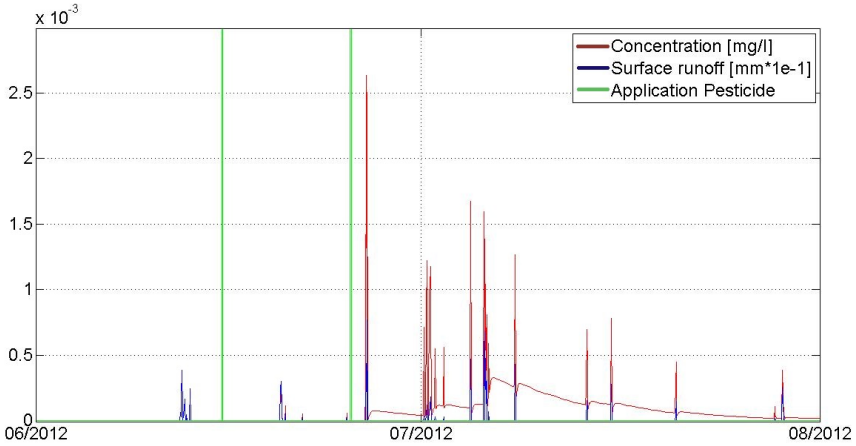

Figure G.8: Results for Mecoprop, using the simple model

Appendix H

Appendix: Summary of calibration trials

Comb N° [1]	Optimizer	Kc	c	Zr	ts	s*	Rsw	phi	tdscal	SS	α	NSE	Nash log	Nash bias
1	SCE	358.93 [2]	13.84	89.68	6.63	0.32	0.50	14.07	106.43	1.23	14.93	0.59	0.71	0.04
3	SCE	358.93	13.84	89.68	6.63	0.32	0.50	14.07	106.43	1.23	14.93	-2.14	-1.53	0.14
5	SCE	257.37	13.95	1035.70	3.01	0.58	0.38	8.67	488.97	1.40	4.57	0.71	0.84	-0.03
5	DREAM	346.71	12.38	807.09	4.41	0.52	0.41	11.57	376.55	1.69	4.07	0.66	0.81	0.20
6	SCE	359.94	14.37	1305.90	1.91	0.55	0.45	5.48	991.50	1.48	4.66	0.77	0.82	-0.03
7	SCE	334.42	21.52	115.83	66.90	0.67	0.01	14.97	1997.10	1.24	5.91	0.65	0.42	-0.65
8	SCE	333.95	21.37	115.17	62.19	0.50	0.34	5.16	1984.90	1.26	6.52	0.70	0.46	-0.05
11	SCE	358.99	23.74	124.79	18.17	0.41	0.84	9.02	47.95	1.29	2.51	-1.87	-1.93	0.12
13	SCE	2.20	3.33	187.38	4.46	0.20	0.06	12.68	370.83	1.42	12.83	0.70	0.83	0.02

[1] Combination corresponding to table 4.1
[2] Values are rounded to 2 decimal degrees

Appendix I

Appendix: Simple Model for Pesticide Transport

I.1 Code: surface_pest.m

Code as described in 3.2.2.

```
function [PEST]=surface_pest_series(param,Extra, Outall)

% %%%%%%%%%%%%%%%%%%%%%%%%%%%%%%%%%%%%%%%%%%%%%%%%%%%%%%%%%%%%%%%%%%%%%%%%%%
% This code is part of the Spatially-Explicit Pesticide Transport (SEPT)
% model of the ECHO laboratory, an extension to the SEHR model EPFL;
% see MainSEHR for details
% %%%%%%%%%%%%%%%%%%%%%%%%%%%%%%%%%%%%%%%%%%%%%%%%%%%%%%%%%%%%%%%%%%%%%%%%%%

%%% in this module, the pesticide on the surface undergoes following
%%% processes:
%%% 1. wash-off with surface runoff water (Qsup)
%%% 2. infiltration of pesticide
%%% 3. volatilization if volatile compound? not yet implemented, will not be?
%%% 4. chemical degradation

%%% initialize variables
dt=Extra.dt;
M0=Extra.appPEST; %[kg] application of pesticide
Qm_river=zeros(length(Extra.date),Extra.Nsc);
Zr=param(Extra.paramind.Zr)/1000;


A=Extra.A(:)*param(Extra.paramind.SS);       % surface area [m2]
L=Outall.L/1000;     % leaching [m/s]
I=Outall.I/1000;     % infiltration [m/s]
Rs=Outall.Rs/1000;   % Surface runoff [m/s]
```

```
27
28 s=Outall.s; %soil moisture [-]
29 s(s==0)=1e-9; %avoid numerical problems for first time step, where s=0
30
31 %%% set parameters
32 theta=param(Extra.paramind.s1);     % fraction water content in the
       source zone (fully saturated at all times)
33 phi=1200;                           % Mass soil over Total Volume [kg/
       m3]
34 d_crust=0.01;                       % thickness of crust layer [m]
35
36 if ¬isfield(Extra, 'kdsurf') && ¬isfield(Extra.paramind, 'kdsurf') %
       here one should apply a calibration, as this half live is highly
       dependant on the specific substance and partitioning etc.
37     DT50=270; %[days]
38     kdsurf=log(2)/DT50/24/3600; %dissipation in the source zone [1/s]
39 end
40
41 if ¬isfield(Extra, 'kdact') && ¬isfield(Extra.paramind, 'kdact') %here
        one should apply a calibration, as this half live is highly
       dependant on the specific substance and partitioning etc.
42     DT50=270; %[days]
43     kdact=log(2)/DT50/24/3600; %dissipation in the source zone [1/s]
44 end
45
46 if ¬isfield(Extra, 'Kd') && ¬isfield(Extra.paramind, 'Kd') %here one
       should apply a calibration, as the partition coefficient is highly
        dependant on the specific substance and partitioning etc.
47     Kd=2;  %[m3/kg]
48 end
49
50 %initialize variables
51 MScrust=zeros(length(Extra.date),Extra.Nsc);        %total mass in the
        source zone [kg]
52 Mcrust_dis=zeros(length(Extra.date),Extra.Nsc);     %disolved mass in
       the source zone [kg]
53 Ccrust_dis=zeros(length(Extra.date),Extra.Nsc);     %concentration of
       the water in the source zone [kg/m3]
54
55 Minf=zeros(length(Extra.date),Extra.Nsc);          % infiltrated mass
        (from crust to soil) [kg]
56 Qm_sup=zeros(length(Extra.date),Extra.Nsc);        % superficial loss
        (from crust to river) [kg/s]
57 Mleak=zeros(length(Extra.date),Extra.Nsc);         % leaked mass (
       from soil to subsurface res) [kg]
58 MSsoil=zeros(length(Extra.date),Extra.Nsc);        % total mass
       stored in soil layer [kg]
59 Msoil_dis=zeros(length(Extra.date),Extra.Nsc);     % dissolved mass
       in soil layer [kg]
60 Csoil_dis=zeros(length(Extra.date),Extra.Nsc);     % concentration in
        soil layer [kg/m3]
61
62 for t=1:length(Extra.date)  %loop on the number of timesteps
63
64     Mcrust_dis(t,:)=MScrust(t,:)/(phi*Kd/theta+1);              % [kg]
65
```

```
66      Ccrust_dis(t,:)=Mcrust_dis(t,:)./(d_crust*theta.*A(:))';    % [kg/
            m3] conc. in the water of the source zone
67
68      Qm_sup(t,:)=Ccrust_dis(t,:).*Rs(t,:).*A(:)';                % [kg/
            s] mass leached directly to river with superficial flow (
            assumption: fully saturated crust layer)
69
70      if Rs(t,:)>(d_crust*theta)'
71          i
72          'flow bigger than available volume'
73      end
74
75      Minf(t,:)=min(MScrust(t,:)- kdsurf*dt.*MScrust(t,:) + M0(t,:) -
            Qm_sup(t,:)*dt,Ccrust_dis(t,:).*I(t,:).*A(:)'*dt);  % [kg]
            mass infiltrated
76
77      MScrust(t+1,:)=MScrust(t,:)- kdsurf*dt.*MScrust(t,:) + M0(t,:) -
            Minf(t,:)-Qm_sup(t,:)*dt ; %[kg] total remaining mass (sorbed
            and dissolved) in the crust
78
79  %     Msoil_dis(t,:)=MSsoil(t,:)./(phi*Kd./s(t,:)+1); %[kg] if
        partitioning in soil layer is desired, activate
80  %     Csoil_dis(t,:)=Msoil_dis(t,:)./(Zr.*A'.*s(t,:)); %[kg/m3] conc.
        in the water of the source zone
81
82      Csoil_dis(t,:)=MSsoil(t,:)/(Zr.*A'.*s(t,:)*Extra.rho); % [kg/m3]
83      Mleak(t,:)=min(MSsoil(t,:)+Minf(t,:)- kdact*dt.*MSsoil(t,:),
            Csoil_dis(t,:).*(L(t,:).*A').*dt); %[kg]
84
85      MSsoil(t+1,:)=MSsoil(t,:)+Minf(t,:)-Mleak(t,:)- kdact*dt.*MSsoil(t
            ,:); %[kg]
86  end
87
88  MScrust(end,:)=[];
89  MSsoil(end,:)=[];
90
91  PEST.appP=M0;
92
93  PEST.Mcrustdis=Mcrust_dis;
94  PEST.Ccrustdis=Ccrust_dis;
95  PEST.Csoil=Csoil_dis;
96  PEST.Qm_sup=Qm_sup;
97  PEST.Msoil_dis=Msoil_dis;
98
99  PEST.MScrust=MScrust;
100 PEST.Mleak=Mleak;
101 PEST.Minf=Minf;
102 PEST.MSsoil=MSsoil;
```

I.2 Code: rseriespest.m

Code as described in 3.2.2.

```
1  function [PEST]=rseries_pest(PEST, param, Extra, Outall)
```

```
%%%%%%%%%%%%%%%%%%%%%%%%%%%%%%%%%%%%%%%%%%%%%%%%%%%%%%%%%%%%%%%%%%%%%%%%%%%%%%
% This code is part of the Spatially-Explicit Pesticide Transport (SEPT)
% model of the ECHO laboratory, an extension to the SEHR model EPFL;
% see MainSEHR for details
%%%%%%%%%%%%%%%%%%%%%%%%%%%%%%%%%%%%%%%%%%%%%%%%%%%%%%%%%%%%%%%%%%%%%%%%%%%%%%

%%% in this module, pesticides undergo following processes:
%%% 1. transport with Qsub towards river network
%%% 2. transport towards deep reservoir
%%% 3. transport with Qprof towards river
%%% 4. chemical degradation

Ssub=Outall.Ssub/1000;          %subsurface water storage [m]
Sprof=Outall.Sprof/1000;        %deep water storage [m]

% Ssub(Ssub==0)=1e-9;
% Sprof(Sprof==0)=1e-9;


Lprof=Outall.Lprof/1000;        % leaching towards deep reservoir [mm/s]

dt=Extra.dt;
A=Extra.A*param(Extra.paramind.SS);                     % area of catchment [m2]

QsubNR=Outall.QsubNR;           %subsurface discharge [m3/s]
QprofNR=Outall.QprofNR;         %deep discharge [m3/s]


Mleak=PEST.Mleak;               % Leaking mass from soil layer

if ¬isfield(Extra, 'kr') && ¬isfield(Extra.paramind, 'kr') %here one could apply a calibration, as the half live is highly dependant on the specific substance and partitioning etc.
    DT50=365; %[days]
    kr=log(2)/DT50/24/3600; %dissipation in the subsurface zone [1/s]
end

MSsub=zeros(length(Extra.date),Extra.Nsc);      %mass [kg] stored in the subsurface reservoir
MSprof=zeros(length(Extra.date),Extra.Nsc);     %mass [kg] stored in the deep reservoir
Csub=zeros(length(Extra.date),Extra.Nsc);       % concentration subsurface reservoir [kg/m3]
Cprof=zeros(length(Extra.date),Extra.Nsc);      % concentration deep reservoir [kg/m3]
Qm_sub=zeros(length(Extra.date),Extra.Nsc);     %[kg/s]mass leaching to river from subsurface reservoir
Qm_prof=zeros(length(Extra.date),Extra.Nsc);    %[kg/s]mass leaching to river from deep reservoir
```

```
44
45 M2deep=zeros(length(Extra.date),Extra.Nsc);     % mass leaching from
       subsurface to deep reservoir [kg]
46
47
48 for t=1:length(Extra.date)
49
50     Csub(t,:)=MSsub(t,:)./(Ssub(t,:).*A(:)'); %[kg/m3] conc. in the
           water of the source zone
51
52     if any(QsubNR(t,:)*dt>Ssub(t,:).*A(:)')
53         'error, flux bigger than stock (Qsub)'
54     end
55
56
57     Qm_sub(t,:)=MSsub(t,:).*QsubNR(t,:)./(Ssub(t,:).*A(:)'); %[kg/s]
58
59     M2deep(t,:)=max(0,min(MSsub(t,:)+Mleak(t,:)-kr*MSsub(t,:)*dt-
           Qm_sub(t,:)*dt,Lprof(t,:).*MSsub(t,:)./Ssub(t,:)));  %[kg]
60
61 %     Qm_sub(t,:)=max(0,QsubNR(t,:).*Csub(t,:));  %[kg/s]mass flow to
       river
62
63
64
65 %     M2deep(t,:)=min(MSsub(t,:)+Mleak(t,:)-kr*MSsub(t,:)*dt-Qm_sub(t
       ,:)*dt,Csub(t,:).*Lprof(t,:).*A(:)'.*dt); %[kg]
66 %     M2deep(t,:)=Csub(t,:).*Lprof(t,:).*A(:)'.*dt; %[kg]
67
68     MSsub(t+1,:)=MSsub(t,:)+Mleak(t,:)-kr*MSsub(t,:)*dt-Qm_sub(t,:)*dt
           -M2deep(t,:); %[kg]
69
70 end
71
72
73 for t=1:length(Extra.date)
74
75     Cprof(t,:)=MSprof(t,:)./(Sprof(t,:).*A(:)'); %[kg/m3] conc. in the
            water of the source zone
76
77     Qm_prof(t,:)=max(0,min(MSprof(t,:)+M2deep(t,:)-kr*MSprof(t,:)*dt,
           MSprof(t,:).*QprofNR(t,:)./(Sprof(t,:).*A(:)'))); %[kg/s]  %[
           kg/s] mass flow to river
78
79     MSprof(t+1,:)=MSprof(t,:)+M2deep(t,:)-kr*MSprof(t,:)*dt-Qm_prof(t
           ,:)*dt; %[kg]
80
81 end
82 MSsub(end,:)=[];
83 MSprof(end,:)=[];
84
85 PEST.Qm_sub=Qm_sub;
86 PEST.Qm_prof=Qm_prof;
87 PEST.MSsub=MSsub;
88 PEST.M2deep=M2deep;
89 PEST.MSprof=MSprof;
90 PEST.Cprof=Cprof;
```

```
91 PEST.Csub=Csub;
```

I.3 Code: pest_norouting.m

Code as described in 3.2.2.

```
1  function [PEST]=pest_norouting(PEST, qsim, Extra)
2
3
4  Qmtot=PEST.Qm_sup+PEST.Qm_sub+PEST.Qm_prof;
5
6  Qmtot=sum(Qmtot,2);
7
8
9  PEST.Ctot=Qmtot./qsim; %kg/m3/s
10
11 PEST.Mtot=Qmtot*Extra.dt;
12
13 'mass balance of pesticide (neg=sim>input)'
14
15 sum(sum(PEST.appP))-sum(PEST.Mtot)-sum(PEST.MScrust(end,:))-sum(
       PEST.MSsoil(end,:))-sum(PEST.MSprof(end,:))-sum(PEST.MSsub(end,:))
```